２０２４年度

博士学位論文

Overcoming Vestibular System Limitations to Prevent Spatial Disorientation

— Central Training and Peripheral Protection —

空間識失調防止のための前庭系の限界の克服

－中枢訓練と末梢保護－

中部大学大学院

工学研究科　ロボット理工学専攻

田所　慎

Overcoming Vestibular System Limitations to Prevent Spatial Disorientation

— Central Training and Peripheral Protection —

By

Shin Tadokoro

A dissertation submitted in partial fulfillment of

the requirements for the degree of Doctor of Engineering

Department of Robotic Science and Technology

Graduate School of Engineering, Chubu University

2024

The reasonable man adapts himself to the world; the unreasonable one persists in trying to adapt the world to himself. Therefore, all progress depends on the unreasonable man.

- George Bernard Shaw (1856–1950)

Acknowledgments

I am deeply grateful for the help and support of many individuals who have made this work possible. First and foremost, I thank my advisor, Prof. Yutaka Hirata, whose patience and unwavering support have shaped me into the scientist I am today. Dr. Hirata also extended the modified Kalman filter model to three dimensions, and Yusuke Shinji implemented it with an eye movement model to simulate the VOR results, which made this research far more practical and powerful, breaking new ground in a long-standing critical issue.

I am indebted to Toshimi Yamanaka for managing the aquatic animals, supporting figure preparation, and creating beautiful fish illustrations that greatly enhanced the clarity of this work. Prof. Nobuyuki Kawai, Prof. Zin Arai, and Prof. Shin-ichi Higashijima provided valuable feedback on the VOR project. Prof. Kawai also mentored me in psychological research on spatial disorientation, allowing me to prepare a presentation for a conference. Although this research did not make it into this thesis, I plan to finalize it for publication in the future.

I also extend my gratitude to Dr. Katsuki Niwa for leading the TJ-014 project; Dr. Takaomi Kurioka, Dr. Daisuke Kamide, and Dr. Atsushi Tamura for their assistance with hair cell count assessments; Dr. Takeshi Matsunobu, Dr. Yasushi Satoh, and Prof. Akihiro Shiotani provided valuable comments on the TJ-014 project. Dr. Niwa, Dr. Kurioka, and Dr. Matsunobu are also the individuals who sparked my initial interest in vestibular research. Prof. Shiotani also supported my academic journey by facilitating my transition from his Department of Otolaryngology to Prof. Hirata's laboratory.

Dr. Norihiko Yamada, Dr. Shinya Bekku, and Dr. Kei Kato, esteemed seniors in the Japan Air Self-Defense Force, encouraged and motivated a helpless flight surgeon frustrated and overwhelmed by frequent aviation accidents, inspiring him to confront the challenges of spatial disorientation research. Their support enabled me to embark on the study abroad program at Chubu University.

I wish to express my heartfelt thanks to Dr. Yoshiro Wada, a respected otolaryngologist and mentor, who connected the young, inexperienced yet passionate otolaryngologist eager to tackle the challenges of spatial disorientation to the powerful and exciting engineering laboratory of Dr. Hirata, making this interdisciplinary journey possible. I am also deeply grateful to Dr. Wada for his continued support, as well as to Prof. Shuuji Kajita and Prof. Hironobu Fujiyoshi, for their service as members of my thesis committee.

Prof. Robert Baker, Prof. Tatyana Yakusheva, and Dr. Jean Laurens, leading figures in vestibular research and neuroscience, elevated this study to a higher level through their insightful discussions and invaluable input. Prof. Shinichi Iwasaki and Dr. Kayoko Kabaya greatly enhanced my clinical knowledge through their guidance and support during clinical case conferences on vestibular disorders. Prof. Atsushi Iriki provided me with the invaluable opportunity to independently apply for grants and lead research as a principal investigator, fostering my growth as a researcher.

Finally, I would like to express my deepest gratitude to my wife and daughters for their unwavering support throughout this process.

The investigation of Visual-Vestibular Neural Training to Resolve Tilt-Translation Ambiguity in Goldfish was supported by JST CREST Grant Number JPMJCR22P5 and JSPS KAKENHI Grant Numbers 20H04286, 19K06756, and 18KK0286. The assessment of TJ-014’s effects on ROS-induced inner ear hair cell loss was supported by JSPS KAKENHI Grant Number 23592504. This research was conducted as part of the official duties of the author, who is employed by the Japan Ministry of Defense, in accordance with the Act on Reimbursement of National Public Officers' Expenses for Studying Abroad (Act No. 70 of 2006). The views expressed in this publication are those of the author and do not necessarily reflect the official policies or positions of the Japan Ministry of Defense. I declare that this study was conducted in the absence of any commercial or financial relationships that could be construed as potential conflicts of interest.

Abstract

Vestibular limitations pose fundamental challenges to spatial orientation, significantly impacting animal behaviors. These sensory limitations can lead to spatial disorientation, a major contributing factor to falls, motion sickness, and aviation accidents. Aviation accidents, in particular, are associated with high fatality rates, with spatial disorientation accounting for 25-33% of the causes. This thesis investigates vestibular limitations from both central (brain) and peripheral (sensor) perspectives, offering insights into their resolution.

To address the central limitations, we examined the adaptive capabilities of the vestibular system in resolving tilt-translation ambiguity, using goldfish as a model organism and the vestibuloocular reflex (VOR) as an indicator of spatial orientation. Goldfish, with their well-characterized oculomotor physiology and distinct motion experience profiles, allowed us to reveal how accumulated motion experiences refine neural estimates of head motion. Our results demonstrated that the VORs of naïve goldfish did not differentiate between translation and tilt. However, after prolonged visual-vestibular neural training, the VORs were able to distinguish between the two types of head motion within three hours. These findings were supported by simulations using a Kalman filter model, which highlighted the role of accumulated motion experience in refining neural estimates. Our behavioral experiments and computational modeling provide novel evidence supporting theoretical frameworks such as frequency segregation and internal model theories. Furthermore, they offer the first evidence of how motion experiences and training contribute to resolving spatial disorientation.

For the peripheral limitations, we explored pharmacological strategies to protect the vestibular system from oxidative stress caused by excessive reactive oxygen species (ROS), which compromise vestibular function. Specifically, we investigated the protective effects of Hangesha-shin-to (TJ-014), a traditional herbal medicine, against ROS-induced ototoxicity in the inner ear hair cells of rat Corti organ explants. Our results demonstrated that TJ-014 effectively mitigates oxidative damage to hair cells, suggesting its potential as a novel and practical therapeutic approach.

This integrative approach, combining experimental, computational, and pharmacological methodologies, advances our understanding of vestibular limitations and their impact on spatial orientation. The findings support the development of enhanced training protocols to reduce spatial disorientation and innovative therapies to preserve vestibular function, contributing to improved safety in various environments, including daily life and aviation operations.

Table of Contents

1. Introduction …1

1.1 Background …1

1.1.1 Importance of Spatial orientation …1

1.1.2 Limitation of vestibular system …1

1.2 Purpose of this thesis …3

1.3 Structure of this thesis …5

2. Materials and Methods …8

2.1 Visual-Vestibular Neural Training to Resolve Tilt-Translation Ambiguity in Goldfish …8

2.1.1 Subjects …8

2.1.2 Surgical procedures …8

2.1.3 Experimental setup …8

2.1.4 Experimental paradigms …16

2.1.5 Data analysis …17

2.1.6 Implementation of the computational model for motion estimation and eye movements …19

2.2 TJ-014 effect in ROS-induced inner ear hair cell loss …25

2.2.1 Subjects …25

2.2.2 Hangesha-shin-to (TJ-014) …25

2.2.3 Cochlear explant culture …26

2.2.4 Cell counts and immunohistochemistry …26

2.2.5 Assessment of hair cell counts …27

2.2.6 Assessment of mitochondrial membrane potential …28

2.2.7 Data analysis …28

3. Visual-Vestibular Neural Training to Resolve Tilt-Translation Ambiguity in Goldfish …29

3.1 Results …29

3.1.1 VOR during translation in dark in naïve animals …29

3.1.2 Changes in VOR during visual-translation training …35

3.1.3 Changes in VOR during translation in the dark along with the training …36

3.1.4 VOR during roll-tilt before and after training …38

3.1.5 Kalman filter simulations …38

3.2 Discussion …46

3.2.1 Adaptive changes in the spatial orientation formed during translation …46

3.2.2 Interpretation based on the Kalman filter model …51

3.2.3 VOR as an indicator of motion estimation …55

4. TJ-014 effect in ROS-induced inner ear hair cell loss …60

4.1 Results …60

4.1.1 Protective effect of TJ-014 …60

4.1.2 TJ-014 suppresses caspase-3 activation …60

4.1.3 TJ-014 suppresses ROS generation …61

4.1.4 TJ-014 protects mitochondrial membrane potential …66

4.2 Discussion …66

5. Conclusion …71

References …73

Appendix: Glossary of terms and abbreviations …89

Supplementary Methods …95

S2.1 Correction for vertical and horizontal eye positions …95

S2.1.1 Correction for vertical eye position …95

S2.1.2 Correction for horizontal eye position …96

S2.1.3 Estimation of the tilt angle of the horizontal eye camera …96

S2.2 Calculation for the rotational angle of the GIA vector. …100

S2.3 Kalman filter model …101

S2.3.1 Model of head and eye motion with sensors …101

S2.3.2 Model in matrix form …102

S2.3.3 Kalman filter algorithm and control feedback …103

Supplementary Results …104

Kalman gains …104

S3.1 Kalman gains in linear Supplementary Results VOR dark before training …104

S3.2 Kalman gains in linear VOR dark after training …105

S3.3 Kalman gains in rotate VOR dark before training …106

S3.4 Kalman gains in rotate VOR dark after training …107

S3.5 Kalman gains in linear VOR light beginning of training …108

S3.6 Kalman gains in linear VOR light end of training …109

Academic Achievements …111

List of Figures

Figure 1.1. Structure of this thesis. …7

Figure 2.1. Definition of 3D axes in animals' head coordination and experimental setup. …12

Figure 2.2. Experimental paradigms for roll-tilt, translation, and visual-translation training, and protocol timeline. …15

Figure 2.3. Modified Kalman filter model incorporating additional components for explaining VOR results. …22

Figure 3.1. Horizontal and vertical VOR responses to translational head acceleration in the dark, showing training effects. …31

Figure 3.2. Horizontal and vertical VOR responses to translational head acceleration with OKS during visual-translation training. …33

Figure 3.3. Horizontal and vertical VOR responses to roll-tilt head rotation in the dark before and after training. …37

Figure 3.4. Simulation results of the modified Kalman filter model validating angular VOR and OKAN responses. …40

Figure 3.5. Simulation results of modified Kalman filter model for translational head acceleration in the dark before and after training. …43

Figure 3.6. Simulation results of modified Kalman filter model for translational head acceleration with OKS during training. …44

Figure 3.7. Simulation results of modified Kalman filter model for roll-tilt head rotation in the dark before and after training. …45

Figure 4.1. Representative fluorescence images of phalloidin-labeled hair cells treated under different conditions. …62

Figure 4.2. Survival ratios of outer hair cells in each group. …63

Figure 4.3. Representative fluorescence micrographs of cleaved caspase-3, F-actin, and DAPI. …64

Figure 4.4. Representative fluorescence micrographs of 8-OHdG, F-actin, and DAPI. …65

Figure 4.5. Representative micrographs of mitochondrial membrane potentials using MitoTracker Red CMXRos. …69

Figure 4.6. Comparing the density of MitoTracker Red CMXRos fluorescence. …70

List of Tables

Table 2.1. Variables in the modified Kalman filter model …23

Table 2.2. Simulation parameters in the modified Kalman filter model …24

1 Introduction

1.1 Background

1.1.1 Importance of Spatial orientation

The ability of animals to safely interact with their surrounding environment is crucial for survival. Efficiently focusing on a target or avoiding obstacles while chasing prey or escaping predators is essential for life. “Spatial orientation” supports these behaviors. Spatial orientation refers to the estimation of an animal's relative location, posture, and motion within a given space (Mehlman and Taube, 2018). It is formed by integrating information from multiple sensory systems, including visual, vestibular, and proprioceptive inputs, enabling precise interactions with the environment.

Over millions of years, animals on Earth have evolved to adapt to a diverse range of environments, transitioning from aquatic to terrestrial, arboreal, and even aerial habitats (Sharma, 2015). However, this evolutionary adaptation is limited by their phylogenetic heritage, including inherent physical capabilities and behavioral traits. Exposure to novel or unfamiliar environments can create a mismatch between the demands of these environments and an animal's innate capabilities for spatial orientation. This mismatch manifests as spatial disorientation (Gillingham, 1992). For instance, human beings, physiologically adapted for terrestrial environments, face significant challenges in aerial settings. This unfamiliarity often leads to spatial disorientation, which has been a contributing factor in numerous aviation mishaps worldwide, resulting in substantial losses of personnel and material (Singh and Navathe, 1994; Cheung *et al.*, 1995; Holmes *et al.*, 2003). Gibb *et al.* (2011) suggested that spatial disorientation accounts for at least 25-33% of all aircraft mishaps and is associated with the highest number of fatalities.

1.1.2 Limitation of vestibular system

Among the sensory systems, two sets of vestibular organs—the semicircular canals and the otoliths—are specialized for sensing head motions in three-dimensional (3D) space. Semicircular canals function like gyroscopes, detecting angular head velocity. However, this information is neither accurate nor sustained during prolonged head motion, as the hair cells in the semicircular canals lack continuous responses over extended periods

(Highstein *et al.*, 2005; Laurens and Angelaki, 2011). On the other hand, otoliths act as accelerometers, sensing gravito-inertial acceleration (GIA), which is the vector sum of linear head acceleration and gravitational acceleration (Laurens and Angelaki, 2011; Kheradmand and Otero-Millan, 2019). Because they detect the combined vector of linear head acceleration and gravitational acceleration, it is impossible to distinguish between linear head motion (translation) and head-tilting relative to gravity (tilt) based solely on otolith output. This issue is known as "tilt-translation ambiguity", which can lead to somatogravic illusions and has been implicated in several fatal aviation accidents (Gillingham and Wolfe, 1985; Clément *et al.*, 2001). Experimental studies in monkeys have shown that primary otolith afferents respond indistinguishably to sinusoidal translation and tilt motions when the trajectories of the two stimuli match (Fernandez and Goldberg, 1976; Angelaki and Dickman, 2000). Interestingly, studies on both humans and non-human primates have demonstrated that perceptions of translation and tilt are not always accurate, leading to instances of spatial disorientation.

Animals are believed to implement neural systems to address these limitations. To supplement insufficient canal response, visual input from retina is integrated with canal signals through the neural system called velocity storage mechanism (VSM) (Raphan *et al.*, 1979; Laurens and Angelaki, 2011). This in turn improves the rotational velocity estimate. To overcome the ambiguity of otolith, animals must accurately perceive ongoing head motions and form the correct spatial orientation. Two major theories have been proposed to explain how the vertebrate neuronal system estimates tilt and translation motion from an ambiguous otolith response (Clément *et al.*, 2022). The frequency segregation theory posits that low-frequency linear accelerations are interpreted as tilts, whereas high-frequency accelerations are correctly interpreted as translations (Paige and Tomko, 1991; Seidman and Paige, 1996; Seidman *et al.*, 1998). In contrast, the integration theory, often referred to as the internal model theory, assumes that the brain utilizes information from multiple sensory sources, e.g., the semicircular canals, vision, and proprioception, to distinguish between these two types of motion (Merfeld *et al.*, 1993; Angelaki *et al.*, 1999; Angelaki *et al.*, 2004; Laurens and Angelaki, 2011). Notably, both theories postulate the existence of an underlying neural mechanism that enables animals to distinguish different types of head motions based on their own motion

experiences (Paige and Tomko, 1991; Telford *et al.*, 1997; Laurens and Angelaki, 2011). However, despite these theoretical frameworks, there are limited experimental studies that explicitly address how animals adaptively learn to estimate head motion from ambiguous vestibular information based on their motion experiences. The practical aspects of motion experience are also expected to help overcome vestibular limitations. For example, aviation pilots undergo spatial orientation training before boarding an aircraft to prevent spatial disorientation. This training involves experiencing simulated conditions that are likely to induce spatial disorientation. However, the effectiveness of these training methods has not yet been experimentally validated.

Additionally, the sensory cells of vestibular organs—inner ear hair cells—are highly vulnerable to oxidative stress, making individuals prone to vestibular disorders (Goto *et al.*, 2009; Kishimoto-Urata *et al.*, 2022). Reactive oxygen species (ROS) are continuously generated in the human body through various sources, including mitochondrial respiration and enzymatic reactions (Bae *et al.*, 2011; Brieger *et al.*, 2012). While ROS play vital roles in physiological processes such as cell signaling, redox homeostasis, and biosynthesis, excessive ROS production can induce oxidative stress, leading to tissue damage (Brieger *et al.*, 2012; Sena and Chandel, 2012). Factors like psychological stress, air pollution, and cigarette smoke are known to increase ROS levels (Møller *et al.*, 1996). ROS-induced inner ear damage can disrupt sensory integration, contributing to spatial disorientation. For pilots, this may increase the risk of aircraft accidents (Tamura and Tadokoro, 2019). Antioxidant therapies have shown potential in preventing ROS-induced inner ear damage in animal studies (Takumida *et al.*, 1999a; Fetoni *et al.*, 2003a; Kikkawa *et al.*, 2009). However, success in the laboratory has not translated to the clinic, and inner ear protection-based treatment strategies for ROS-induced ototoxicity have been disappointing thus far.

1.2 Purpose of this thesis

The overall aim of this thesis is to establish a solid scientific foundation for developing methods to overcome vestibular limitations and prevent spatial disorientation. This involves employing an engineering approach addressing the central nervous system and a histological approach targeting peripheral sensory organs.

First, my collaborators and I hypothesized that animals can adaptively and neurologically change their head motion estimation in response to accumulated motion experiences. In other words, we proposed that the accumulation of a well-designed set of sensory stimuli could efficiently resolve spatial disorientation. This concept—experimentally investigating whether training could indeed prevent spatial disorientation—had not been conclusively demonstrated before. We conducted behavioral experiments using goldfish to evaluate their VOR as an indicator of 3D head motion estimates during interaural linear translation and roll-tilt, both before and after visual-vestibular neural training that involved interaural linear translation and visual stimuli. Goldfish were selected as our model species due to the comprehensive understanding of their neuroanatomy and the physiology underlying various oculomotor behaviors (Gestrin and Sterling, 1977; Sterling, 1977). Importantly, because they have minimal experience with interaural linear translation in their natural habitat, they are favorable for assessing the impact of motion experience by comparing results before and after the experimental intervention. To acquire further computational understanding of this neurological adaptive process during the training, we extended the Kalman filter model of spatial orientation formation originally developed by Laurens and Angelaki (2017) and replicated the changes in the VOR that we observed in the goldfish following the training.

In addition to verifying the adaptive changes in the central nervous system, we explored a pharmacological approach that offers protective effects on inner ear hair cells against oxidative stress, a potential cause of spatial disorientation. Since the use of drugs with undesirable side effects for aircraft operation is restricted by regulations (Flight Standards Division, 2005), we focused on drugs that do not have these restrictions. Hangesha-shin-to (TJ-014) is a traditional Kampo formula used in Japanese herbal medicine, commonly for treating diarrhea, dyspepsia, gastritis, stomatitis, psychoneurosis, and chemotherapy-induced stomatitis. We focused on the antioxidant effects of the ingredients baicalein, baicalin, wogonin, and berberine, which are components of TJ-014 (Usami *et al.*, 1998; Shieh *et al.*, 2000). We hypothesized that TJ-014 could be a promising therapeutic drug for ROS-induced ototoxicity. In this study, we examined whether TJ-014 could protect hair cells from gentamicin-induced damage using organ of Corti explants. The organ of Corti, a specialized sensory epithelium in the cochlea, develops from hair cells and

supporting cells along the cochlear duct floor (Kelley, 2007). The cochlea, along with the vestibular organs (otoliths and canals), forms the inner ear, and the hair cells in these organs share similar structures and functions, both being vulnerable to ROS-induced ototoxicity (Selimoglu, 2007). The organ of Corti from rats can be readily dissected and cultured, as established in previous methods (Van De Water and Ruben, 1974; Sobkowicz *et al.*, 1993), making it suitable for evaluating the therapeutic effects on ROS-induced ototoxicity in inner ear hair cells. Aminoglycosides (AGs), including gentamicin (GM), are widely prescribed antibiotics, but their ototoxicity is well known and irreversible (Rizzi and Hirose, 2007). The generation of reactive oxygen species (ROS) is one of the earliest events in AG ototoxicity, playing a key role in hair cell death by activating transcription factors such as c-Jun and p53 (Sugahara *et al.*, 2006; Choung *et al.*, 2009; Tabuchi *et al.*, 2011). Thus, we employed rodents with GM-induced inner ear damage as a widely used model for ROS-induced inner ear damage (Takumida *et al.*, 1999b; Fetoni *et al.*, 2003b; L. Poirrier *et al.*, 2010). In evaluating the protective effects on inner ear hair cells, we assessed hair cell (HC) counts, oxidative stress and apoptotic pathways by immunohistochemistry for cleaved caspase-3, 8-hydroxy-2'-deoxyguanosine (8-OHdG), and mitochondrion-selective probes.

Ultimately, this work aims to both design a groundbreaking training protocol based on a comprehensive understanding of the neurological mechanisms that cause and resolve spatial disorientation, and contribute to the development of practical pharmacotherapies for inner ear damage that potentially evokes spatial disorientation.

1.3 Structure of this thesis

This thesis is composed of five chapters, based on research conducted through my collaborative efforts at Chubu University (Tadokoro *et al.*, 2024), detailed in Chapter 3, and at National Defense Medical College (Niwa *et al.*, 2016), detailed in Chapter 4.

Chapter 1 provides an introduction, outlining the background, purposes, and structure of this thesis. It also highlights vestibular limitations and proposes measures to address them.

Chapter 2 describes the subjects, materials, experimental apparatus, and methods used in the two types of animal experiments, as well as the newly implemented computational model, to validate the measures proposed in Chapter 1.

Chapter 3 reports on the evaluation of visual-vestibular neural training designed in this study to resolve tilt-translation ambiguity. It examines whether the somatogravic illusion caused by this ambiguity occurs in goldfish and whether such effects can be overcome via training that integrates visual and vestibular stimuli, using goldfish VOR as an indicator of motion estimation. This chapter also reports the simulation results of goldfish VOR using a newly proposed Kalman filter model, developed in collaboration with Mr. Yusuke Shinji and Prof. Yutaka Hirata. The model simulates the process of integrating multisensory information from the semicircular canals, otoliths, and retina to estimate self-motion and generate reflexive eye movements to stabilize vision. Based on the simulation results, this chapter discusses the underlying neural mechanisms behind the goldfish VOR.

Chapter 4 investigates the protective effects of Hangesha-shin-to (TJ-014) against GM-induced inner ear hair cell loss. It highlights TJ-014's ability to mitigate hair cell damage by suppressing oxidative stress.

Chapter 5 concludes the thesis by summarizing the findings and their practical implications for preventing spatial disorientation. This chapter discusses the integration of central training (visual-vestibular neural training) with peripheral protection strategies, offering recommendations for future research directions and potential applications in high-risk environments, such as aviation and space exploration.

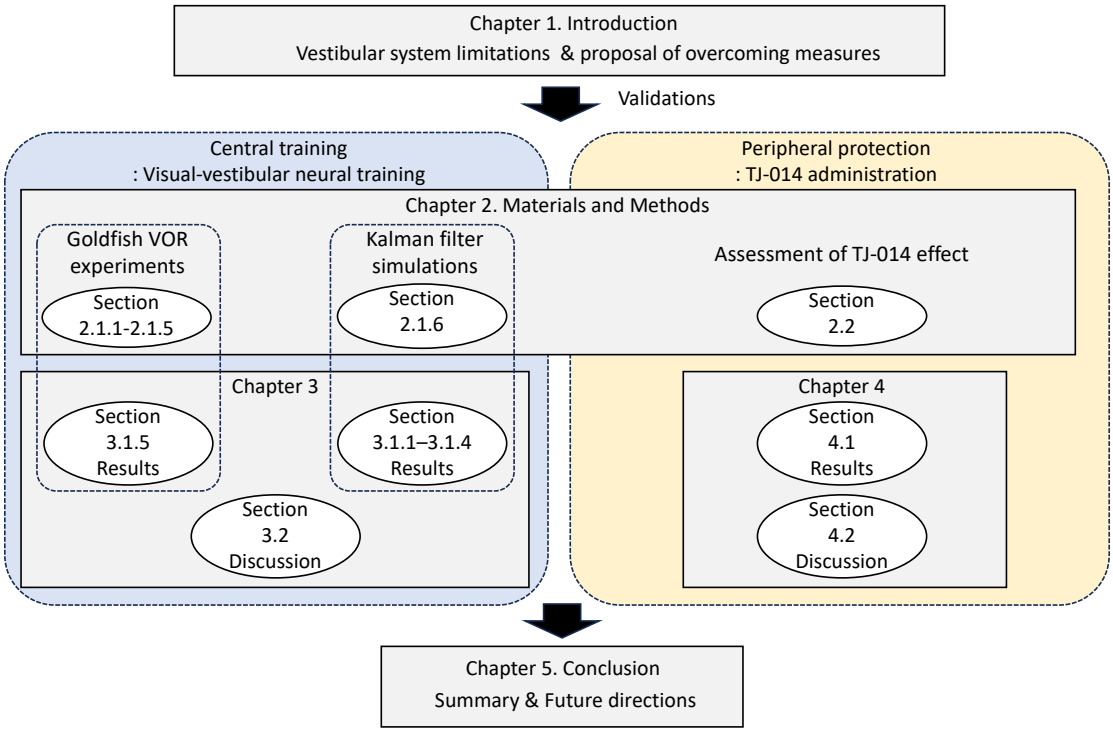


Figure 1.1. Structure of this thesis.

2 Materials and Methods

2.1 Visual-Vestibular Neural Training to Resolve Tilt-Translation Ambiguity in Goldfish

2.1.1 Subjects

Goldfish (*Carassius auratus*) of both sexes, 10–15 cm long, were obtained from an authorized supplier (Maru-u, Japan). Thirteen goldfish were used in this study. They were maintained in a separated home aquarium at 25 °C on a 12 h light/dark cycle and the water quality was monitored biweekly. Their spindle-shaped bodies, which may have prevented naïve goldfish from accumulating linear acceleration along the interaural axis, were also advantageous for our investigation to compare their behavior before and after exposure to linear acceleration.

Procedures for animal preparation were adopted from those previously described (Pastor *et al.*, 1994; Marsh and Baker, 1997; Aksay *et al.*, 2000; Debowy and Baker, 2011; Miki *et al.*, 2018), and are detailed in the following subsubsections. All relevant guidelines were followed for the use and care of animals in this study, and the Animal Welfare Committee of Chubu University approved all experimental and surgical procedures (Approval ID: 202210010).

2.1.2 Surgical procedures

The goldfish were anesthetized by immersion in a solution 1:20.000 wt/vol of MS222 (tricaine methanesulfonate, A5040; Sigma-Aldrich, USA). A headpost set up with two screws and a pedestal of dental acrylic cemented to self-tapping screws was fastened to the frontal bones to provide head stabilization during the experiments (Pastor *et al.*, 1994).

2.1.3 Experimental setup

Water tank

A keyhole-shaped aquarium was designed for the experiments (Figure 2.1C). It comprised clear and transparent plexiglass to effectively transmit external visual stimuli.

The cylindrical part of the tank was designed to ensure that, when the fish was in the center of the tank, the angle between the eyes of the goldfish and the tank wall remained consistently perpendicular. This design maintained a 0-degree angle of incidence for the light reaching the goldfish's eyes, thereby preventing excessive refraction. Had the forward wall of the tank been planar, even if transparent, beyond the critical angle (49° for water and air), visual stimuli on the display would not reach the goldfish's eyes. This would result in undesirable visual stimulation, as the image within the tank would reflect like a mirror. Hence, it was necessary for the tank to be cylindrical. Using an endoscope, we confirmed that the display from outside the tank does not appear distorted from the center of the cylinder. Goldfish were comfortably fixed using a headpost at the center of the cylindrical part of the aquarium. The centers of the bilateral semicircular canals were carefully positioned at the center of the cylinder. Aerated water at 25 °C was filled in the sealed aquarium and circulated to appropriately maintain the animals throughout the experiment.

Vestibular and visual stimulation

Stimulus coordination

The definition of 3D axes in the animals' head coordination, corresponding to vestibular and visual stimulus coordination (as our animals' heads were restrained in a water tank that was securely fixed on the visual-vestibular stimulation apparatus) used in the current study, is illustrated in Figure 2.1A. Arrowheads indicate positive directions for both linear and rotational motions. The rotational axes of the eyes were parallel to those of the head (Figure 2.1A, right panel). Yaw and roll-tilt head rotations occur around the z- and x-axes, respectively, which typically induce horizontal and vertical VOR in goldfish, respectively. Positive horizontal (measured in the left eye) and vertical (measured in the right eye) movements were rightward and downward, respectively (see "***Eye movement recording***" in this subsubsection).

Vestibular stimulation

A custom-made tilt-rotation platform consisting of a rotation table connected to a DC motor (tilt motor) via a timing belt (Figure 2.1B, C, D) was used to generate the roll-tilt vestibular stimulation. The aquarium was securely attached to the rotation table, such that

the anteroposterior axis (x-axis) of the goldfish was aligned with the rotation axis of the device. The entire tilt-rotation platform was fixed on a slider-type actuator (Slider, EZSHM6H080AZMC; Oriental Motor, Japan) driven by a stepping motor (Translation motor, AZM66MC; Oriental Motor, Japan) such that its rotation axis was orthogonal to the direction of the slider motion (Figure 2.1C, D). The commands to drive the tilt and translation motors were generated using Spike2 software (Cambridge Electronic Design, UK) and provided via the Power1401 interface. A potentiometer (CP-45H; Midori Precision, Japan) attached to the tilt-rotation axis was used to measure the tilt angle of the rotation table. An acceleration sensor (KXR94-2050; Akizuki Denshi Tsusho, Japan) installed on the rotation table measured the GIA component along the interaural axis (y-axis) of the fish.

Visual stimulation

The optokinetic stimulus (OKS) was presented on a 13.3-inch liquid-crystal display monitor with a refresh rate of 60 Hz (KNH133-133-ZH; Shenzhen Kenuohua Electronics, China) fixed on a slider and positioned 70 mm in front the center of the cylindrical section of the aquarium (Figure 2.1C). The monitor covered approximately 129° of the animal's visual field. The center of the cylinder corresponded to the location of the animal's semicircular canals and was close to the eyes. The OKS was created using the Unity game engine (Unity Technologies, USA). The OKS velocity command was generated using LabVIEW software (National Instruments, USA) and transferred to Unity via Transmission Control Protocol/Internet Protocol communication to move the vertical black-and-white stripes. OKS moved sinusoidally in synchrony with the translational vestibular stimulation at the same frequency (0.5 Hz), with a maximum amplitude of 38°/s. For example, the OKS moves rightward during the leftward movement of the slider. Presented on a flat display aligned parallel to the y-axis, the OKS physically traversed along the y-axis, manifesting its motion as a linear velocity; hence, no visual motion was observed along the x-axis. The angular velocity at 38°/s, which is the maximum amplitude of the OKS velocity, is equivalent to 0.055 m/s as a linear velocity along the y-axis at the direct front of the goldfish on the display.This visual scene was intended to convey to the goldfish the direction of its actual physical self-motion during translational motion. While considerably slower in comparison to the maximum linear velocity of translational

motion (0.64 m/s, as detailed in section 2.1.4), this deliberate speed adjustment was implemented due to concerns that an excessively rapid OKS might be imperceptible to the goldfish. Additionally, the choice was influenced by the limitation of the liquid-crystal display monitor with a refresh rate of 60 Hz, which may not smoothly render the OKS. Due to the possibility of independent software (Spike2 and LABVIEW) potentially generating stimulation signals slightly out of phase, we synchronized OKS motion with vestibular stimulation by having the LabVIEW software receive a copy of commands for the vestibular apparatus (tilt motor or translation motor) from Spike2 via a USB-6009 data acquisition (DAQ) device (National Instruments). For the experiments conducted in the dark (section 2.1.4), the OKS display was turned off to obtain complete darkness.

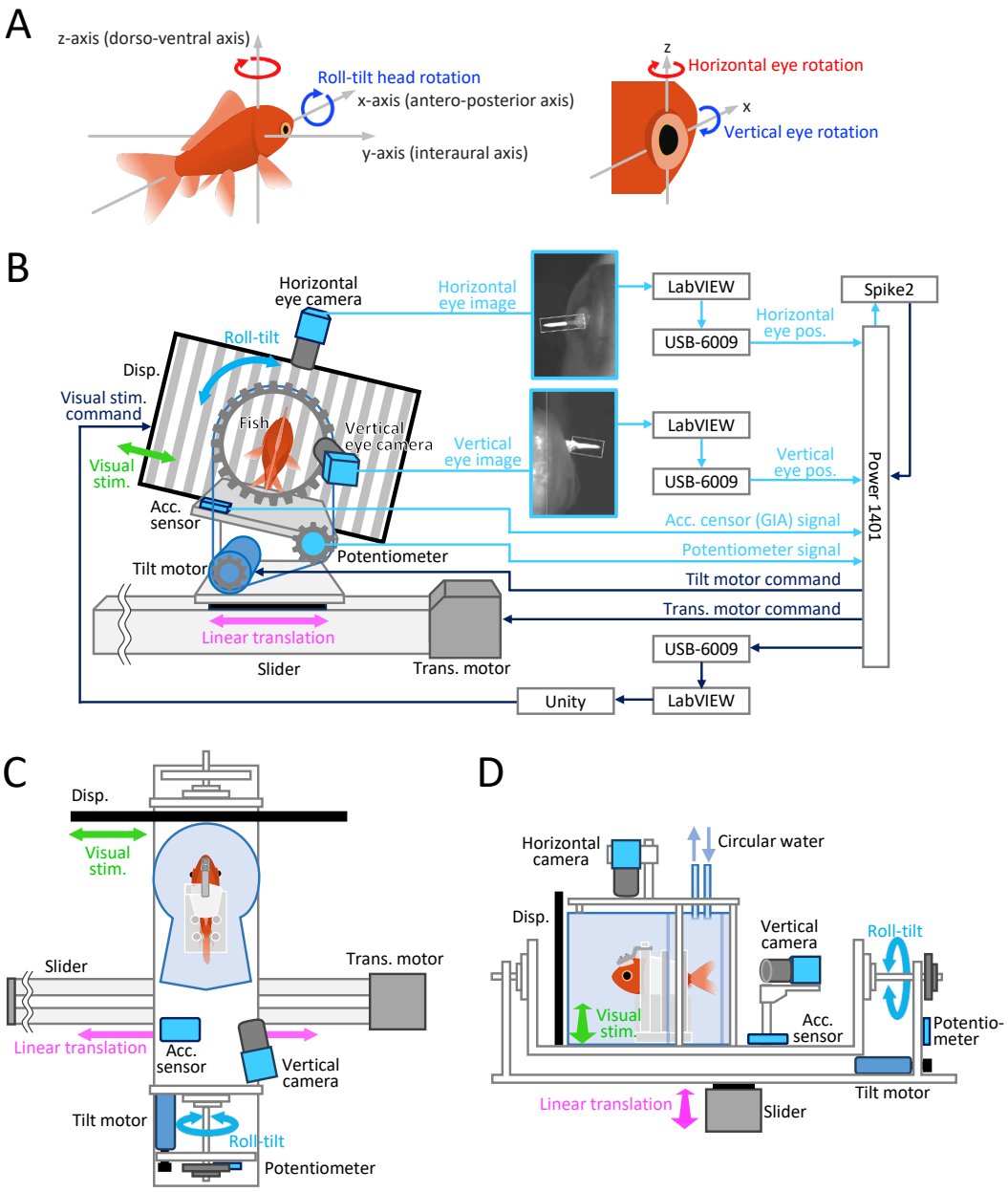


Figure 2.1. (A) Definition of 3D axes in the animals' head coordination. Positive directions are indicated by arrow heads for both linear and rotational motion. To clarify, yaw and roll-tilt rotations are those around z and x-axis, respectively, which typically induce horizontal and vertical VOR, respectively. Positive directions of yaw (horizontal) and roll (vertical) rotations are clockwise, i.e., rightward in both eyes and downward in the right eye, respectively. (B), (C), and (D) Experimental setup. (B) Rear view of the system (left) and its configuration diagram (right). The aquarium is removed in this view.

Note, visual stimulus and linear translation were not given during actual roll-tilt test paradigm. (C) Top view. Horizontal eye camera is removed in this view. (D) Left side view. Disp.: display; stim.: stimulus; Acc.: acceleration; Trans.: translation; pos.: position.

Eye movement recording

The rotational axes of the eye used in this study are parallel to those of the head. Horizontal and vertical eye movements are rotations around the z- and x-axes, respectively, passing through the eye's center of rotation (Figure 2.1A). Vertical VOR eye movements are induced by head rotation around the x-axis in lateral-eyed animals such as goldfish, whereas the same vestibular stimulation induces torsional VOR in front-eyed animals such as primates. Horizontal and vertical eye movements were extracted from video images acquired at 601 fps using two CMOS cameras (DMK33UX273; Imaging Source, Germany) equipped with infrared filters (IR-86; Fujifilm Corporation, Japan). The eyes were illuminated using an infrared light source (AE-LED56; Akizuki Denshi Tsusho, Japan) to capture clear images (Figure 2.1B). The camera to measure horizontal eye movements was placed atop the aquarium to capture the left eye, whereas the camera to measure vertical eye movements was placed behind the aquarium at a slightly oblique position (10° to the right) to capture the right eye. This inclination ensured an unobstructed view of the goldfish eye movements from the rear (Figure 2.1C). It has been demonstrated and reconfirmed that goldfish binocular eye movements are conjugated during VOR and that their eye velocity traces are identical (Pastor *et al.*, 1994). Positive horizontal (left eye) and vertical (right eye) eye movements occurred in the rightward and downward directions, respectively (Figure 2.1A).

To accurately measure the eye rotation angles, a small cone-shaped marker, coated with thermoplastic containing titanium dioxide, was attached to each eye. It was affixed to a peripheral part of the cornea outside the edge of the pupil (Figure 2.1B) using a cyanoacrylate adhesive after the administration of surface anesthesia using lidocaine, just before the goldfish was placed in the aquarium.

The images acquired from the two cameras were individually sent to two different personal computers (PCs) via USB 3.0, and the eye positions (rotation angles) were measured at 200 Hz using custom-made software developed using the LabVIEW Vision

Toolkit (National Instruments). The zero eye position (0°) was set to the null eye position, where the eyes asymptotically drift back after spontaneous saccades in the dark (Straube *et al.*, 1991; Kaneko, 1997; Beck *et al.*, 2004; Major *et al.*, 2004). Corrections for the vertical eye position obtained from a 10° oblique camera were applied to the data (see Supplementary Methods section S2.1.1). A potentially slight tilt of the horizontal eye camera away from the z-axis can detect an erroneous horizontal component arising from purely vertical eye movements. Corrections for the horizontal eye position data are also provided (see Supplementary Methods sections S2.1.2 and S2.1.3).

Horizontal and vertical eye position data extracted from the separate PCs were converted to voltage signals via the respective DAQ device (USB-6009 interface) connected to the respective PCs and transferred to Power1401 to record them in synchrony with other sensor data at a sampling frequency of 1000 Hz in 16-bits in the Spike2 program (Figure 2.1B).

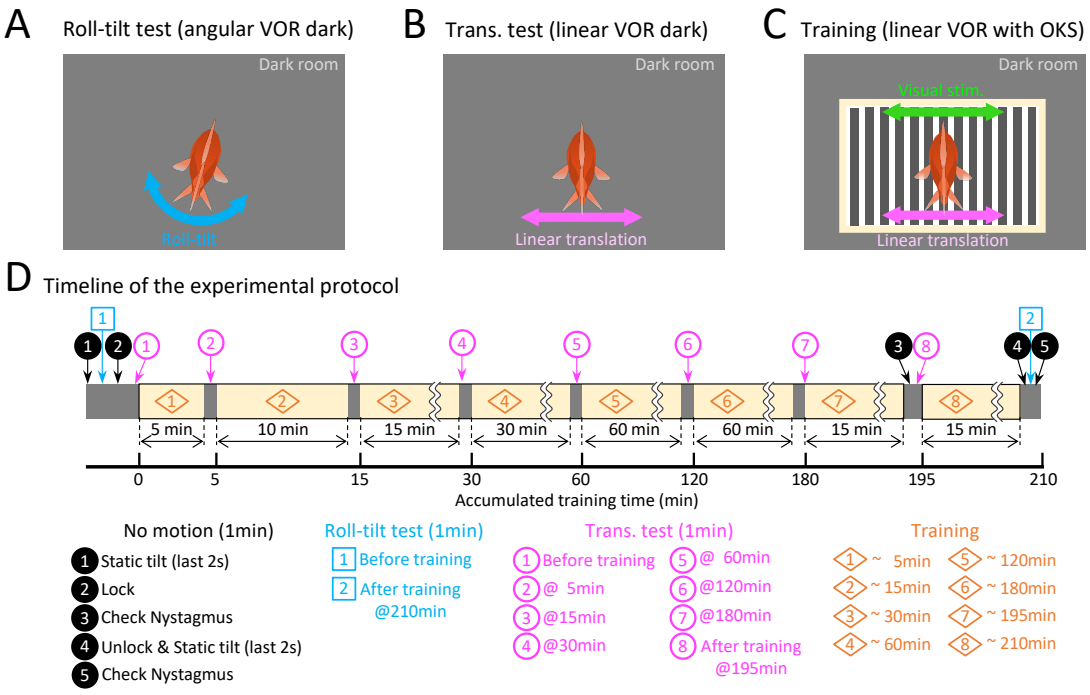


Figure 2.2. Experimental paradigm. (A), (B), and (C) are graphical explanations of the roll-tilt test (angular VOR in the dark), translation test (linear VOR in the dark), and training (linear VOR along with OKS), respectively. (D) Schematic overview of the timeline of the experimental protocol. The times in the titles of each paradigm of translation test and training are the accumulated times of training experienced up to that point, which differs from the overall elapsed time because of the test segments inserted before and during training. Trans.: translation.

2.1.4 Experimental paradigms

All animals were subjected to identical experimental paradigms, as summarized in Figure 2.2D. After preparing for recording, the animals were acclimated to the apparatus for 60 min before the experimental intervention. The total measurement time per animal was 225 min (210 min for training, 8 min for the translation test, 2 min for the roll-tilt test, and 5 min for no motion). The swimming behavior of all animals was carefully inspected for at least 30 min after the experiment to confirm their normal behavior.

Before training, 1 min of eye movement observation (no motion) was conducted in the dark without any stimulation to confirm the absence of abnormal eye movements, such as nystagmus. During the last 2 s of "no motion," the initial tilt position was gradually shifted to 12.7° in a clockwise manner to provide symmetrical tilt-rotation stimulation about the earth's vertical axis (z-axis). From this initial position, a roll-tilt rotational stimulus was applied for 1 min in the dark to evaluate the roll-tilt VOR in the animal's naïve state (Figure 2.2A, D, Roll-tilt test). The angular velocity of the roll-tilt stimulation was a sinusoid at 0.5 Hz, with maximum speed and acceleration of 40 °/s and 0.22 G, respectively. Subsequently, another "no motion" period was allowed for 1 min, during which the tilt-rotation table was locked to the slider to prevent unintended rotation during the subsequent translation stimulations. A linear translational stimulus was then applied in the dark for 1 min to evaluate the translational VOR in the naïve state (Figure 2.2B, D, Translation test, magenta circled number 1). The velocity of the translation stimulation was sinusoid at 0.5 Hz; with a maximum linear speed and acceleration of 0.64 m/s and 0.2 G, respectively.

Then, the training and test paradigms were conducted for a total of 218 min (Figure 2.2C, D, Training). During the training period, the same linear translational stimulus as that in the Translation test was provided with the OKS, which moved synchronously with the translation velocity (see "Visual stimulation" in section 2.1.3). Seven translation tests, each lasting 1 min, were performed during the training and test paradigms at 5, 15, 30, 60, 120, 180, and 195 min (Figure 2.2D, magenta circled numbers 2–8). The no motion period was imposed before the final translation test (Figure 2.2D, magenta number 8) to observe the eye movements immediately after training. After completing all the training

periods, the rotation table was unlocked during another 1-min “no motion” observation, followed by roll-tilt testing to evaluate the roll-tilt VOR after training (Figure 2.2A, D, Roll-tilt test). Finally, “no motion” observations were conducted in the dark to confirm the absence of abnormal eye movements.

Because this study focuses on exploring the potential selective adaptability of the otolith-ocular system and the motion estimation system, particularly focusing on their ability to achieve visually guided reinterpretation of translation and tilt, we selected 0.5 Hz as the frequency of sinusoidal stimuli. In primates, translational head motion along the y-axis induces a gradual shift in the VOR axis from torsional to horizontal in the intermediate-frequency range of approximately 0.1–1 Hz (Paige and Seidman, 1999; Merfeld *et al.*, 2005a). During translational head motion along the y-axis at low frequencies (< 1/7 Hz) in goldfish, a vertical VOR was observed around the x-axis (Takabayashi *et al.*, 2003). Therefore, we concluded that a frequency of 0.5 Hz was appropriate for our sinusoidal stimuli, as it is within the intermediate frequency range where the shift in the VOR axis can be observed. Notably, this frequency aligns with the frequency used in a previous translational cross-axis VOR adaptation study (Wei and Angelaki, 2001), which aimed to evaluate the adaptive changes in motion interpretation during translation (see section 3.2.1).

2.1.5 Data analysis

All the data recorded at a sampling rate of 1000 Hz were anti-aliased using an 11-point moving average filter with a cut-off frequency of 40.27 Hz and then resampled at 100 Hz for offline analysis. After downsampling, the high-frequency noise components in the vestibular stimuli were eliminated by applying a 21-point moving average filter twice with a cut-off frequency of 2.11 Hz. Similarly, the high-frequency noise components in the eye movement recordings were eliminated by applying an 11-point moving average filter twice, with a cut-off frequency of 4.03 Hz.

Calculation of linear velocity, tilt angular velocity, and equivalent GIA angular velocity

From the recorded vestibular stimulus data (linear acceleration along the y-axis and roll-tilt rotational angle around the x-axis), linear velocity, tilt angular velocity, and the velocity of GIA vector rotation (GIA angular velocity) were calculated as follows:

Linear velocity during linear translation was calculated by integrating the y-axis data of the acceleration sensor using the MATLAB (MathWorks, USA) 'cumtrapz' function (Figures 3.1 and 3.2). The tilt angular velocity was calculated by differentiating the potentiometer angle data using a 3-point low-pass differentiation filter (Figure 3.3). To obtain GIA angular velocity, we first calculated the rotational angle of the GIA vector relative to the earth's vertical axis (z-axis), which rotates around the goldfish's antero-posterior axis (x-axis) using the arctangent of acceleration as $\theta_{\mathrm{GIA}} = \tan^{-1}(\mathrm{Acc.\,Sensor\ Value})$ during translational motion following Lichtenberg (1982) and arcsine of acceleration as $\theta_{\mathrm{GIA}} = \sin^{-1}(\mathrm{Acc.\,Sensor\ Value})$ during the roll-tilt motion (see Supplementary Methods section S2.2). The GIA angular velocity was obtained by differentiating the rotational angle of the GIA vector using a 3-point low-pass differentiation (Figures 3.1–3.3). High-frequency noise components amplified by differentiation processing in the vestibular stimuli were eliminated again by applying a 21-point moving average filter twice, with a cut-off frequency of 2.11 Hz. For the GIA angular velocity, the counterclockwise direction was defined as positive to better illustrate its relationship with the tilt angular velocity. The GIA angular velocity was presented to show that translational acceleration stimulation (Figures 3.1 and 3.2) and roll-tilt stimulation (Figure 3.3), which are currently used, generated almost identical stimulation to that of otoliths.

Eye velocity evaluation

Horizontal and vertical eye velocities were obtained by differentiating the eye position data using a 3-point low-pass differentiation. High-frequency noise components amplified by the differentiation processing of eye velocities were eliminated by applying an 11-point moving average filter twice with a cutoff frequency of 4.03 Hz. To evaluate the VOR, saccades and high-frequency noise, if present, were eliminated from the horizontal and vertical eye position data by applying a custom-made automatic

desaccading algorithm. The eliminated portions of the data were excluded from further analyses. The eye velocity traces from all individual animals were time-aligned and averaged throughout the experiment, as they all underwent identical experimental sequences. Notably, because of desaccade processing, the averaging processing at each time point was not always by the same number of samples, especially immediately after sudden vestibular or visual stimulation following the no-motion period, where eye velocity tended to be unstable due to startle-like responses.

For quantitative evaluation, individual eye velocity data were averaged over stimulus cycles for the entire 1-min test period and for the last 5 min of the training periods. Sinusoidal curve fits were performed to obtain estimates of amplitude and phase from these individually averaged VOR eye velocity data by using the MATLAB 'fittype' function where frequency was fixed to 0.5 Hz (stimulus frequency). The individually averaged eye velocity data and estimated amplitudes were averaged across all individuals. The amplitudes of the horizontal eye velocity during the roll-tilt test and first translation test paradigms were not well approximated because of their minimal and unstable horizontal eye movement. This lack of stability may have been influenced by both the small magnitude of these eye velocities and startle-like responses following sudden vestibular stimulation after the "no motion" period.

Differences in the estimated eye velocity amplitudes between the first and last paradigms of the translation test, roll-tilt test, and training were evaluated using the Wilcoxon rank-sum test, along with individually estimated eye velocity amplitudes.

2.1.6 Implementation of the computational model for motion estimation and eye movements

Laurens and Angelaki (2017) used the framework of the Kalman filter, a widely used mathematical technique for implementing statistically optimal dynamic estimation, which continuously updates self-motion estimates and computes sensory prediction errors. We employed their model of spatial orientation formation to interpret our results. This model was designed to treat both active and passive head movements as inputs, with process noise incorporated into the input. The role of process noise is discussed in detail in section 3.2.2. We then revised the model to simulate VORs in response to translation and tilt head

motion in goldfish (lateral-eyed animals) based on estimates of 3D head motion and visual stimulation (OKS) states. Moreover, we introduced the estimated state of gravity ($\widehat{\boldsymbol{G}}$) from the previous time step, obtained using the Kalman filter, into the Kalman gain matrix. This enabled us to describe the calculation of state estimates realistically, addressing the issue posed by Laurens' model regarding the calculation of state estimates using the real state of gravity acceleration ($\boldsymbol{G}$), which the brain cannot inherently perceive. Notably, this modification simultaneously rendered our model nonlinear. The validity of this nonlinearity will be discussed in section 3.2.2. In the revised model, the states to be estimated by the Kalman filter algorithm are head linear acceleration $\boldsymbol{A}$, head linear velocity $\boldsymbol{B}$, head rotation velocity $\boldsymbol{\Omega}$, gravitational acceleration $\boldsymbol{G}$, eye rotation velocity $\boldsymbol{P}$, visual rotation velocity $\boldsymbol{\Phi}$, and semicircular canals endolymph rotation velocity $\boldsymbol{C}$ (all 3D vectors are summarized in Tables 2.1 and 2.2). For the sensors, the model incorporated semicircular canals, otoliths, and the retina, similar to the Laurens and Angelaki (2017) model. We assumed that, when animals looked forward (see section 3.2.3), the reflexive eye velocity around each axis was generated in the opposite direction to the head rotation velocity and head linear velocity states and in the same direction as the visual rotation state, according to the following equations:

$$P_x^u(t) = h\left(\widehat{\Phi}_x(t) - \widehat{\Omega}_x(t)\right) \tag{2.1}$$

$$P_y^u(t) = h\left(\widehat{\Phi}_y(t) - \widehat{\Omega}_y(t) + r\hat{B}_z(t)\right) \tag{2.2}$$

$$P_z^u(t) = h\left(\widehat{\Phi}_z(t) - \widehat{\Omega}_z(t) - r\hat{B}_y(t)\right) \tag{2.3}$$

where $P_x^u(t)$, $P_y^u(t)$, and $P_z^u(t)$ represent the eye motor command $\boldsymbol{P}^u$ around the x-, y-, and z-axes, respectively, as defined in Figure 2.1A. The coefficient h was set to 0.8 based on the rotational VOR gain of goldfish as reported in Pastor (Pastor *et al.*, 1992; Pastor *et al.*, 1994). The coefficient r was determined to be 4 to replicate the translational VOR experiment presented in this paper. The state estimate is represented using the hat operator, which is computed via the Kalman filter. The sign of the vertical eye motor command $P_x^u(t)$ (i.e., up and downward) switches for each eye in lateral-eyed animals. Equation

(2.1) applies to the right eye, as observed in this study. The structure of the model is depicted in Figure 2.3, and a detailed description of the model and the mathematical equations used are provided in the Supplementary Methods section S2.3.

The following simulations were conducted to confirm the validity of the model and evaluate the 3D VOR induced as well as 3D head motion states estimated by the Kalman filter: angular VOR in the dark induced by the angular velocity stimuli of sinusoidal waves (frequency: 0.5 Hz, amplitude: 38°/s) around each axis, optokinetic response (OKR) induced by visual stimuli of sinusoidal wave (frequency: 0.5 Hz, amplitude: 38°/s), and optokinetic response after nystagmus (OKAN) around the z-axis after the visual stimuli is turned off. Subsequently, using the same set of model parameters as those used for model validation, we simulated the following: 1) translational VOR induced by the translational acceleration stimuli of sinusoidal waves (frequency: 0.5 Hz, amplitude: 0.2 G) along the y-axis, 2) visual-translational VOR induced by visual stimuli of sinusoidal wave (frequency: 0.5 Hz, amplitude: 38°/s) around the z-axis and translational acceleration stimuli of the sinusoidal wave (frequency: 0.5 Hz, amplitude: 0.2 G) along the y-axis, 3) angular VOR induced by the angular velocity stimuli of sinusoidal wave (frequency: 0.5 Hz, amplitude: 38°/s) around the x-axis. Furthermore, to express the animal's increased experience in translation acceleration, we increased the standard deviation (SD) of linear head acceleration input along the y-axis (Table 2.2, σ_y^A) from 0.001 G before training to 0.180 G after training, whereas other parameters were unchanged.

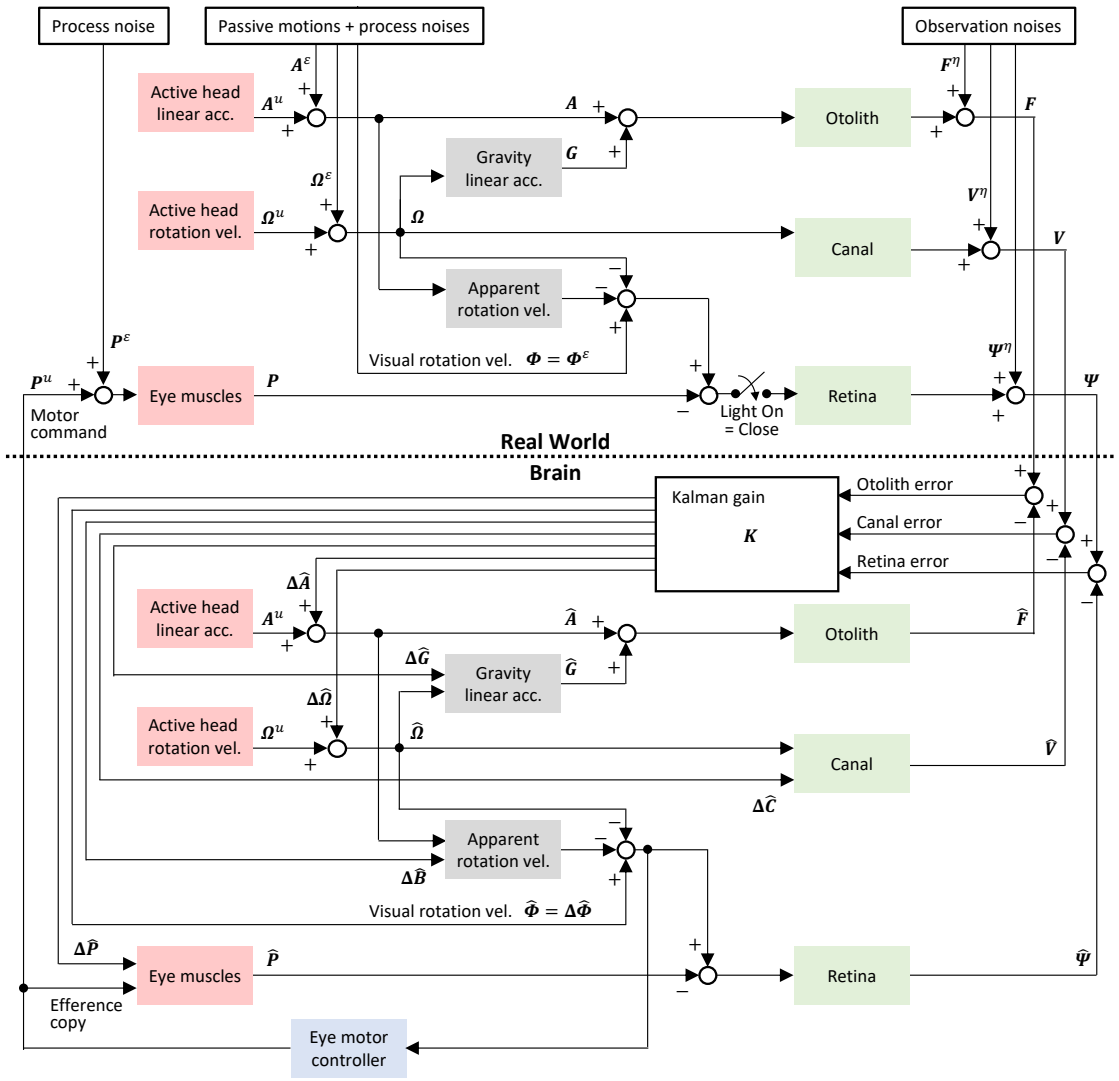


Figure 2.3. Modified Kalman filter model, where each variable and coefficient is defined in Table 2.1. The eye motor control model, retina model, apparent rotation velocity model, and Eye motor controller were added to the Kalman filter model in Laurens and Angelaki (2017) to explain our results of VOR. The apparent rotational velocity model outputs the visual rotational velocity around the head caused by linear acceleration, which is used to linear VOR in the Eye motor controller (Equations (2.1), (2.2), (2.3)). To assist in the interpretation of our experiments, particularly with the interpretation of eye movements, passive motion and process noise, we have also described a world system outside the brain that was not specified in the Kalman filter model by Laurens and Angelaki (2017). vel.: velocity; acc.: acceleration.

Table 2.1. Variables in the Kalman filter model

Motion variables	
$\boldsymbol{A}$	Head linear acceleration
$\boldsymbol{\Omega}$	Head rotation velocity
$\boldsymbol{G}$	Gravity acceleration
$\boldsymbol{B}$	Head linear velocity
$\boldsymbol{P}$	Eye rotation velocity
$\boldsymbol{C}$	Semicircular canals endolymph rotation velocity
$\boldsymbol{\Phi}$	Visual rotation velocity
Sensory variables	
$\boldsymbol{F}$	Otolith signal
$\boldsymbol{V}$	Semicircular canal signal
$\boldsymbol{\Psi}$	Retina signal
Input variables & noises	
$\boldsymbol{A}^{u}$	Active motion of head linear acceleration
$\boldsymbol{\Omega}^{u}$	Active motion of head rotation velocity
$\boldsymbol{P}^{u}$	Eye motor command
$\boldsymbol{A}^{\varepsilon}$	Process noises + passive stimuli of head linear acceleration
$\boldsymbol{\Omega}^{\varepsilon}$	Process noises + passive stimuli of head rotation velocity
$\boldsymbol{\Phi}^{\varepsilon}$	Process noises + passive stimuli of visual rotation velocity
$\boldsymbol{P}^{\varepsilon}$	Process noise of eye motor command
$\boldsymbol{F}^{\eta}$	Observation noise of otolith signal
$\boldsymbol{V}^{\eta}$	Observation noise of semicircular canal signal
$\boldsymbol{\Psi}^{\eta}$	Observation noise of retina signal
Feedback signals & gain	
$\boldsymbol{\Delta\widehat{A}}$	Feedback signal to correct estimation of head linear acceleration
$\boldsymbol{\Delta\widehat{G}}$	Feedback signal to correct estimation of gravity acceleration
$\boldsymbol{\Delta\widehat{\Omega}}$	Feedback signal to correct estimation of head rotation velocity
$\boldsymbol{\Delta\widehat{B}}$	Feedback signal to correct estimation of head linear acceleration
$\boldsymbol{\Delta\widehat{P}}$	Feedback signal to correct estimation of eye velocity
$\boldsymbol{\Delta\widehat{C}}$	Feedback signal to correct estimation of semicircular canal dynamics
$\boldsymbol{K}$	Kalman gain

Table 2.2. Simulation parameters in the Kalman filter model

	Variables	Values
Δt	simulation time step	0.002 s
τ_C	canal dynamics time const	0.5 s
τ_m	muscle dynamics time const	0.003 s
r	reciprocal of viewing point length	4
h	Eye control gain	0.8
Standard deviation (SD) of noises & passive signals		
σ^{Ω}	Head rotation velocity SD of process noises + passive stimuli	40 °/s
σ_x^A	Head linear acceleration SD of process noises + passive stimuli along x-axis	0.001 G
σ_y^A	Head linear acceleration SD of process noises + passive stimuli along y-axis	0.001 G or 0.180 G
σ_z^A	Head linear acceleration SD of process noises + passive stimuli along z-axis	0.001 G
σ^{Φ}	Visual rotation velocity SD of process noises + passive stimuli	1 °/s
σ^P	Eye velocity process noise SD	3 °/s
σ^V	Canal observation noise SD	3 °/s
σ^F	Otolith observation noise SD	0.02 G
σ^{Ψ}	Retinal slip observation noise SD	30 °/s

2.2 TJ-014 effect in ROS-induced inner ear hair cell loss

2.2.1 Subjects

The pregnant Sprague-Dawley rats (Japan SLC, Hamamatsu, Japan) used in this study were cared for at the Institute of Laboratory Animals of the National Defense Medical College. The Animal Research Committee of the National Defense Medical College approved all experimental protocols, which were performed in accordance with the National Institutes of Health Guidelines for the Care and Use of Laboratory Animals (Approval ID: 12096).

2.2.2 Hangesha-shin-to (TJ-014)

TJ-014 a dried powder extract prepared by Tsumura & Co. (Tokyo, Japan), manufactured from a mixture of *Pinellia tuber* (relative quantity = 5.0), *Scutellaria root* (2.5), *Glycyrrhiza* (2.5), *processed ginger* (2.5), *Ginseng* (2.5), *Jujube* (2.5), and *Coptis Rhizome* (1.0). TJ-014 (Lot number: 2100014010) was dissolved in the initial medium described below before use, with the extract yield being 24%. The quality variation among batches is minimized by using only Japanese pharmacopeias, and the specific amount of baicalin, glycyrrhizic acid, and berberine; the presence of the spots of active ingredients of the seven herbal components are ascertained in every batch. Detailed chemical profile of Hange-sha-shin-to extract is described in Japanese pharmacopeia 16th edition supplement I: 2508–2511 (http://www.pmda.go.jp/files/000152883.pdf). TJ-014 is ordinarily used for diarrhea, dyspepsia, gastritis, stomatitis, and psychoneurosis. Furthermore, we typically use TJ-014 for the management of chemotherapy-induced stomatitis. In fact, its efficacy is widely recognized (Kono, 2010).

TJ-014 solution was prepared prior to organ culture. Firstly, TJ-014 extract was dissolved into the initial medium described below to a 1 mg/mL concentration using a magnetic stirrer in a sterile environment at 37 ℃ for 1 h. Secondly, the TJ-014 solution was filtered by using a DISMIC®-13CP disposable syringe filter unit (Toyo Roshi, Tokyo, Japan) and gradually diluted to obtain 1, 10, or 100 μg/mL concentrations for the initial medium.

2.2.3 Cochlear explant culture

Postnatal day 3–5 (P3–5) rats were deeply anesthetized with isoflurane and decapitated. The basal turn of the organ of Corti was dissected within 10 min and cultured by following previously reported methods (Van De Water and Ruben, 1974; Sobkowicz *et al.*, 1993). Control explants were maintained in Dulbecco's Modified Eagle's Medium (DMEM) with 10% fetal bovine serum (FBS), 25 mM HEPES, and 30 U/mL penicillin, and were cultured in an incubator at 37 ℃ with 5% CO_2 and 95% humidity. GM explants were maintained in the above-described initial medium plus 50 μM of GM. TJ- 014 explants were maintained in the initial medium plus 50 μM of GM with 0, 1, 10, or 100 μg/mL of TJ-014. These five groups were cultured for up to 48 h. At least 10 cultures were used for each condition tested.

2.2.4 Cell counts and immunohistochemistry

At the end of the culturing procedures, the explants were fixed with 4% paraformaldehyde (PFA) in phosphate-buffered saline (PBS) for 20 min and permeabilized with 5% Triton X- 100 (Sigma, St. Louis, USA) in PBS with 10% FBS for 10 min. The specimens were stained with rhodamine phalloidin probe (1:100, rhodamine phalloidin, Invitrogen, Eugene, USA) at room temperature for 45 min. Phalloidin is a specific marker for cellular F-actin and labels the stereociliary arrays and cuticular plates of HCs.

Caspase-3 activation was detected using cleaved caspase-3 antibody (1:100, Cleaved Caspase-3 D175 Rabbit Antibody, Cell Signaling Technology, Beverly, USA). Specimens were then counterstained with Alexa 488 (1:200 Alexa Fluor® 488 Goat Anti-Rabbit IgG, Invitrogen).

To evaluate oxidative stress, we used anti-8-OHdG monoclonal antibody (1:10 JaICA, Hukuroi, Shizuoka, Japan). 8-OHdG is one of the predominant methods of inducing free radical DNA lesions and used as an indicator of free radical formation. Specimens were then counterstained with Alexa 488 (1:200 Alexa Fluor® 488 Goat Anti-Mouse IgG, Invitrogen). After rinsing in PBS, the cochlear explants were mounted on slides with an antifade mounting medium (VECTASHIELD with DAPI; Vector Laboratories, Burlingame, USA). DAPI labeling was used to identify condensed HC nuclei.

To evaluate the mitochondrial membrane potential, we used mitochondrion-selective probes (MitoTracker® Red CMXRos, Molecular Probes®, Eugene, USA) at a concentration of 200 nM and observed the mitochondrial membrane potential in live cells. After the cochlear explant culture procedure, these explants were washed three times in the initial medium and bathed in 200 nM MitoTracker® for 30 min. Subsequently, explants were washed three times in the initial medium and observed through a confocal microscope. All procedures to evaluate mitochondrial membrane potential were conducted in a chamber slide system coated with poly-L-lysine, which prevents explant removal during washing.

Before this procedure, we examined the lowest concentration of MitoTracker® Red CMXRos that produced low background fluorescence and clear optimal detection, because the probe itself is cytotoxic and must be used at as low of a concentration as possible.

Evaluation of the number of hair cells and caspase-3 immunostaining was conducted at the time point of 24 h and 48 h after the start of organ culture. However, the time points of the 8-OHdG immunostaining and MitoTracker® Red CMXRos staining are 12 h and 24 h because ROS induced by GM challenge generate within 1 hour after GM treatment (Choung *et al.*, 2009) and the signal of 8-OHdG could not be detected 48 h after the start of organ culture in all conditions. Additionally, MitoTracker® Red CMXRos signal also disappeared after 48 h after the start of organ culture in all conditions. So, evaluation of ROS and mitochondrial membrane potential was conducted at an earlier timing.

All fluorescent images were captured with a Nikon C2 confocal microscope (Nikon C2, Nikon Instruments Company, Tokyo, Japan).

2.2.5 Assessment of hair cell counts

Quantitative results were obtained by evaluating 30 outer hair cells (OHCs) associated with 10 inner hair cells (IHCs) in a given microscopic field. The average HC survival rate in three different parts from one organ of Corti was calculated and compared between groups. For minimizing bias, we selected three persons who did not know the slides groups counted OHCs.

2.2.6 Assessment of mitochondrial membrane potential

A collapse of the mitochondrial membrane potential, one of the causes of GM-induced HC apoptosis, was observed by using the MitoTracker® Red CMxRos selective mitochondrion probe. This probe is taken up only by mitochondria with normal membrane potentials. We compared the color tone density of OHCs using ImageJ 1.46r (Wayne Rasband, National Institutes of Health, Bethesda, USA). Parts of the nine OHCs, with three cells in each outer hair cell (OHC) row, were selected randomly in a given microscopic field and used for evaluation.

2.2.7 Data analysis

All data are expressed as the mean ± standard deviation. Comparisons of percentages of surviving OHCs and the density of MitoTracker® Red CMXRos were performed by a one-way analysis of variance (ANOVA) with Tukey's multiple comparison test using JMP® 10.0.0 (SAS Institute Inc., USA).

3 Visual-Vestibular Neural Training to resolve Tilt-Translation Ambiguity in Goldfish

3.1 Results

Among the 13 animals used in this study, one showed unstable eye movements and VOR adaptation and was therefore excluded from further data analyses and evaluation. First, we show the interaural (y-axis) translational VOR in the dark for the remaining 12 animals before training (section 3.1.1). We then show how translational VOR is altered by visual stimulation combined with head translation during training (section 3.1.2), followed by post-training translational VOR in the dark (section 3.1.3). We also demonstrate the tilt (around the anteroposterior x-axis) of the VOR tested before and after training (section 3.1.4). Finally, we present the simulation results of the Kalman filter model (section 3.1.5).

3.1.1 VOR during translation in dark in naïve animals

Figure 3.1A shows the horizontal (red) and vertical (blue) eye velocities averaged for all animals (n = 12) during translational acceleration stimulation in the dark before training (Figure 2.2D; magenta circle 1). Red and blue shadows indicate plus or minus one standard deviation. The top panel shows the linear velocity (along the y-axis) converted from acceleration stimulation (see section 2.1.5). The second panel from the top shows the tilt angular velocity, which is zero during this stimulation, and the GIA angular velocity calculated from the translational acceleration (see section 2.1.5), both around the x-axis. The GIA angular velocity revealed that stimulation during this paradigm and roll-tilt stimulation (shown in Figure 3.3) generated almost identical stimulation to that of the otoliths. Clearly, robust vertical VOR with an average amplitude of 12.5°/s was induced, whereas very small, if any, horizontal VOR was observed in naïve animals. In contrast to naïve goldfish, naïve primates have shown horizontal VOR around the z-axis during interaural translation (at 0.5 Hz) rather than around the x-axis (torsional VOR in the case of front-eyed animals) (Paige and Tomko, 1991; Angelaki *et al.*, 1999; Wei and Angelaki, 2001). The human VOR around the x-axis, which is similar to the results observed in our goldfish, was found at lower frequencies. Specifically, at frequencies of 1/200–1/40 Hz and 1/5–2/5 Hz, torsional VOR (equivalent to the vertical VOR in goldfish) around the

x-axis, rather than horizontal VOR, has been demonstrated during interaural translation in upright humans (Lichtenberg *et al.*, 1982; Seidman and Paige, 1996).

These results are confirmed in a cycle average format in the inset of Figure 3.1C (before training at 0 min), illustrating the horizontal (red) and vertical (blue) eye velocity traces averaged over the stimulus cycles (magenta). A slight phase lag (35.7°) in reference to the stimulus velocity was noted for the vertical VOR eye velocity. Similar to the present findings in goldfish, previous results on human torsional VOR eye velocity during interaural translation also demonstrated a phase delay from the sinusoidal GIA angular velocity. For instance, in humans, this phase lag reaches approximately 22.5° at 1/200 Hz and 48.6° at 1/5 Hz (Lichtenberg *et al.*, 1982; Seidman and Paige, 1996).

Before examining how these translational VORs in the dark change throughout the training process, we demonstrate the progression of the horizontal and vertical eye velocities during the training paradigm in the next subsubsection.

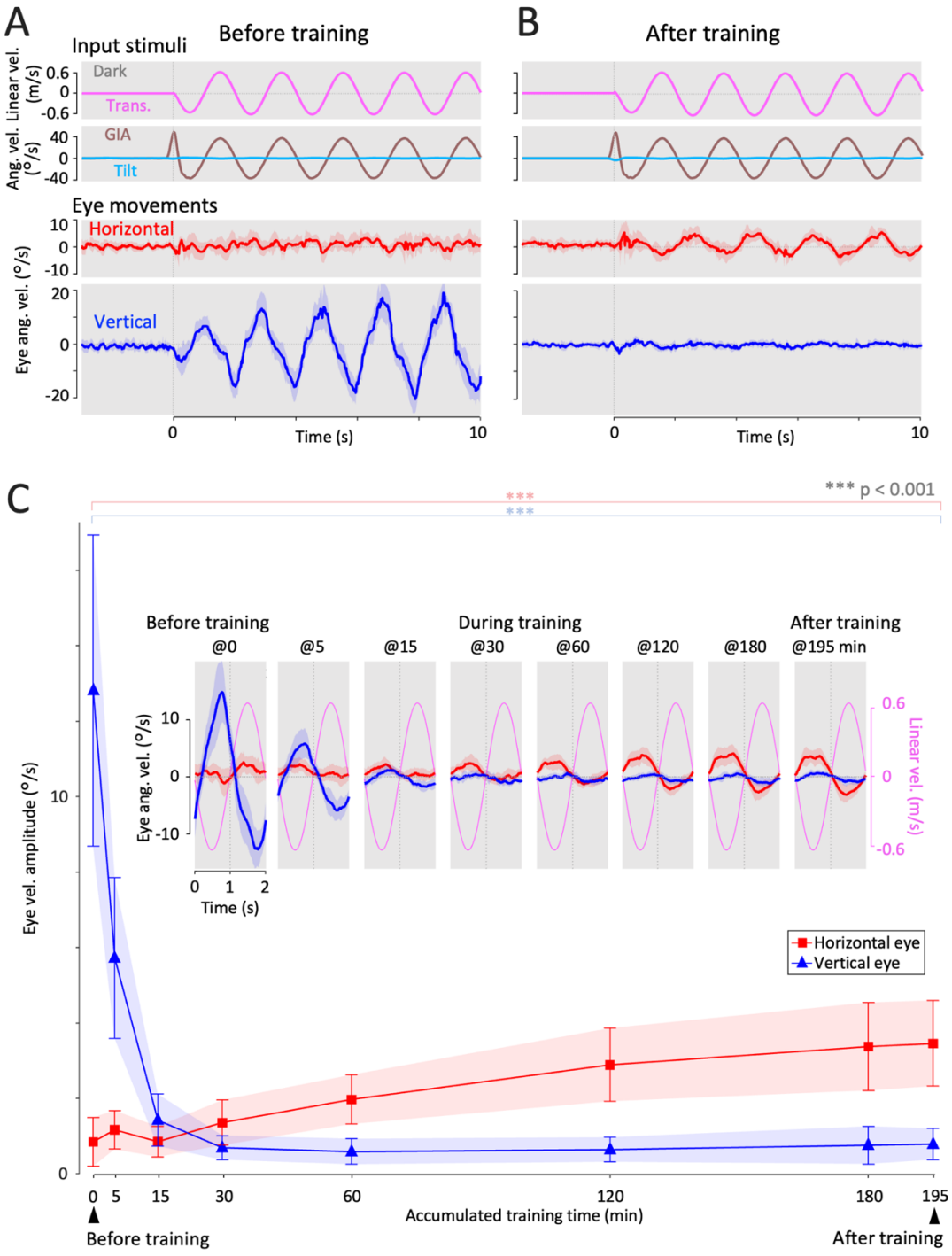

A
Before training
Input stimuli
Linear vel. (m/s)
0.6
0
-0.6
Dark
Trans.
Ang. vel. (°/s)
40
0
-40
GIA
Tilt
Eye movements
Eye ang. vel. (°/s)
10
0
-10
Horizontal
20
0
-20
Vertical
0
Time (s)
10
B
After training
0
Time (s)
10
C
*** p < 0.001
***
***
Before training
During training
After training
@0
@5
@15
@30
@60
@120
@180
@195 min
Eye ang. vel. (°/s)
10
0
-10
0 1 2
Time (s)
0.6
0
-0.6
Linear vel. (m/s)
Horizontal eye
Vertical eye
Eye vel. amplitude (°/s)
10
0
0 5 15 30 60 120 180 195
Accumulated training time (min)
Before training
After training

Figure 3.1. Horizontal and vertical VOR in response to interaural translational head acceleration in the dark (translation test) before, during, and after visual-translation training. (A) and (B) Horizontal (second panels from the bottom, red) and vertical (bottom panels, blue) eye velocities, around the z- and x-axes respectively, averaged over all animals (n = 12) during translational acceleration stimulation in the dark before (A) and after (B) training. Red and blue shadows indicate plus or minus one standard deviation. The top panels show linear velocity along the y-axis converted from the acceleration stimulation (see section 2.1.5). The second panels from the top show tilt (rotation around the y-axis) angular velocity, which is 0 during this stimulation and GIA angular velocity calculated from the translational acceleration, both around the x-axis. (C) Inset illustrating the horizontal (red) and vertical (blue) eye velocity traces averaged over stimulus cycles (magenta). The angular velocity traces around different axes (horizontal eye velocity around the z-axis and vertical eye velocity around the x-axis) and linear velocity along the y-axis traces are depicted in the same figures. Below the insets, changes in the mean amplitudes of horizontal and vertical VORs (learning curves) are plotted. Red and blue shadows indicate plus or minus one standard deviation. The increase in mean (±SD) amplitude of horizontal eye velocity and the decrease in mean amplitude of vertical eye velocity before and after training are significant (0.3 ± 0.6 vs. 3.4 ± 1.1 °/s, $p < 0.001$ for horizontal eye velocity; 12.5 ± 4.1 vs. 0.7 ± 0.4 °/s, $p < 0.001$ for vertical eye velocity, Wilcoxon rank-sum test). vel.: velocity; ang.: angular; trans.: translation; GIA: gravito-inertial acceleration; ***: $p < 0.001$.

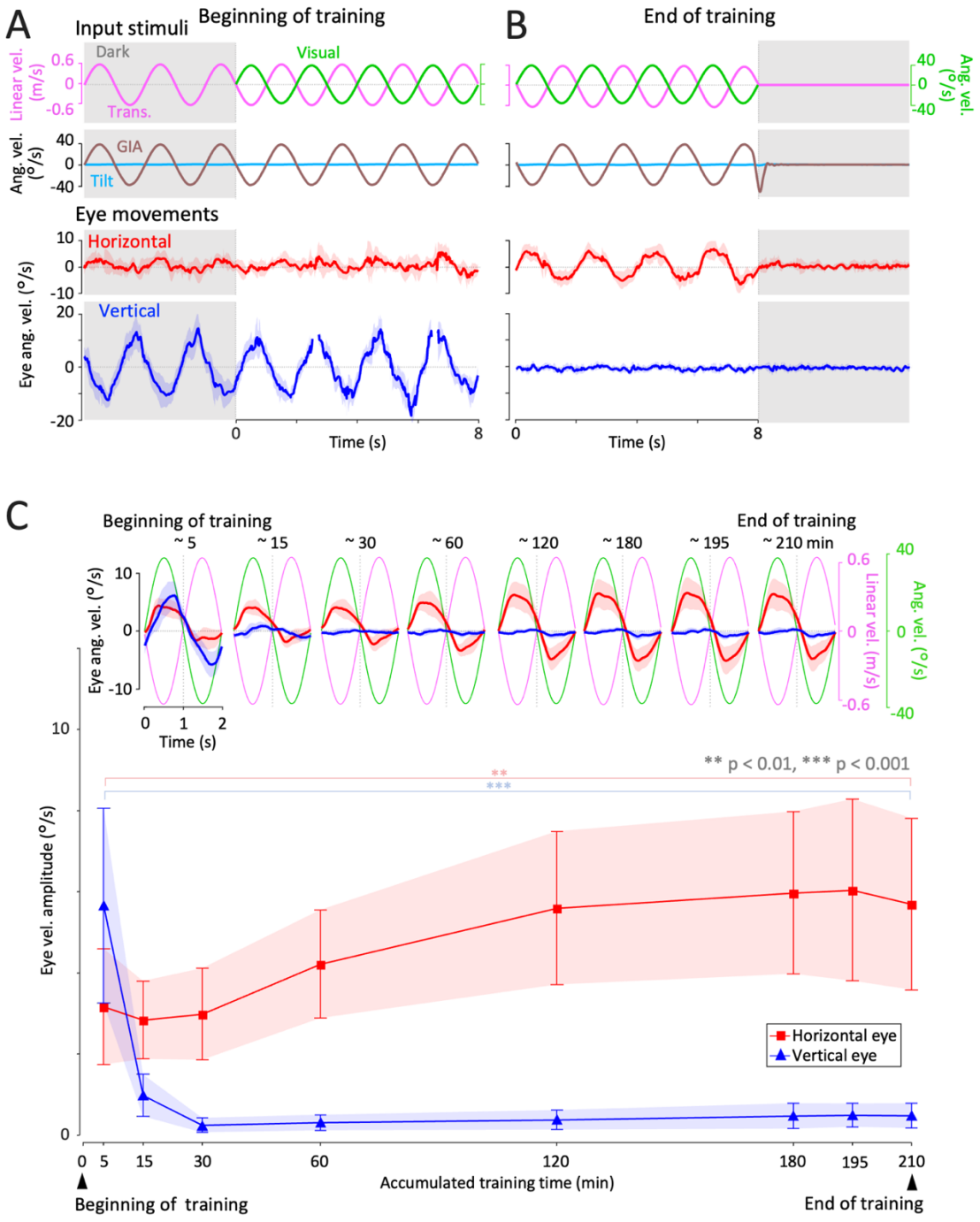

A
Input stimuli
Beginning of training
B
End of training
Linear vel. (m/s)
0.6
0
-0.6
Dark
Visual
Trans.
Ang. vel. (°/s)
40
0
-40
GIA
Tilt
Eye movements
Horizontal
Vertical
Eye ang. vel. (°/s)
10
0
-10
20
-20
Time (s)
0
8
C
Beginning of training
End of training
~ 5
~ 15
~ 30
~ 60
~ 120
~ 180
~ 195
~ 210 min
Eye ang. vel. (°/s)
Linear vel. (m/s)
Ang. vel. (°/s)
Time (s)
0 1 2
** p < 0.01, *** p < 0.001
Eye vel. amplitude (°/s)
Horizontal eye
Vertical eye
0 5 15 30 60 120 180 195 210
Accumulated training time (min)
Beginning of training
End of training

Figure 3.2. Horizontal and vertical VORs in response to interaural translational head acceleration along with OKS (training) during visual-translation training. (A) and (B) Horizontal (second panels from the bottom, red) and vertical (bottom panels, blue) eye velocities around the z- and x-axes, respectively, averaged over all animals (n = 12) during translational acceleration stimulation along with OKS at the beginning (A) and end (B) of the training. Red and blue shadows indicate plus or minus one standard deviation. The top panels show linear velocity along the y-axis converted from the acceleration stimulation (see section 2.1.5), and OKS velocity represented as an angular velocity around the z-axis. The second panels from the top show tilt angular velocity, which is 0 during this stimulation and GIA angular velocity calculated from the translational acceleration, both around the x-axis. (C) Inset illustrating horizontal (red) and vertical (blue) eye velocity traces averaged over stimulus cycles (magenta). The angular velocity traces around different axes (horizontal eye velocity and visual stimulus velocity both around the z-axis, vertical eye velocity around the x-axis) and linear velocity along the y-axis traces are depicted in the same figures. Eye velocities and visual stimulus velocity are depicted in different scales. Below the insets, changes in the mean amplitudes of horizontal and vertical VORs (learning curves) are plotted. Red and blue shadow indicate plus or minus one standard deviation. The increase in mean (±SD) amplitude of horizontal eye velocity and the decrease in mean amplitude of vertical eye velocity between the beginning and end of the training are significant (3.1 ± 1.4 vs. 5.6 ± 2.1 °/s, $p < 0.01$ for horizontal eye velocity; 5.6 ± 2.3 vs. 0.4 ± 0.3 °/s, $p < 0.001$ for vertical eye velocity, Wilcoxon rank-sum test). vel.: velocity; ang.: angular; trans.: translation; GIA: gravito-inertial acceleration; **: $p < 0.01$; ***: $p < 0.001$.

3.1.2 Changes in VOR during visual-translation training

Figure 3.2 illustrates changes in the horizontal and vertical VOR eye velocity during training, in which the same translational acceleration stimulus as in the test was combined with visual stimulation. Figure 3.2A and B illustrate the horizontal (red) and vertical (blue) eye velocities for four stimulus cycles (8 s) averaged for all animals at the beginning (A) and end (B) of training. At the beginning of training, a clear vertical VOR was induced, whereas little horizontal VOR was observed. After 3 h of training, the relationship was reversed, where a robust horizontal VOR and almost no vertical VOR were induced.

The insets in Figure 3.2C illustrate the horizontal (red) and vertical (blue) eye velocity averaged over stimulus cycles (linear velocity in magenta, visual stimulus velocity in green) during the initial 5 min, 10–15 min, 25–30 min, and thereafter. At the beginning of the training (0–5 min), the amplitudes of the horizontal and vertical VOR eye velocity are 3.1 and 5.6 °/s, respectively. The mean amplitude of horizontal VOR increased gradually along with the training time while that of the vertical VOR rapidly decreased to almost zero in the initial 30 min of training. The increase in mean (±SD) amplitude of the horizontal eye velocity and the decrease in mean amplitude of the vertical eye velocity between the beginning and end of the training are significant (3.1 ± 1.4 vs. 5.6 ± 2.1 °/s, $p < 0.01$ for horizontal eye velocity; 5.6 ± 2.3 vs. 0.4 ± 0.3 °/s, $p < 0.001$ for vertical eye velocity).

The learning curves of the changes in horizontal and vertical VOR amplitudes during training are illustrated in the insets below. Red and blue shadows indicate plus or minus one standard deviation for the horizontal and vertical VOR amplitudes, respectively. The learning curves indicated that the initial noncompensatory VOR (large vertical and smaller horizontal eye velocities) became more compensatory (almost no vertical or larger horizontal eye velocities) to reduce retinal image slip during the training stimulus as training progressed. In the next subsubsection, we illustrate how these changes in the VOR during training are reflected in eye movements during the test stimulus in the dark.

3.1.3 Changes in VOR during translation in the dark along with the training

Figure 3.1B illustrates the horizontal (red) and vertical (red) VOR eye velocities during translation in the dark after 3 h of training in the same format as in Figure 3.1A, showing those at the beginning of training. Notably, the horizontal VOR was robust, whereas the vertical VOR was significantly suppressed after training. The insets in Figure 3.1C show the averaged horizontal and vertical VOR eye velocity traces during translation stimulation in the dark tested during and after training (5–195 min) in the same format as before training (0 min). Below the insets, changes in the mean amplitudes of the horizontal (red) and vertical (blue) VOR (learning curves) are plotted. Notably, the amplitude of the horizontal VOR gradually increased, whereas that of the vertical VOR rapidly decreased to almost zero within 30 min, similar to the learning curves during training (Figure 3.2C). The increase in mean (±SD) amplitude of horizontal eye velocity and the decrease in mean amplitude of vertical eye velocity before and after training are significant (0.3 ± 0.6 vs. 3.4 ± 1.1 °/s, $p < 0.001$ for horizontal eye velocity; 12.5 ± 4.1 vs. 0.7 ± 0.4 °/s, $p < 0.001$ for vertical eye velocity).

The learning curves indicated that the vertical-dominant VOR responding to translational head motion in the dark became horizontally dominant after training. In naïve goldfish, the vertical VOR is robustly induced by roll-tilt head motion. Since the vertical VOR during translation is suppressed after training, it might also be suppressed during roll-tilt head rotation. This possibility is discussed in the next subsubsection.

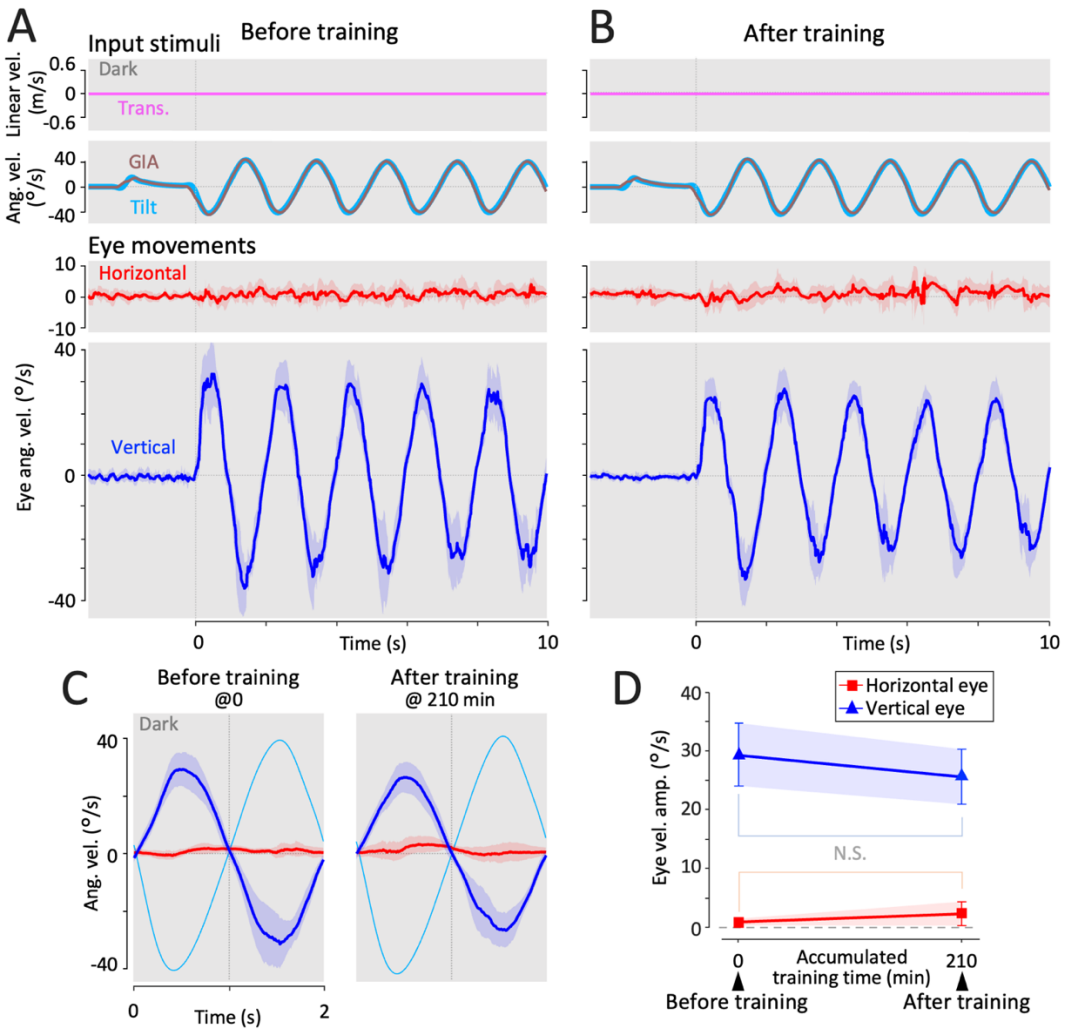


Figure 3.3. Horizontal and vertical VOR in response to roll-tilt head rotation in the dark (roll-tilt test) before, and after visual-translation training. (A) and (B) Horizontal (second panels from the bottom, red) and vertical (the bottom panels, blue) eye velocities around the z- and x-axes respectively, averaged over all animals (n = 12) during roll-tilt stimulation in the dark before (A) and after (B) training. Red and blue shadows indicate plus or minus one standard deviation. The top panels show linear velocity along the y-axis, which is 0 during this stimulation. The second panels from the top show tilt angular velocity and GIA angular velocity both around the x-axis. (C) Horizontal (red) and vertical (blue) eye velocity traces averaged over stimulus cycles (cyan). Angular velocity traces around different axes (horizontal eye velocity around the z-axis, vertical eye velocity and tilt angular velocity both around the x-axis) are depicted in the same figures.

(D) Changes in the mean amplitudes of horizontal and vertical VORs (learning curves). Red and blue shadows indicate plus or minus one standard deviation. Both horizontal and vertical eye velocities show no significant differences between before and after training (0.6 ± 0.6 vs. 1.3 ± 2.0 °/s, $p = 0.157$ for horizontal eye velocity; 29.1 ± 5.4 vs. 25.4 ± 4.7 °/s, $p = 0.060$ for vertical eye velocity, Wilcoxon rank-sum test). vel.: velocity; ang.: angular; trans.: translation; GIA: gravito-inertial acceleration; N.S.: not significant.

3.1.4 VOR during roll-tilt before and after training

Figure 3.3 illustrates changes in the horizontal and vertical VOR eye velocities during roll-tilt stimulation in the dark before and after training (Figure 2.2D, cyan rectangles 1 and 2) in the same format as in Figures 3.1 and 3.2.

Both before (A) and after training (B), vertical eye velocity traces were prominently observed (blue, bottom panels), not suppressed, compensatory to roll-tilt angular velocity and GIA angular velocity in the dark (the second panels from the top), while the horizontal eye velocity remained minimal (red, the second panels from the bottom). As illustrated in Figure 3.3D, the mean eye velocity amplitudes in both horizontal (red) and vertical (red) VOR were not significantly different before and after training (0.6 ± 0.6 vs. 1.3 ± 2.0 °/s, $p = 0.157$ in horizontal eye velocity; 29.1 ± 5.4 vs. 25.4 ± 4.7 °/s, $p = 0.060$ in vertical eye velocity).

3.1.5 Kalman filter simulations

To interpret these results, we added a VOR and OKR simulation model (Figure 2.3) to a previously proposed Kalman filter model for spatial orientation (Laurens and Angelaki, 2017) and employed it in our analysis. We first validated the model by confirming that it reproduces basic vestibular-visual oculomotor behaviors in goldfish and then applied the model to interpret changes in the VOR and those corresponding to spatial orientation formation.

Model validation

Figure 3.4A shows the model simulation results for the angular VOR in the dark around each rotational axis. Robust compensatory eye velocity was reproduced as reported in

previous behavioral experiments (Tweed *et al.*, 1994; Migliaccio *et al.*, 2010). The stimuli (linear head, angular head, and angular visual velocities) were estimated as provided. For example, when head rotation was provided in the dark around the x-axis (Figure 3.4A, panel in the first column from the left and second row from the top), eye velocity was produced only around the x-axis in the opposite direction to head rotation (Figure 3.4A, panel in the first column from the left and third row from the top), while head rotation around the x-axis was estimated close to the provided head rotation (Figure 3.4A, panel in the first column from the left and second row from the bottom).

Figure 3.4B shows the model simulation result of the OKR and OKAN, which were induced by constant velocity visual stimulation around the z-axis for 60 s, followed by no stimulation in the dark. It has been demonstrated in goldfish and other species, including primates, that eye velocity gradually increases around the z-axis to catch up with the visual stimulus velocity while the stimulation is presented (OKR) and keeps moving in the dark for a while after the stimulation is turned off (OKAN) (Cohen *et al.*, 1977; Miki *et al.*, 2020). As in the experimental data, the model reproduced both OKR and OKAN eye velocities (Figure 3.4B, fourth panel from the top). Notably, head rotation around the z-axis was estimated instead of the visual stimulation velocity as the source of the OKR and OKAN eye velocities, as shown in the second panel from the bottom of Figure 3.4B. In addition, owing to the similarity of visual stimuli caused by rotational and linear head velocity, the slightly accumulated head linear velocity along the y-axis was estimated while visual stimulation was provided, and it persisted after OKS was terminated (third panel from the bottom, Figure 3.4B). All other estimated self-motions from Figure7A to B were close to zero.

The simulated erroneous estimation of head rotation along with OKR and OKAN also suggests the reproduction of “vection,” an erroneous perception of head rotation in the opposite direction of the visual stimulus (Thilo *et al.*, 1999; Kleinschmidt, 2002; Nooij *et al.*, 2018). All lines in Figure 3.4 were averaged from 12 simulations, similar to the results of the goldfish experiments (Figures 3.5–3.7).

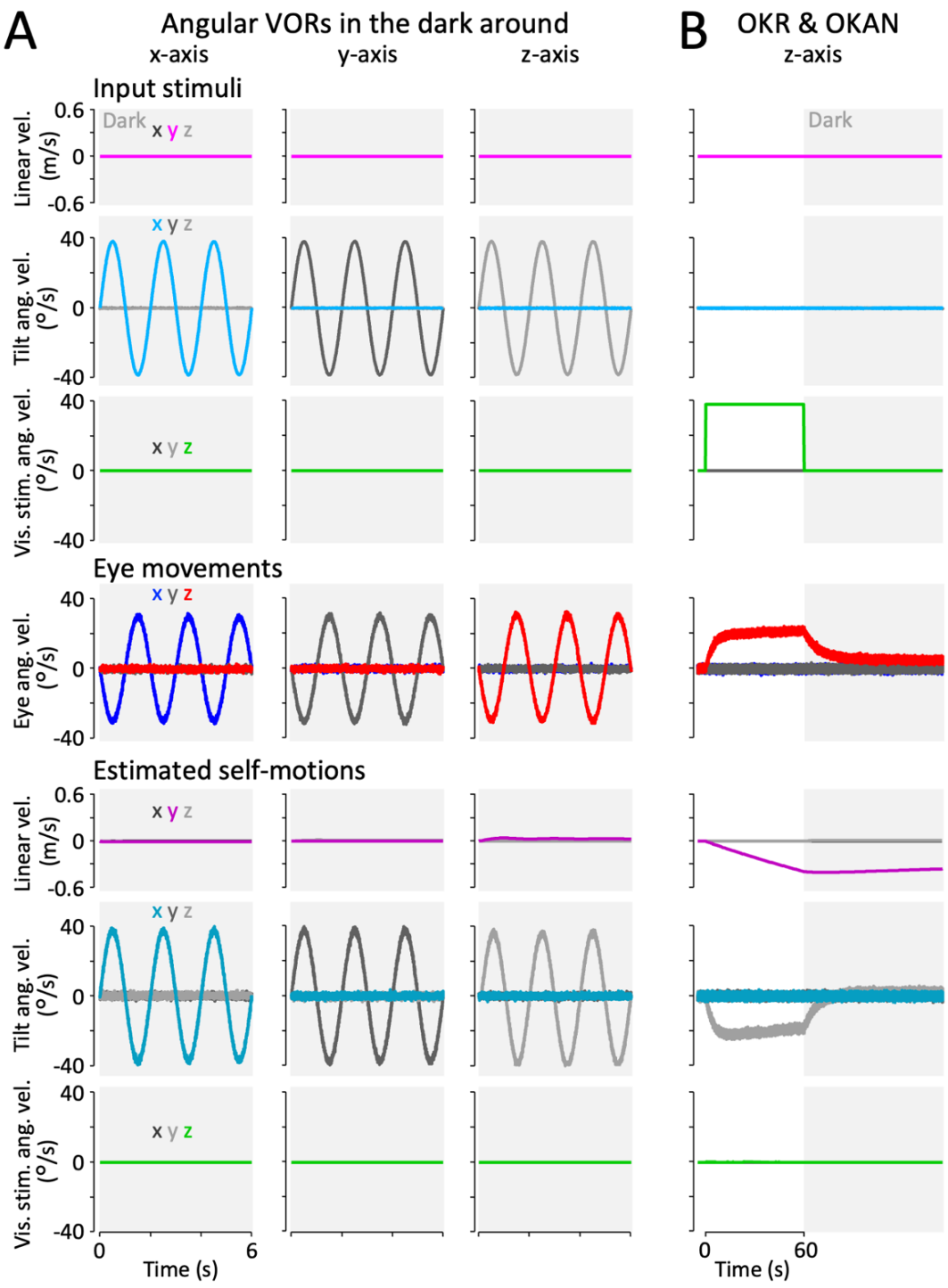


Figure 3.4. Results of the modified Kalman filter model simulation for model validation. (A) Simulation results of angular VORs around the x-, y-, and z-axes. (B) Simulation results of OKAN around the z-axis. In (A) and (B), **the top three rows** represent input stimuli (vestibular or visual), **the fourth row from the top** depicts eye movements, and

the bottom three rows show internally estimated self-motions corresponding to their respective input stimuli. The colors 'x,' 'y,' and 'z' in the inset of the leftmost column indicate the directions (rotation around the x-, y-, z-axes, or translation along the x-, y-, z-axes). All traces display the average results of the 12 simulation runs. Traces representing minimal values overlap at the baseline and are not all visible. vel.: velocity; ang.: angular; vis.: visual; stim.: stimulus.

Translation and tilt VOR before, during, and after training

Using the same set of model parameters as those used for the model validation, we simulated the VOR in response to translational acceleration and tilt stimulation in the dark, which were used in the current experiment (frequency: 0.5 Hz, GIA amplitude: 0.2 G). Figure 3.5 shows the simulation results of the translated VOR in the dark before and after training. Before training, the horizontal VOR eye velocity was minimal, as shown in Figure 3.5A, whereas the vertical VOR was robustly generated, as the current result shown in Figure 3.1A. Notably, the vertical VOR was caused by a false estimate of the tilt angular velocity around the x-axis (fourth panel from the top, Figure 3.5A), whereas the linear velocity was estimated to be almost zero. To express the animal's increased experience in translation acceleration, we increased the standard deviation of the linear head acceleration input along the y-axis (Table 2.2, σ_y^A) from 0.001 G before training to 0.180 G after training while other parameters were unchanged. This manipulation resulted in changes in the VOR after training, as found in the current experiment shown in Figure 3.1B. Robust horizontal VOR eye velocity was produced, while the vertical VOR was significantly suppressed after training, as illustrated in Figure 3.5B (after training). Notably, both the linear translation, and tilt angular velocities were correctly estimated after training.

Figure 3.6 illustrates the simulation results of the VOR with the parameter set for the beginning of training (same as the model validation) and for the end of training in response to visual-translation stimulation. As the current results shown in Figure 3.2A and B, the minimal horizontal eye velocity before training was enhanced after training (Figure 3.6, third row from the top), whereas the distinctive vertical eye velocity before training was suppressed significantly after training (Figure 3.6, fourth row from the top).

Similarly, Figure 3.7 shows the simulation of VOR with the parameter set before and after training in response to the roll-tilt stimulus in the dark, reproducing the current results (Figure 3.3A and B). In other words, the horizontal and vertical VORs were unchanged after the training (Figure 3.7, third and fourth rows from the top). All other estimated self-motions from Figure 3.5 to Figure 3.6 were close to zero.

The Kalman gains utilized in this simulation are presented in the Supplementary Results. These Kalman gains were computed using the formula provided in the Supplementary Methods section S2.3.

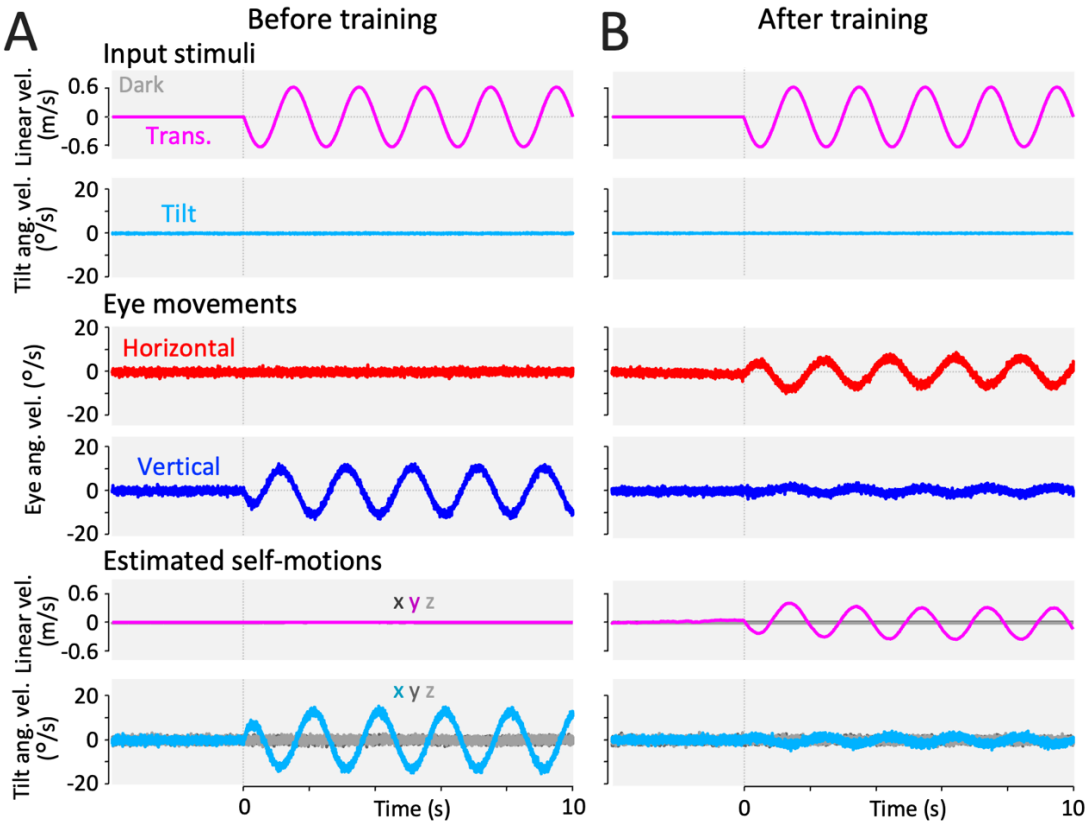


Figure 3.5. Results of the modified Kalman filter model simulation in response to interaural translational head acceleration in the dark. In the Kalman filter model, the process noise + passive stimuli standard deviation of interaural linear acceleration was set to a small value (0.001 G) at (A) and a large value (0.180 G) at (B), to reproduce the translation test paradigms before and after training. **The top two rows** show input stimuli, with linear velocity stimulation along the y-axis (magenta) and tilt angular velocity around the x-axis (cyan). Tilt angular velocity around the x-axis is 0 during this stimulation. **The third and fourth rows from the top** show the simulation results of horizontal eye velocity around the z-axis (red) and vertical eye velocity around the x-axis (blue). **The bottom two rows** show the simulation results of linear velocity along the x-, y-, and z-axes (dark gray, dark magenta, and light gray, respectively) and angular velocity around the x-, y-, and z-axes (dark cyan, dark gray, and light gray, respectively), estimated by the Kalman filter. Eye movements and estimated self-motions traces show the average traces of the 12 simulation runs. vel.: velocity; ang.: angular.

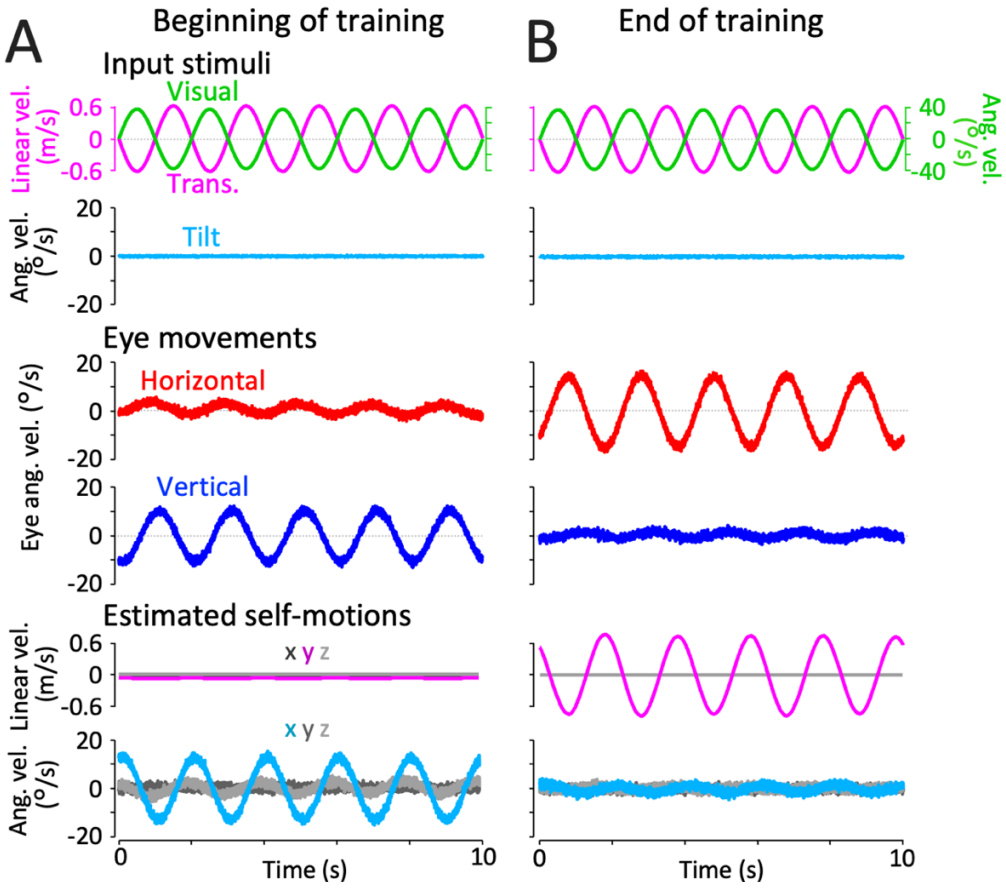


Figure 3.6. Results of the modified Kalman filter model simulation in response to interaural translational head acceleration along with OKS. In the Kalman filter model, the process noise + passive stimuli standard deviation of interaural linear acceleration was set to a small value (0.001 G) at (A) and a large value (0.180 G) at (B) to reproduce training paradigms at the beginning and end of the training. **The top two rows** show input stimuli, with linear velocity stimulation along the y-axis (magenta), OKS velocity around the z-axis (light green), and tilt angular velocity around the x-axis (cyan). Tilt angular velocity is 0 during this stimulation. **The third and fourth rows from the top** show the simulation results of horizontal eye velocity around the z-axis (red) and vertical eye velocity around the x-axis (blue). **The bottom two rows** show the simulation results of linear velocity along the x-, y-, and z-axes (dark gray, dark magenta, and light gray, respectively), and angular velocity around x, y, and z-axis (dark cyan, dark gray, and light gray, respectively), estimated by the Kalman filter. Eye movements and estimated self-motions traces show the average traces of the 12 simulation runs. vel.: velocity; ang.: angular.

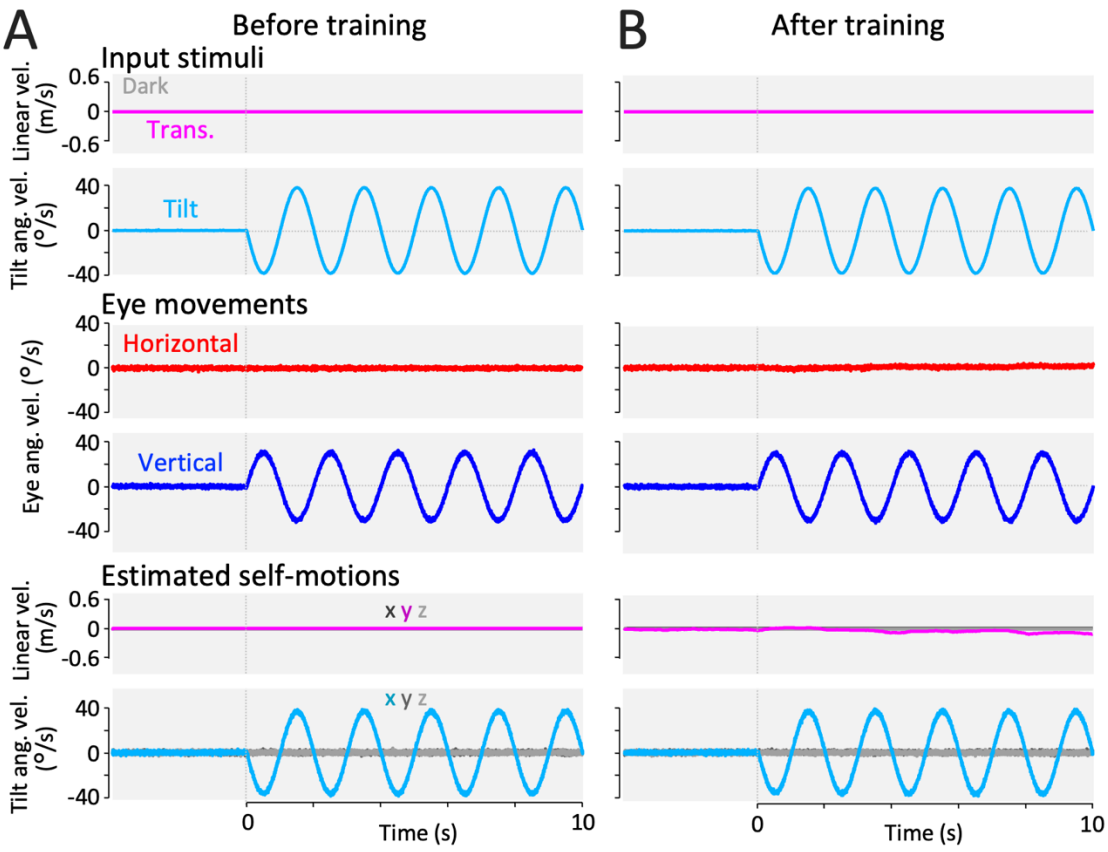


Figure 3.7. Results of the modified Kalman filter model simulation in response to roll-tilt head rotation in the dark. In the Kalman filter model, the process noise + passive stimuli standard deviation of interaural linear acceleration was set to a small value (0.001 G) at (A) and a large value (0.180 G) at (B) to reproduce roll-tilt test paradigms before and after training. **The top two rows** show input stimuli, with linear velocity stimulation along the y-axis (magenta) and tilt angular velocity around the x-axis (cyan). Linear velocity stimulation (magenta) is 0 during this stimulation. **The third and fourth rows** from the top show the simulation results of horizontal eye velocity around the z-axis (red) and vertical eye velocity around the x-axis (blue). **The bottom two rows** of panels show the simulation results of linear velocity along the x-, y-, and z-axes (dark gray, dark magenta, and light gray, respectively), and angular velocity around the x-, y-, and z-axes (dark cyan, dark gray, and light gray, respectively), estimated by the Kalman filter. Eye movements and estimated self-motions traces show the averaged traces of 12 simulation runs. vel.: velocity; ang.: angular.

3.2 Discussion

3.2.1 Adaptive changes in the spatial orientation formed during translation

It has long been argued how the tilt-translation ambiguity arising from peripheral sensory organs (i.e., the otolith) can be resolved to accurately estimate spatial orientation. Notably, humans perceive translational motion in parallel with presenting horizontal VOR during high-frequency (>4 Hz) periodic interaural translations (Telford *et al.*, 1997; Paige *et al.*, 1998; Merfeld *et al.*, 2005a; Clément *et al.*, 2022), whereas tilt perception and torsional or vertical VOR are induced during low-frequency (<1/20 Hz) or sustained linear accelerations in the dark (Seidman and Paige, 1996; Seidman *et al.*, 1998; Moore *et al.*, 2001; Clément *et al.*, 2001; Zupan and Merfeld, 2005; Merfeld *et al.*, 2005a; Clément *et al.*, 2022). The VORs in monkeys have also been found to behave similarly (Paige and Tomko, 1991; Paige *et al.*, 1998). In particular, tilt perception during low-frequency or sustained linear acceleration is referred to as "somatogravic illusion," which has been causing many fatal aviation accidents (Gillingham and Wolfe, 1985; Clément *et al.*, 2001). These phenomena indicate that, in the case of high-frequency periodic linear translation, both humans and monkeys can resolve the ambiguous otolith response and interpret the translation as translation. However, with low-frequency translation or sustained linear acceleration, the ambiguity remains unresolved, resulting in the misinterpretation of translation as a tilt. Two theories have been proposed as the neural mechanisms interpreting the phenomena observed during linear translation.

The first is the frequency-selective segregation theory (Paige and Tomko, 1991; Seidman and Paige, 1996; Seidman *et al.*, 1998). Paige *et al.* suggested that animals possess high-pass filters for estimating linear translation and low-pass filters for estimating tilt, thus facilitating discrimination between the two types of motion using ambiguous otolith signals. In their theory, the brain filters out high-frequency linear excursions, such as everyday walking, thereby reducing the impact of transient linear motion on tilt detection. Although these low-pass filters also reduce high-frequency otolith-based tilt detection, they are effectively complemented by canal-based tilt-detection methods. A high-pass filter aids in translational estimation to avoid misinterpreting commonly experienced prolonged tilts as translations.

The other theory is referred to as the integration or internal model theory. Over the subsequent decades, multiple theoretical studies have suggested that the brain resolves ambiguity by explicitly solving motion equations to estimate gravity and inertial (translational) motion (Merfeld *et al.*, 1993; Merfeld, 1995; Hess and Angelaki, 1997; Mergner and Glasauer, 1999; Merfeld *et al.*, 1999; Bos and Bles, 2002; Zupan *et al.*, 2002; Laurens and Droulez, 2007; MacNeilage *et al.*, 2008). Merfeld unified these theories (Merfeld *et al.*, 1993), proposing a comprehensive model integrating the properties of otolith organs and semicircular canals using two distinctive mechanisms: velocity storage mechanism (VSM) and tilt estimator. The tilt estimator mathematically integrates gravity vector changes tracked by resolving Goldstein's equation of motion (Goldstein, 1980; Angelaki *et al.*, 2004). Laurens and Angelaki further unified visual motion information and suggested that this integrator functions as a low-pass filter for tilt estimation (Laurens and Angelaki, 2011). The high-frequency otolith signal (GIA), which was not utilized in the tilt estimation, was interpreted as linear inertial acceleration during passive motion. This concept aligns with the frequency-selective segregation framework (Laurens and Angelaki, 2011).

Both of these major theoretical frameworks are supposed to be appropriate for the natural motion experiences of animals (e.g., linear motion at low frequencies is very rare in nature) (Paige and Tomko, 1991; Telford *et al.*, 1997; Laurens and Angelaki, 2011); Laurens and Angelaki further claimed that animal motion experiences adaptively affect neural mechanisms (Laurens and Angelaki, 2011). However, few experimental studies have explored how animals adaptively learn to estimate their self-motion using ambiguous sensory information. To unveil the adaptive mechanism, we hypothesized that animals could adapt their estimation mechanisms based on their accumulated motion experiences and conducted behavioral experiments to test this hypothesis.

Current experiments can be succinctly described as an assessment of the cross-axis VOR adaptation in response to translational vestibular stimuli. Furthermore, this assessment serves as an indicator of adaptive changes in spatial orientation (section 3.2.3). While only one study of cross-axis VOR adaptation during translation has been previously conducted in monkeys (Wei and Angelaki, 2001), current study using goldfish yielded

surprising results that were entirely distinct from those of monkeys, providing novel and crucial insights into the process of adaptive changes in spatial orientation. Below, we provide a detailed discussion of the current results in conjunction with simulations using the modified Kalman filter model.

Translational VOR adaptation in goldfish

Before training, naïve goldfish displayed vertical eye velocity (around the x-axis) during interaural translation (along the y-axis) in the dark, rather than horizontal VOR (around the z-axis), which should be more adequate to stabilize vision if the visual scene is presented in front of the fish (Figure 3.1, Translation test before training). The occurrence of VOR around the x-axis in naïve goldfish during 0.5 Hz translation is suggested to be a consequence of erroneous tilt estimation (see section 3.2.3). The gradual increase in the vertical VOR response to translation (along the y-axis) over the first 10 s (Figure 3.1A) appears analogous to the phenomenon observed in the horizontal VOR response to yaw rotation in goldfish. We previously observed this phenomenon in an unreported experiment. It was characterized by the goldfishes' initial low sensitivity (gain) after having been in darkness and at rest for some time and then exposed to vestibular stimulus, whereafter their sensitivity gradually increased. The cause is unclear; however, a similar phenomenon may have occurred in the vertical VOR response to translation (along the y-axis, Figure 3.1A). However, in the vertical VOR response to tilt (around the x-axis, Figure 3.3A), the gain is large directly following the stimulus onset. Considering the differences in which vestibular organs are stimulated in specific movements—the canal and otolith are stimulated simultaneously during tilt, while only the canal is stimulated during yaw rotation and only the otolith during translation—we postulate that the simultaneous stimulation of the canal and otolith leads to this large gain immediately after the stimulus onset.

At the beginning of training, the goldfish exhibited vertical VORs around the x-axis. Although these vertical VORs are based on tilt estimation, they do not contribute to the reduction of retinal slip generated by the presentation of lateral OKS moving parallel to the y-axis. Persistent retinal slip might teach goldfish the impropriety of vertical VOR, thereby implying an error in the tilt estimation process, leading to a reduction in vertical

VOR. It is important to note that persistent retinal slip alone is insufficient to explain the currently observed rapid suppression of the vertical VOR. The canal prediction error based on the absence of actual tilt rotation, as well as persistent retinal slip, is considered to have contributed to the remarkably rapid suppression (see ***Role of canal prediction error in rapid translational VOR suppression*** in this subsubsection). Simultaneously, when goldfish perform translational estimation in response to translational vestibular stimuli and express horizontal VOR, this leads to a reduction in retinal slip and visual stability. The reduction in retinal slip might have kept telling the goldfish that their translational estimation was accurate, which, in turn, could explain the current observation of a gradual increase in translational estimation-based horizontal VOR during training (Figure 3.2C).

Changes in the eye movements of these goldfish were not transient responses (corrections) to the visual stimuli. Both the VOR with OKS (training paradigm) and the response to translational vestibular stimuli in the dark (translation test paradigm) revealed astonishingly rapid suppression of the vertical VOR around the x-axis and a gradual increase in the horizontal VOR around the z-axis (Figure 3.1C). This suggests that the goldfish's interpretation (motion state estimation) of the translational vestibular stimuli has changed. After 3 h of training, despite a gradual increase in the horizontal vestibulo-ocular reflex (VOR), this gain remained relatively small given the speed of the slider. The limited gain suggests that it is challenging for goldfish to estimate a translation of 0.64 m/s solely from vestibular signals because interaural translation occurs too rarely in goldfish to estimate adequately.

During the roll-tilt tests, both before and after training, the amplitude of the horizontal VOR remained consistently low, whereas the amplitude of the vertical VOR remained substantially high. There were no significant differences before and after the training (Figure 3.3).

Taken together, it is evident that post-training goldfish VOR can distinguish between interaural translation and roll-tilt, even in the dark, suggesting that they no longer misinterpret translation as tilt, but correctly interpret it as translation, while tilt is still properly perceived as tilt.

Role of canal prediction error in rapid translational VOR suppression

The rapid suppression of VOR responses to conflicting OKS observed in goldfish has not been previously documented in both the common angular VOR adaptation (Kuki *et al.*, 2004) and the prior case of translational cross-axis VOR adaptation (Wei and Angelaki, 2001). Typically, angular VOR adaptation results in a faster increase than decrease in learning (Kuki *et al.*, 2004). Furthermore, prior to this study, although only Wei (2001) had investigated the cross-axis adaptive plasticity of translational VOR, she did not observe any evident suppression of non-compensatory VOR (Wei and Angelaki, 2001). She investigated monkeys before and after a 2-h exposure to either vertical or torsional OKS accompanied by interaural translation stimuli (0.5 Hz). Akin to the goldfish horizontal VOR enhancement (around the z-axis), the monkeys' adaptation gradually progressed during OKS exposure (around the x- or y-axis), enhancing their torsional or vertical VOR (around the x- or y-axis, respectively). However, despite not compensating for the vertical or torsional OKS, the monkeys' horizontal VOR remained largely unchanged. Interestingly, it was robustly elicited, even at the moment of exposure to the conflicting torsional OKS around the x-axis. Wei's monkey initially exhibited a VOR around the z-axis during interaural translation at 0.5 Hz in contrast to goldfish in current study, which initially exhibited a VOR around the x-axis in response to the same stimulus. Thus, they aimed to adapt the monkeys from the VOR around the z-axis to either the VOR around the x- or y-axis in their study.

The rapidly vanishing vertical VOR around the x-axis in goldfish in response to conflicted horizontal OKS and the persistent horizontal VOR around the z-axis in monkeys, especially in response to conflicted torsional OKS around the x-axis, may be explained by the absence of observed canal signals during translation. In particular, during the actual roll-tilt rotation, both otoliths and canals should be observed by animals; however, during the translational motion-induced roll-tilt illusion, canal signals will not be observed. To avoid the error between the canal signals actually observed during translation and the erroneous canal signals predicted based on the roll-tilt illusion (canal prediction error), both trained goldfish and naïve monkeys might have rapidly discarded the erroneous tilt estimation and converged their estimation toward translation.

There are other questions regarding why naïve goldfish can initially only perform roll-tilt estimation and not translational estimation despite the presence of canal prediction errors, why they become capable of translational estimation through training, and why naïve monkeys are already capable of translational estimation from the beginning. Differences in the probability distribution (i.e., their motion experiences) of passive translation are generally used to explain the distinctions between the high- and low-frequency translational VOR in primates (Paige and Tomko, 1991; Telford *et al.*, 1997; Laurens and Angelaki, 2011), similarly, differences in the animals' experiences can also explain the differences in translational VOR between goldfish and primates at the same frequency (0.5 Hz). The impact of the probability distributions of passive motion and sensory prediction errors on motion estimation is detailed in section 3.2.2.

3.2.2 Interpretation based on the Kalman filter model

The Kalman filter, which is a mathematical algorithm developed by Rudolf Kalman in the early 1960s, integrates sensor measurements to provide optimal estimates of directly unobservable states in dynamic systems. In 2017, Laurens and Angelaki introduced the Kalman filter into their previous model (Laurens and Angelaki, 2011) and utilized it as a computational mechanism to estimate the head motion states based on visual and vestibular sensor information (i.e., semicircular canals and otoliths) (Laurens and Angelaki, 2017). Their new model, which incorporates a Kalman filter, updates the estimates of head motion states, including linear and rotational motion, by adding corrective values obtained by multiplying the Kalman gain with the sensory prediction error between the observed and predicted sensory signals.

To interpret the results of the current VOR adaptation study, we revised the model to simulate VORs in response to translation and tilted head motion in goldfish, based on the estimates of 3D head motion and visual stimulation (OKS) states. To reproduce the observed changes in the VOR (decrease in the vertical VOR and increase in the horizontal VOR) after training, we varied the parameter representing the variance in linear acceleration along the y-axis. This allowed us to replicate the cross-axis VOR adaptation in goldfish presented in this study and investigate adaptive changes in spatial orientation, as depicted in Figures 3.5–3.7.

In the Kalman filter model, passive motion is estimated by adding correction values based on sensory prediction errors to the predicted estimates (stationary estimations derived from efference copies) generated by the internal model. In other words, the Kalman filter converges the motion state estimates toward the appropriate values by minimizing the sensory prediction errors. This concept aligns with the idea that both trained goldfish and naive monkeys attempt to avoid canal prediction errors and converge their estimations toward translation (as discussed in section 3.2.1).

Similarly, the Kalman filter model, as mentioned below, is also capable of describing the impact of differences in the probability distribution (i.e., the difference of motion experiences between the goldfish and monkey) during passive translation. These differences presumably led to distinct estimations, such as roll-tilt estimation in naïve goldfish versus translational estimation in trained goldfish and naïve monkeys. Within the model, the magnitude of the weighting of the correction values based on sensory prediction errors (Kalman gain) depends on the variance in the probability distribution of the passive motion that the animal anticipates. Animals that do not move voluntarily are generally in a state of rest, although they may occasionally experience passive movements because of being pushed or carried. Therefore, the probability distribution of passive motion is typically centered around zero with a small variance. As animals gain more experience with passive motion, the probability distribution becomes wider and the variance increases. For instance, the daily locomotion and jumping activities of naïve monkeys encompass abundant translational and rotational components along the x-, y-, and z-axes (Carriot *et al.*, 2017). This provided young animals being carried by their parents with rich passive experiences and potentially broadened the probability distribution of each passive motion. Passive motions with relatively wide probability distributions (e.g., roll-tilting in naïve goldfish and high-frequency translational motion in primates) can be largely updated in their motion state estimates through corrections based on sensory prediction errors, even when predicting stationary motion using deficient efference copies of motion commands that are generated only during voluntary motion. However, in passive motion with a small variance in the probability distribution, the magnitude of correction based on sensory prediction errors tends to be small. For instance, it is reasonable to assume that goldfish, which possess a spindle-shaped body

mainly designed for forward motion, had significantly less exposure to 0.5 Hz and 0.2 G interaural translation compared to humans and monkeys who commonly experience daily 3D-linear excursions. Furthermore, fish such as goldfish, which live independently from their parents shortly after hatching, can be confidently postulated to have less passive motion, excluding drift, compared to young primates that are carried by their parents. This minimal exposure results in a small variance in the probability distribution, which is expected to result in minimal translational estimation. In the Kalman filter model, passive motion is described as a perturbation affecting the motion state variable (Laurens and Angelaki, 2017). This input was treated as process noise because it is unpredictable in the brain (Madhani *et al.*, 2022). The process noise of individuals who encounter a larger than normal range of experienced motion (e.g., a sailor) could be larger (Madhani *et al.*, 2022). In the Kalman filter framework, process noise describes actual motion that is unintended ("passive") and not motion that is commanded by the brain ("active") (Madhani *et al.*, 2022). In our model simulations, we specifically manipulated the variance of this process noise (Table 2.2, σ_y^A).

Based on the simulation results, the results of the goldfish experiments can be interpreted as follows.

Naive goldfish assume that the variance in the probability distribution of translational movements is small; therefore, they do not update their translational estimates and estimate them to remain small, despite the sensory prediction error from the observed sensory signals. After training, the goldfish perceived the probability distribution of translation as having a large variance; therefore, the weight of the translational correction based on the sensory prediction error increased, and the increase in the estimated translation movements caused the goldfish to move their eyes in the horizontal direction. The increase in translational variance that goldfish assume after training can be attributed to training involving the OKS. Therefore, these results support the possibility that goldfish have a neural mechanism for acquiring optimal spatial orientation by updating the variances of self-motion through visual and vestibular information.

If the goldfish solely responded independently to the otolith and canal reaction, without considering tilt and translation estimation, it would be expected to observe a similar

amount of change in VOR responses during tilt after training to those during translation, such as the emergence of enhanced horizontal VOR and reduction of vertical VOR due to the component of the otolith adaptation, even when considering that the canal response remained relatively large during tilt. However, our results did not align with these expectations. This indicated that the 3D VOR system was adapted to differentiate between tilt and translation.

Additionally, given that altering the tilt estimator function affects its frequency filtering (Laurens and Angelaki, 2011), adjusting the process noise might similarly influence its frequency filtering and alter the frequency cutoff for the tilt or translation estimation. However, in this study, we could not verify whether the frequency cutoff for tilt or translation estimation was shifted by training, which may have manipulated the variance in the process noise. This is because the 0.8-meter-long slider currently available is unable to measure the goldfish VOR across a sufficient range of frequencies. To address this, we plan to prepare a longer slider to test additional frequencies and evaluate any shift in the frequency cutoff in future studies.

The assumption of small variance in the probability distribution of goldfish translational movements and how it is linked to their living environment can be validated in future studies by equipping fish with an inertial measurement unit attached to their heads. This allows the distribution of motion within their actual living environment to be measured and verifies whether it aligns with our assumption. Concerns about the unit potentially impeding swimming can be alleviated by measuring sufficiently large fish, such as fully grown goldfish or carp, which share ecological similarities with typical-sized goldfish.

The Kalman filter model in this study appears to represent visual- and vestibular-based motion state estimates in the initial pathways formed before conscious motion perception formation within subsequent pathways (see detail in section 3.2.3). While the simulation results suggest that retinal slip during visual-translation training contributed to updating the variance of the passive motion probability distribution (variance of process noise), the adjustment algorithm responsible for manipulating the parameter is not encompassed within the Kalman filter and will be implemented in our subsequent studies.

As shown in the Supplementary Results, Kalman gains vary with the stimulus because this model includes estimated gravity in the calculation of Kalman gains. This implies that our model is nonlinear, even though the Kalman filter itself has been designed for linear systems. Unlike Laurens' model, which operates linearly and maintains a state transition matrix with constant Kalman gain values over time. This is because we introduced the $\widehat{\boldsymbol{G}}$ from the previous time step, obtained using the Kalman filter, into the Kalman filter gain matrix. This enabled us to describe the calculation of state estimates realistically, addressing the issue posed by Laurens' model regarding the calculation of state estimates using the real state of $\boldsymbol{G}$, which the brain cannot inherently perceive. Despite the model becoming nonlinear as a consequence, we do not view it as a critical issue for interpreting the experimental data in the present study. This is because our objective in this modeling was not to derive a model where the animal's brain always accurately estimates the external world but to replicate the experimental results and examine how the animal's brain interprets sensory stimuli to output eye movements. In addition, we consider that the brains of animals, which sometimes have erroneous estimations, may not implement a model that functions accurately at all times. The success of the reproduction itself is demonstrated in the results. Nevertheless, this model should be further refined by incorporating an extended or unscented Kalman filter to make it more generalized because the generalization of the model should contribute to its reliability.

Moreover, the neural mechanisms and brain regions responsible for this variance adjustment occurring outside the framework of the Kalman filter model remain unknown. One possible brain network involved in this learning process could be located in the cerebellum, which has ample evidence of involvement in processing inertial motion and gravity signals (Yakusheva *et al.*, 2007). In any case, further investigation of this process is warranted.

3.2.3 VOR as an indicator of motion estimation

Instead of the unobservable motion perception of goldfish, we employed VOR as an indicator of motion estimation. The human torsional VOR around the x-axis and the horizontal VOR around the z-axis serve as rational eye movements for stabilizing vision

in front-eyed animals during roll-tilt and interaural translation, respectively. Hence, we interpreted the VORs around the x- and z-axes as the consequences of roll-tilt and interaural translation estimation, respectively. Although goldfish have relatively more lateralized eye positions than humans, we applied this concept to goldfish by assuming that they are also looking forward. This assumption is supported because the area where fish feed actively is located anteriorly, where their mouths are located, and prior studies (Tamura, 1957; Fernald, 1982; Zaunreiter *et al.*, 1991) have demonstrated binocular vision in the frontal visual field of some fish. Specifically, some reports suggest that binocular vision is available even in goldfish and their close relatives, Japanese dace, both of which belong to the Cyprinidae family (Hester, 1968; Inoue and Kuroiwa, 1975). Any uneasiness regarding the assumption that laterally eyed fish are looking forward is alleviated by two factors. First, the optical axis (the axis passing through the center of curvature of a lens or spherical mirror parallel to the axis of symmetry) does not coincide with the visual axis (the axis or chief ray of the actual pencil of rays that enter the pupil and converge to the fovea, coincident with the direction of gaze), even in humans (Liou and Brennan, 1997). Another is the observation that similar to primates, the visual axis in some fish (presumed to correspond to the area of high cone density on the retina) is directed forward—in the direction of active feeding behavior (Yamanouchi, 1956; Kimura and Tamura, 1966; Kawamura and Tamura, 1973; Somiya and Tamura, 1973; Kawamura, 1979; Kawamura and Ohashi, 1988; Momose *et al.*, 2003). Moreover, the eyes of goldfish are not completely lateral but slightly oriented forward, so their "optical axis" is not entirely parallel to the y-axis but is slightly directed forward. Consequently, even if goldfish do not exhibit binocular vision and their direction of sight coincides with the optical axis, compensatory eye movements for translation along the y-axis are likely to be horizontal around the z-axis. Furthermore, the induction of horizontal VOR in light with OKS in the forward field of view in this study itself could be considered an example of reflexive eye movement that stabilizes the frontal visual field in goldfish.

The VOR in the dark predominantly reflects head-motion estimations based solely on vestibular information. Similarly, because the VOR also shares pathways with the OKR (Raphan *et al.*, 1979), the VOR in light reflects head motion estimations based on both visual and vestibular information. Furthermore, motion perception is thought to be

formed through the integration of multimodal sensory information, such as vestibular, visual, and possibly proprioceptive inputs (Shaikh *et al.*, 2013; Angelaki and Laurens, 2020). Considering the hierarchical information processing in the brain, it seems reasonable to assume that high-spatiotemporal-resolution visual and vestibular information are initially used for primary self-motion estimation and swiftly employed in rapid motor control. Subsequently, it is suggested that additional sensory inputs (e.g., proprioception) would be integrated into this initial estimation to form conscious motion perception, which appears to require more time. In fact, the visual field stabilization provided by the VOR operates with a short latency of approximately 10 ms (Miles *et al.*, 2004), which is significantly faster than the perceptual process (Barnett-Cowan and Harris, 2009). Therefore, we considered the VOR, which we adopted as an indicator of motion estimation, to share initial pathways with motion perception and to reflect a more quantitative and rapid vestibular-based motion estimation than motion perception itself.

The foundational premise of our idea is the presence of a shared neural mechanism that potentially contributes to the VOR and motion perception (Shaikh *et al.*, 2013; Angelaki and Laurens, 2020). Previous findings have demonstrated that VORs reflect animal perceptions of head motion. For example, it has been demonstrated that humans perceive translational motion in parallel with presenting horizontal VOR during high-frequency (>4 Hz) periodic interaural translations (Telford *et al.*, 1997; Paige *et al.*, 1998; Merfeld *et al.*, 2005a; Clément *et al.*, 2022), while tilt perception and tortional VOR were induced during low-frequency (<1/20 Hz) or sustained linear accelerations in the dark (Seidman and Paige, 1996; Seidman *et al.*, 1998; Moore *et al.*, 2001; Clément *et al.*, 2001; Zupan and Merfeld, 2005; Merfeld *et al.*, 2005a; Clément *et al.*, 2022). These VORs compensate for perceived head motion in front-eyed animals, although the torsional VOR does not compensate for actual translational head motion. Similarly, both self-motion perception and VOR amplitude exhibited comparable high-pass filter like characteristics with increasing stimulus frequency from 0.025 to 0.4 Hz during whole body yaw rotation (Mergner *et al.*, 1991; Mergner *et al.*, 1998). Likewise, the similarity in the time constants of decay of post-rotational motion perception and VOR, both in normal subjects (Okada *et al.*, 1999; Bertolini *et al.*, 2011) and cerebellar patients (Bronstein *et al.*, 2008; Bertolini *et al.*, 2012), has been reported. Another similarity between perception and VOR is the

amount of noise as a function of the amplitude. Both dynamics depend on the sensory noise (observation noises of otolith signal $\boldsymbol{F}^{\eta}$, and semicircular canal signal $\boldsymbol{V}^{\eta}$ in Figure 2.3) (Nouri and Karmali, 2018; Madhani *et al.*, 2022). These lines of evidence confirm parallel changes in head motion perception and VOR (Pettorossi *et al.*, 2013). However, discrepancies between the VOR and motion perception have also been observed in specific situations (Zupan and Merfeld, 2005; Merfeld *et al.*, 2005b; Merfeld *et al.*, 2005a; Grabherr *et al.*, 2008; Clément *et al.*, 2008; Pettorossi *et al.*, 2013; Clément *et al.*, 2022). For instance, whereas the VOR and motion perception during interaural translation align at sufficiently high or low frequencies (Seidman and Paige, 1996; Telford *et al.*, 1997; Seidman *et al.*, 1998; Paige *et al.*, 1998; Moore *et al.*, 2001; Clément *et al.*, 2001; Zupan and Merfeld, 2005; Merfeld *et al.*, 2005a; Clément *et al.*, 2022), they do not align within the intermediate frequency range of approximately 0.1–1 Hz (Paige and Seidman, 1999; Merfeld *et al.*, 2005a; Clément *et al.*, 2022). Within this intermediate frequency range, translational acceleration stimulation along the y-axis induces a gradual shift in the VOR axis from torsional to horizontal in primates (Paige and Seidman, 1999; Merfeld *et al.*, 2005a). Conversely, within this range (specifically, 0.15–0.6 Hz), humans perceive linear translation (Merfeld *et al.*, 2005a; Clément *et al.*, 2022). Other studies on tilt and linear acceleration (Zupan and Merfeld, 2005; Merfeld *et al.*, 2005b; Merfeld *et al.*, 2005a; Clément *et al.*, 2008) and yaw rotation (Grabherr *et al.*, 2008; Pettorossi *et al.*, 2013) have also reported discrepancies between the VOR and perceived motion. These dual contradictory phenomena—the concordance and discordance between VOR and motion perception—may be explained by the presence of a vestibular-based common neural mechanism that contributes to both VOR and motion perception, along with subsequent neural mechanisms that exclusively affect motion perception. Indeed, studies involving the GABAergic medication 4-aminopyridine in humans and labyrinthectomy in monkeys have demonstrated significant impairments in the VOR and partial impairments in motion perception (Shaikh *et al.*, 2013; Angelaki and Laurens, 2020). These findings indicate that these interventions selectively disrupt the vestibular-based shared neural mechanisms contributing to both the VOR and motion perception, whereas the subsequent neural mechanisms exclusively affecting motion perception remain almost unaffected. This suggests that the coexistence of both shared and unshared pathways (Shaikh *et al.*, 2013; Angelaki and Laurens, 2020), also supports our idea that rapid vestibular-based motion

estimation is initially output as the VOR and that additional sensory inputs are subsequently integrated, forming motion perception.

4 TJ-014 effect in ROS-induced inner ear hair cell loss

4.1 Results

4.1.1 Protective effect of TJ-014

We assessed the therapeutic potential of TJ-014 to protect against GM-induced ototoxicity, presumed to be ROS-induced, at concentrations of 1, 10, and 100 μg/mL. The surviving OHCs were counted in F-actin-labeled surface preparations (Figure 4.1); the percentage of OHC survival in each group is shown in Figure 4.2. At 24 h after GM exposure, the surviving OHC percentages in the control group, the group treated with GM alone, and the groups treated with 1, 10, and 100 μg/mL of TJ-014 were 98.7 ± 13.7%, 83.3 ± 12.9%, 95.9 ± 6.39%, 96.2 ± 3.4%, and 98.4 ± 2.24%, respectively. Significant difference was observed between the groups treated with 1, 10, and 100 μg/mL of TJ-014 and the group treated with GM alone ($p < 0.01$) (Figure 4.2). At 48 h after GM exposure, the surviving OHC percentages in the control group, the group treated with GM alone, and the groups treated with 1, 10, and 100 μg/mL of TJ-014 were 89.7 ± 13.6%, 18.5 ± 8.57%, 29.4 ± 12.7%, 31.3 ± 10.2%, and 66.6 ± 14.3%, respectively. Significant differences were observed between the groups treated with 10 and 100 μg/mL of TJ-014 and the group treated with GM alone ($p < 0.01$) (Figure 4.2). These results showed that TJ-014 protected OHCs in a concentration-dependent manner against GM-induced toxicity in this rat model of cochlear damage.

4.1.2 TJ-014 suppresses caspase-3 activation

The time course of caspase-3 activation (a marker for apoptosis) was examined using fluorescent immunostaining for cleaved caspase-3 at 24 h and 48 h after GM exposure. Stronger immunoreactivity for cleaved caspase-3 was observed at 48 h after GM exposure than at 24 h. In the 24 h group, caspase-3 activation was observed in the groups treated with 1 mg/mL of TJ-014 and GM alone. In the 48 h group, strong immunoreactivity for cleaved caspase-3 was observed in the group treated with GM alone. In contrast, the number of cleaved caspase-3 positive OHCs was decreased by TJ-014 treatment, and these effects were correlated with increased TJ-014 concentrations (Figure 4.3). These results indicate that TJ-014 suppresses caspase-3 activation in a concentration-dependent

manner and strongly suggest that TJ-014 inhibits OHC apoptosis following GM exposure. OHCs in 24 h control group look disturbed compared to OHCs in 48 h control group, but no caspase-3 signal was detected. So, these disturbed OHCs images are probably artifact.

4.1.3 TJ-014 suppresses ROS generation

To confirm that GM causes ROS-induced ototoxicity and to evaluate the ROS-suppressing effect of TJ-014, we examined the time course of DNA oxidative damage in OHCs using 8-OHdG fluorescent immunostaining at 12 and 24 h post-GM exposure. Strong immunoreactivity for 8-OHdG was observed at 12 h post-GM exposure. Among the 12-hour groups, robust 8-OHdG immunoreactivity was detected in OHCs in the GM-alone group, while the number of 8-OHdG-positive OHCs decreased with TJ-014 treatment in a concentration-dependent manner (Figure 4.4). In the 24-hour groups, 8-OHdG-positive OHCs were detected only in the GM-alone group. These results indicate that while GM promotes ROS generation, TJ-014 effectively suppresses ROS production in a concentration-dependent manner. OHCs in 12 h control group look disturbed compared to OHCs in 24 h control group, but no 8-OHdG signal was detected. So, these disturbed OHCs images are also artifact.

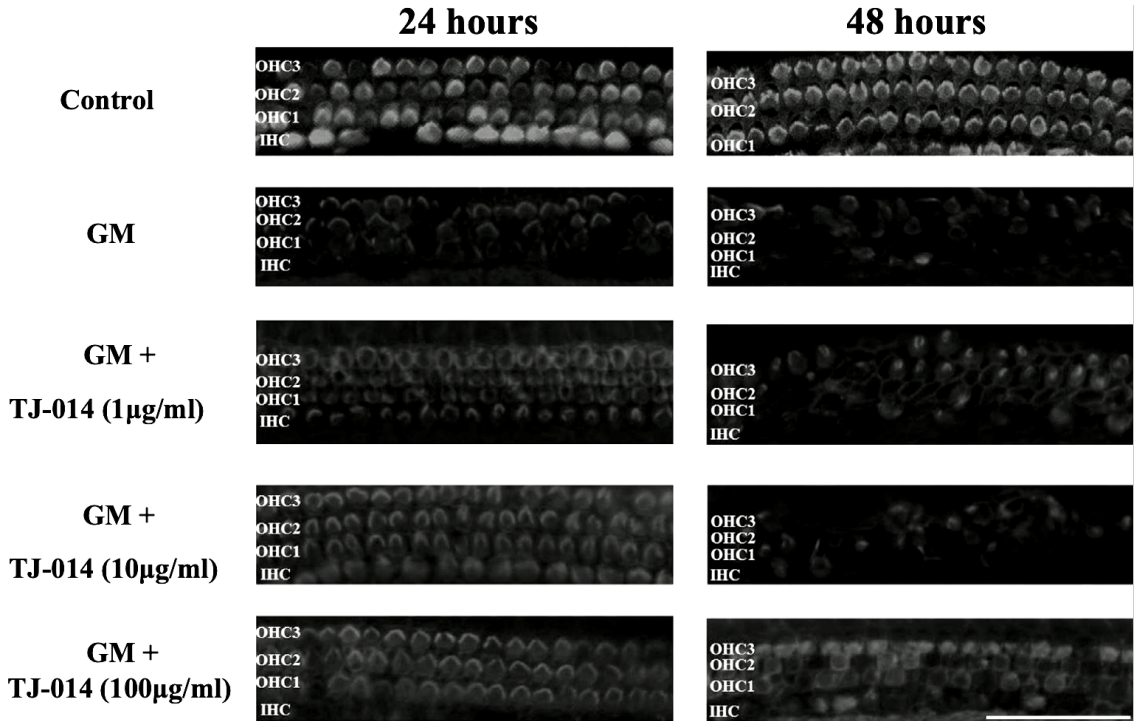


Figure 4.1. Representative fluorescence images of phalloidin-labeled hair cells treated under each condition: control, GM alone, or GM + TJ-014 (1, 10, or 100 μg/mL) at 24 and 48 h after GM exposure. In the group treated with GM alone, the images indicate that the number of surviving HCs is lower than in the TJ-014 treatment groups and that the shapes of the OHCs are warped. These effects are correlated with increasing TJ-014 concentration. HC, hair cell; GM, gentamicin; IHC, inner hair cell; OHC1, OHC2, OHC3, the first, second, and third rows of the outer hair cells, respectively. Scale bar, 50 μm.

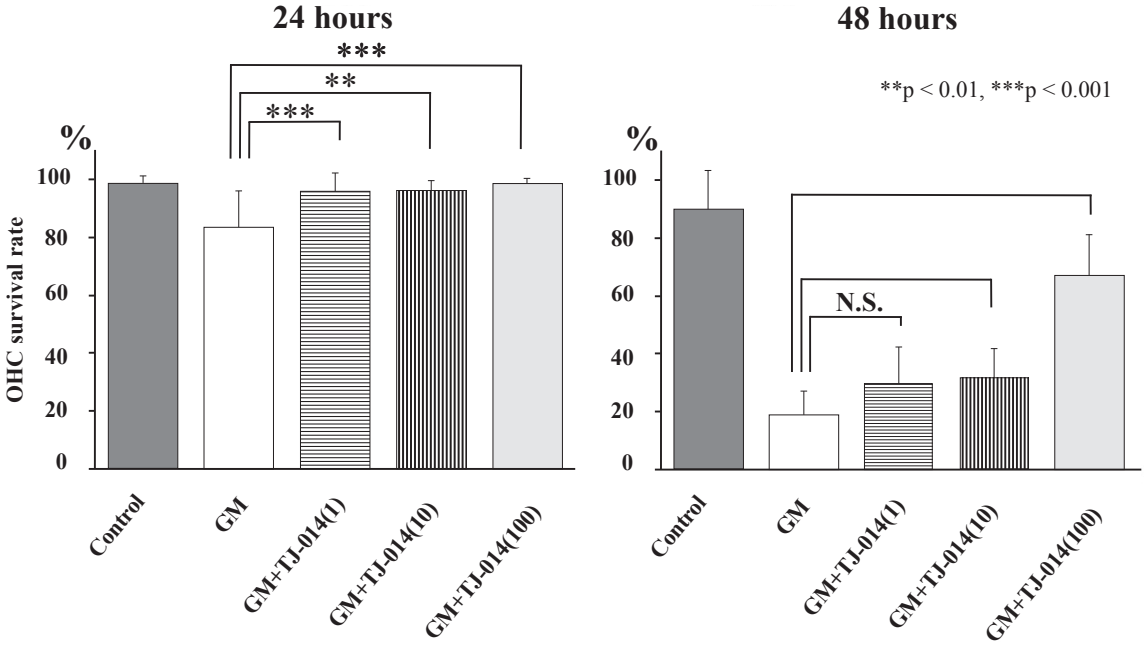


Figure 4.2. The survival ratios of the OHCs in each group. In the 24 h group, TJ-014 treatment significantly increased the OHC survival ratio compared with that of GM alone. Additionally, in the 48 h group, TJ-014 treatment (10 and 100 μg/mL) significantly increased the OHC survival ratio compared with that of GM alone. Error bars show the standard deviation (one-way ANOVA with Tukey's multiple comparison test). GM, gentamicin; OHC, outer hair cell; N.S., not significant; **: $p < 0.01$; ***: $p < 0.001$.

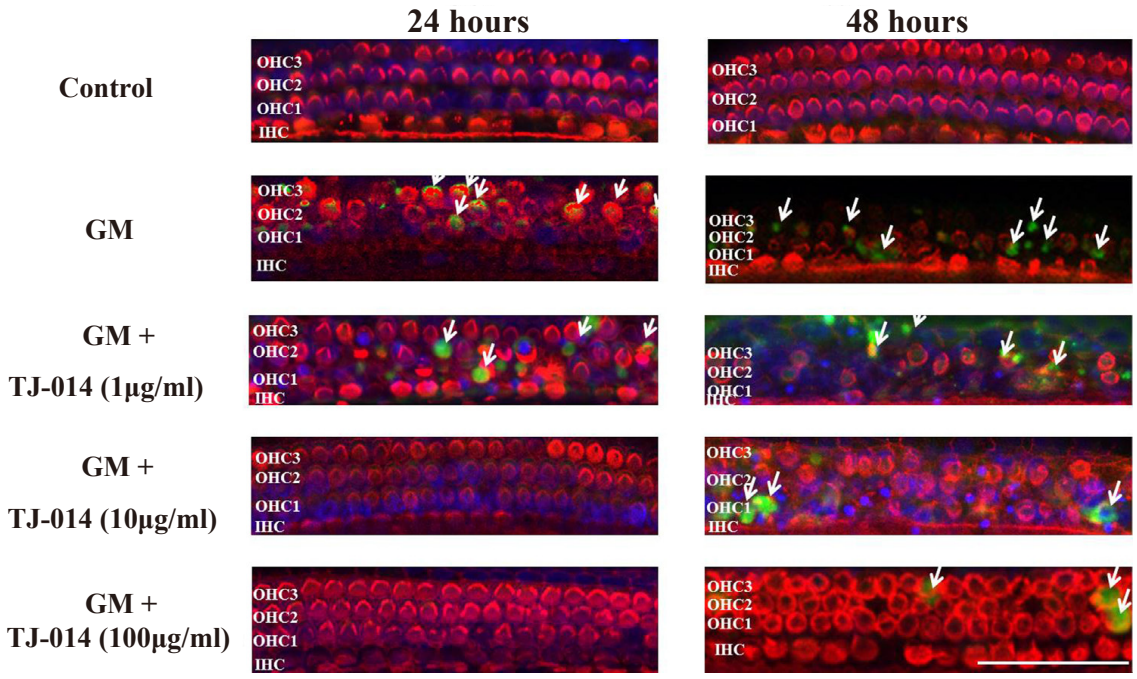


Figure 4.3. Representative fluorescence micrographs of cleaved caspase-3 (green), F-actin (red), and DAPI (blue). Many OHCs positive for cleaved caspase-3 are observed 48 h after GM exposure. OHCs treated with GM alone and GM + TJ-014 (1 mg/mL) show strong immunoreactivities for cleaved caspase-3. In contrast, less immunoreactivity is observed in the TJ-014 treatment (10 and 100 μg/mL) groups. These effects are correlated with increasing TJ-014 concentration. Arrows indicate OHCs exhibiting strong cleaved caspase-3 immunoreactivity. GM, gentamicin; IHC, inner hair cell; OHC1, OHC2, OHC3, the first, second, and third rows of the outer hair cells, respectively. Scale bar, 50 μm.

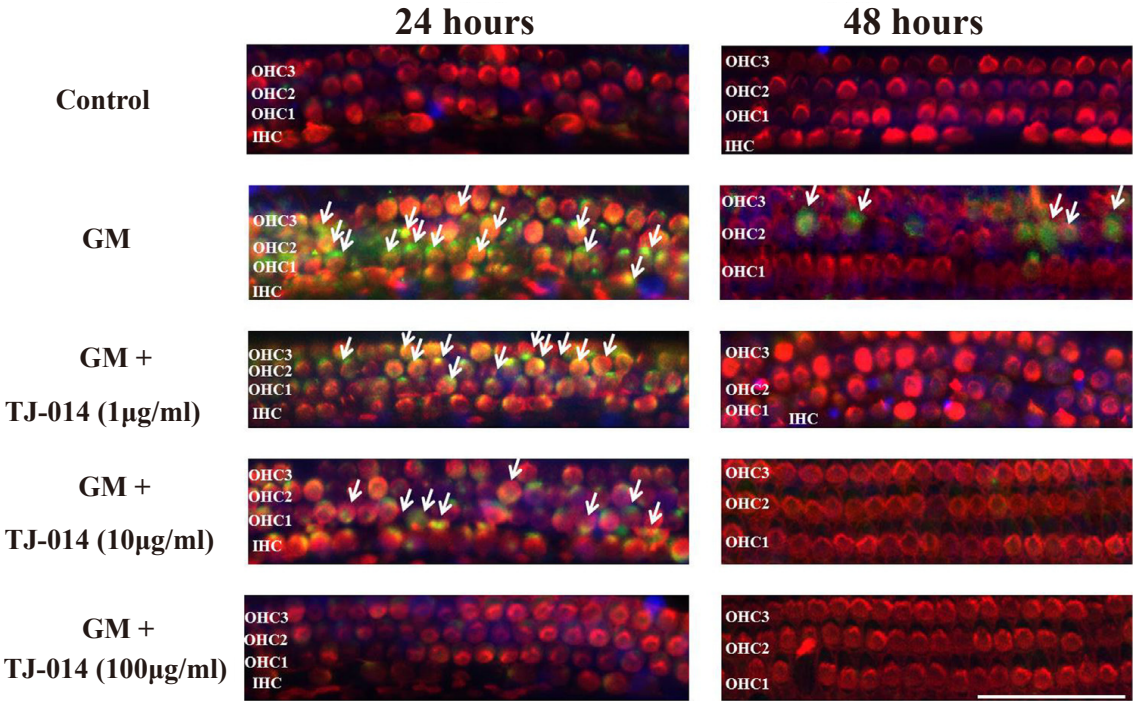


Figure 4.4. Representative fluorescence micrographs of 8-OHdG (green), F-actin (red), and DAPI (blue). Strong immunoreactivity for 8-OHdG is observed 12 h after GM exposure. OHCs treated with GM alone show strong immunoreactivities for 8-OHdG. In contrast, less immunoreactivity is observed in the TJ-014 treatment groups. These effects are correlated with increasing TJ-014 concentrations. Arrows indicate OHCs exhibiting strong 8-OHdG immunoreactivity. GM, gentamicin; IHC, inner hair cell; OHC1, OHC2, OHC3, the first, second, and third rows of the outer hair cells, respectively. Scale bar, 50 μm.

4.1.4 TJ-014 protects mitochondrial membrane potential

The time course of mitochondrial membrane potential damage (preceeding event to caspase-3 activation) was examined using MitoTracker® Red CMxRos in live cells at 12 h and 24 h after GM exposure. At both 12 h and 24 h, mitochondrial membrane potential damage was significantly suppressed in the group treated with 100 μg/mL of TJ- 014, although severe damage to the membrane potential was observed in the group treated with GM alone (Figure 4.5). Subsequently, we quantified the fluorescence level of the OHC mitochondrial membrane potential in each group (Figure 4.6). The mitochondrial membrane potential level in the TJ-014 (100 μg/mL) treatment group was significantly increased compared with that in the GM alone group at both 12 h and 24 h after GM exposure. These results show that TJ-014 protects the mitochondrial membrane potential of OHCs from ROS-induced damage following GM exposure.

4.2 Discussion

This study is the first report to evaluate the potential effects of TJ-014 against ROS-induced HC damage. There has been no paper about the beneficial effect of an oriental drug extract for ROS-induced HC damage.

A paper referred to the effects of baicalein, which is an ingredient of TJ-014, on the prevention of noise-induced hearing loss (Kang *et al.*, 2010), but discussed only function without a proposed mechanism. According to papers about the protective effect of TJ-014 for mucositis, the mechanisms of action of TJ-014 are mainly via anti-inflammatory effects through the enhancement of corticosterone and the suppression of Cyclooxygenase-2 (COX-2) and Prostaglandin E2 (PGE2) (Yamashita *et al.*, 2015). Berberine, which is also an ingredient of TJ-014, significantly protected gastric mucosa damaged with ethanol through the induction of endothelial nitric oxide synthase (eNOS) mRNA expression and the inhibition of inducible nitric oxide synthase (iNOS) mRNA expression in the stomach (PAN *et al.*, 2005). It is known that the induction of high-output iNOS usually occurs in an oxidative environment, and a high level of NO has the opportunity to react with a superoxide anion (O^-), leading to peroxynitrite ($ONOO^-$) formation and cell toxicity, protein tyrosine nitration, hydroxyl radical production, and

tissue damage (Guo, 2003; Ding *et al.*, 2005). In cases of cochlear damage by lipopolysaccharide (LPS) and acoustic overstimulation, iNOS expression was enhanced (Takumida *et al.*, 2000; Shi *et al.*, 2003; Shi and Nuttall, 2003). Additionally, another paper reported that guinea pigs that received a single intravenous administration of gentamicin showed rapid and profound hearing loss from upregulated expression of iNOS in the cochlea (Liu *et al.*, 2008).

This study shows that TJ-014 strongly suppressed ROS generation, damage to the mitochondrial membrane potential, and activation of caspase-3 in a concentration-dependent manner. These results suggest that the origin of the protective effect of TJ-014 is ROS scavenging. ROS scavenging leads to stabilization of the mitochondrial membrane potential and suppresses the activation of caspase-3. As a result, TJ-014 inhibits OHC apoptosis, as shown in this study.

Traditional oriental medicinal compounds contain undiscovered ingredients and antagonists, so there is a possibility that the effects of TJ-014 are not quite so simple. It is not clear if TJ-014 suppresses oxidative stress in the inner ear after being administered orally; however, drugs change into various substances after being metabolized in the intestine. For instance, CEP-1347, an inhibitor of the c-Jun N-terminal kinase apoptotic pathway, provided almost complete protection from AG-induced HC loss in culture (Pirvola *et al.*, 2000), but only achieved a modest 30% reduction in HC loss in vivo (Ylikoski *et al.*, 2002). Additionally, in vivo research using mature mice showed that the molecular features of classical apoptosis could not be detected during 14 days of continuous kanamycin administration (Jiang *et al.*, 2006), in contrast to organ cultures derived from neonatal animals. Therefore, a considerable body of literature implicates caspase- and JNK-dependent apoptotic pathways in HC death, though most of these studies were carried out in cells or organ cultures derived from neonatal animals. Moreover, around the time of cochlear maturation, a greater susceptibility to aminoglycoside antibiotics exists, clearly differentiating the response in a neonatal organ culture from that in a mature animal. Thus, there is a possibility that an in vivo study will lead to completely different results.

Keeping these points in mind, we plan to conduct an in vivo study and compare the results with those of the present study.

In conclusion, TJ-014 significantly suppressed oxidative stress by scavenging ROS and protected OHCs from apoptosis in vitro. The results strongly indicate the potential of TJ-014 to prevent inner ear disorders associated with ROS, thereby reducing the risk of spatial disorientation.

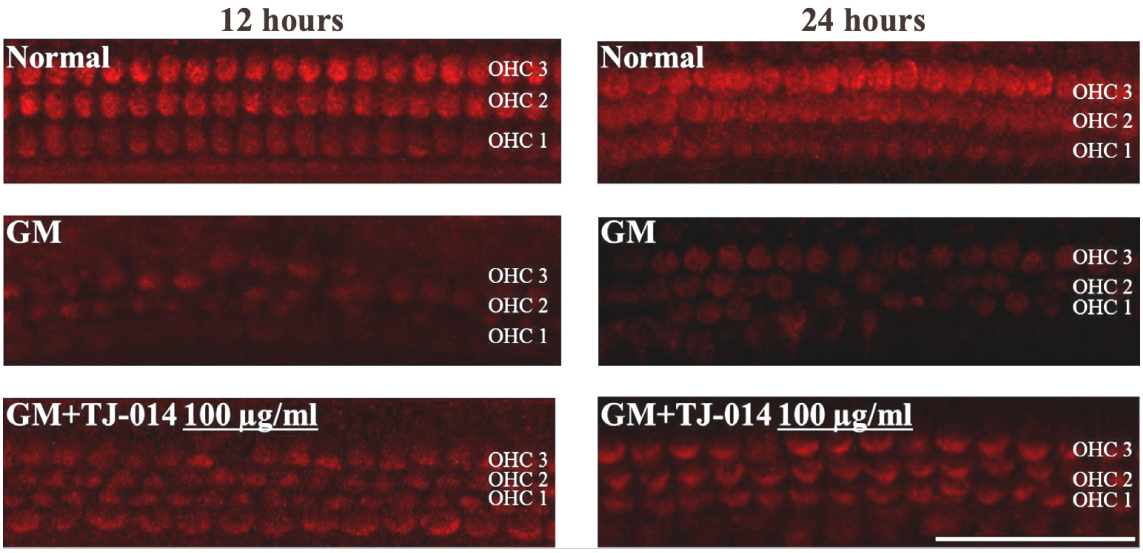


Figure 4.5. Representative micrographs of normal mitochondrial membrane potentials using MitoTracker® Red CMXRos, a selective mitochondrial probe. In the groups treated with GM alone, a collapse of the mitochondrial membrane potential is observed. In contrast, the mitochondrial membrane potentials of the HCs are in better condition in the group treated with GM + TJ-014 (100 µg/mL). GM, gentamicin; OHC1, OHC2, OHC3, the first, second, and third rows of the outer hair cells, respectively. Scale bar, 50 µm.

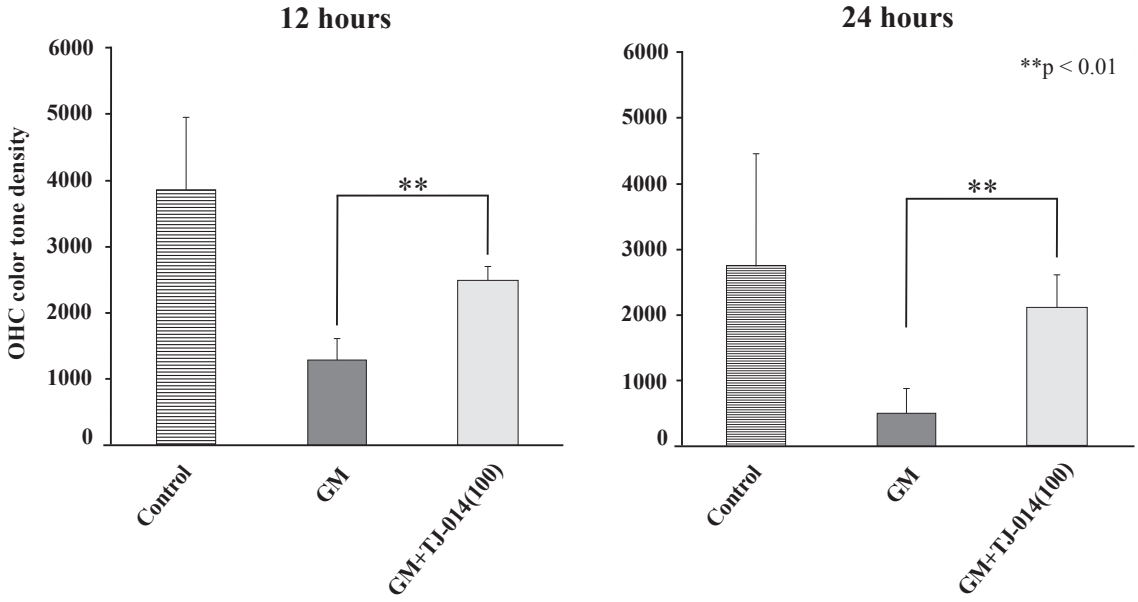


Figure 4.6. Comparisons of the density of MitoTracker® Red CMXRos using ImageJ. The mitochondrial membrane potential level in the TJ-014 (100 μg/mL) treatment group was significantly increased compared with that in the GM alone group at both 12 h and 24 h after GM exposure. Error bars show the standard deviation (one-way ANOVA with Tukey's multiple comparison test). GM, gentamicin; OHC, outer hair cell; **: $p < 0.01$.

5 Conclusion

This thesis investigated approaches to overcoming the limitations of the vestibular system to prevent spatial disorientation, emphasizing both visual-vestibular neural training and peripheral organ protection. Through two complementary studies, we addressed critical challenges in vestibular function, including the adaptive resolution of tilt-translation ambiguity and protective therapy for oxidative stress-induced damage to sensory cells, to advance our understanding of spatial orientation and provide practical solutions to spatial disorientation.

Central Training: Visual-Vestibular Neural Training to Resolve Tilt-Translation Ambiguity

The first study explored the adaptive capabilities of the central nervous system to resolve tilt-translation ambiguity based on accumulated motion experiences. Behavioral experiments using goldfish revealed that visual-vestibular neural training involving interaural linear translation and visual stimuli enhanced their vestibulo-ocular reflex (VOR) performance. Pre- and post-training analyses demonstrated that goldfish improved their head motion estimates, reducing errors associated with tilt-translation ambiguity. By extending the Kalman filter model of spatial orientation, we replicated these behavioral changes computationally, offering insights into the neural mechanisms underlying adaptive process. These findings underscore the importance of experience-based training protocols in mitigating spatial disorientation, particularly for environments where natural motion experiences are insufficient, such as aviation and space exploration.

Peripheral Protection: Preventing ROS-Induced Inner Ear Damage

The second study demonstrated the potential of the Kampo formula Hangesha-shin-to (TJ-014) as a protective agent against oxidative stress-induced damage to inner ear hair cells. Using rat organ of Corti explants, we showed that TJ-014's active components, including baicalein, baicalin, wogonin, and berberine, reduced ROS-induced apoptosis and preserved hair cell integrity under gentamicin-induced stress. Immunohistochemical analyses confirmed that TJ-014 mitigated oxidative stress and apoptosis, highlighting its capacity to prevent ROS-mediated ototoxicity. These findings provide a foundation for

developing pharmacological interventions targeting vestibular disorders associated with oxidative stress, particularly for high-risk groups such as aviation personnel. However, further translational studies are required to validate the clinical efficacy and safety of TJ-014 under real-world conditions.

Integration and Future Directions

By addressing both central and peripheral mechanisms, this thesis highlights a holistic approach to tackling spatial disorientation. The findings emphasize the need for integrated strategies that combine training protocols that leverage the brain's plasticity to adapt to novel motion environments with pharmacological protection of the vestibular organs. Future research should aim to:

1. Enhance Training Protocols: Develop and experimentally validate advanced training programs for pilots and astronauts, incorporating simulated motion environments to accelerate adaptive learning.

2. Elucidate Neural Mechanisms: Investigate the detailed neural circuits and plasticity mechanisms involved in resolving sensory ambiguities, using animal models and advanced brain activity visualization techniques.

3. Expand Translational Applications: Conduct clinical trials to assess the feasibility of TJ-014 and related antioxidants for protecting vestibular function in humans, particularly in high-stress occupational settings.

Ultimately, this work contributes to the scientific understanding of vestibular limitations and their solutions, paving the way for innovations in preventing spatial disorientation. By integrating central training and peripheral protection, it offers a comprehensive framework to enhance spatial orientation, ensuring safety and performance in challenging environments.

References

Aksay E, Baker R, Seung HS and Tank DW (2000) 'Anatomy and discharge properties of pre-motor neurons in the goldfish medulla that have eye-position signals during fixations', *Journal of Neurophysiology*, 84(2):1035–1049, doi:10.1152/jn.2000.84.2.1035.

Angelaki DE and Dickman JD (2000) 'Spatiotemporal processing of linear acceleration: primary afferent and central vestibular neuron responses', *Journal of Neurophysiology*, 84(4):2113–2132, doi:10.1152/JN.2000.84.4.2113.

Angelaki DE and Laurens J (2020) 'Time course of sensory substitution for gravity sensing in visual vertical orientation perception following complete vestibular loss', *eNeuro*, 7(4):1–13, doi:10.1523/ENEURO.0021-20.2020.

Angelaki DE, McHenry MQ, Dickman JD, Newlands SD and Hess BJM (1999) 'Computation of inertial motion: neural strategies to resolve ambiguous otolith information', *Journal of Neuroscience*, 19(1):316, doi:10.1523/JNEUROSCI.19-01-00316.1999.

Angelaki DE, Shaikh AG, Green AM and Dickman JD (2004) 'Neurons compute internal models of the physical laws of motion', *Nature*, 430(6999):560–564, doi:10.1038/nature02754.

Bae YS, Oh H, Rhee SG and Yoo Y Do (2011) 'Regulation of reactive oxygen species generation in cell signaling', *Molecules and Cells*, 32(6):491–509, doi:10.1007/s10059-011-0276-3.

Barnett-Cowan M and Harris LR (2009) 'Perceived timing of vestibular stimulation relative to touch, light and sound', *Experimental Brain Research*, 198(2–3):221–231, doi:10.1007/S00221-009-1779-4.

Beck JC, Gilland E, Tank DW and Baker R (2004) 'Quantifying the ontogeny of optokinetic and vestibuloocular behaviors in zebrafish, medaka, and goldfish', *Journal of Neurophysiol*, 92:3546–3561, doi:10.1152/jn.00311.2004.

Bertolini G, Ramat S, Bockisch CJ, Marti S, Straumann D and Palla A (2012) 'Is vestibular self-motion perception controlled by the velocity storage? Insights from patients with chronic degeneration of the vestibulo-cerebellum', *PloS one*, 7(6), doi:10.1371/JOURNAL.PONE.0036763.

Bertolini G, Ramat S, Laurens J, Bockisch CJ, Marti S, Straumann D and Palla A (2011) 'Velocity storage contribution to vestibular self-motion perception in healthy human subjects', *Journal of Neurophysiology*, 105(1):209–223, doi:10.1152/JN.00154.2010.

Bos JE and Bles W (2002) 'Theoretical considerations on canal-otolith interaction and an observer model', *Biological Cybernetics*, 86(3):191–207, doi:10.1007/S00422-001-0289-7.

Brieger K, Schiavone S, Miller Jr and Krause K (2012) 'Reactive oxygen species: from health to disease', *Swiss Medical Weekly*, doi:10.4414/smw.2012.13659.

Bronstein AM, Grunfeld EA, Faldon M and Okada T (2008) 'Reduced self-motion perception in patients with midline cerebellar lesions', *Neuroreport*, 19(6):691–693, doi:10.1097/WNR.0B013E3282FBF9F6.

Carriot J, Jamali M, Chacron MJ and Cullen KE (2017) 'The statistics of the vestibular input experienced during natural self-motion differ between rodents and primates', *Journal of Physiology*, 595(8):2751–2766, doi:10.1113/JP273734.

Cheung B, Money K, Wright H and Bateman W (1995) 'Spatial disorientation-implicated accidents in Canadian forces, 1982-92.', *Aviation, Space, and Environmental Medicine*, 66(6):579–85.

Choung YH, Taura A, Pak K, Choi SJ, Masuda M and Ryan AF (2009) 'Generation of highly-reactive oxygen species is closely related to hair cell damage in rat organ of corti treated with gentamicin', *Neuroscience*, 161(1):214–226, doi:10.1016/j.neuroscience.2009.02.085.

Clément G, Beaton KH, Reschke MF and Wood SJ (2022) 'Effects of motion paradigm on human perception of tilt and translation', *Scientific Reports*, 12(1):1–14, doi:10.1038/s41598-022-05483-6.

Clément G, Denise P, Reschke MF and Wood SJ (2008) 'Human ocular counter-rolling and roll tilt perception during off-vertical axis rotation after spaceflight', *Journal of Vestibular Research*, 17(5–6):209–215, doi:10.3233/VES-2007-175-602.

Clément G, Moore ST, Raphan T and Cohen B (2001) 'Perception of tilt (somatogravic illusion) in response to sustained linear acceleration during space flight', *Experimental Brain Research*, 138(4):410–418, doi:10.1007/S002210100706.

Cohen B, Matsuo V and Raphan T (1977) 'Quantitative analysis of the velocity characteristics of optokinetic nystagmus and optokinetic after-nystagmus', *Journal of Physiology*, 270(2):321–344, doi:10.1113/JPHYSIOL.1977.SP011955.

Debowy O and Baker R (2011) 'Encoding of eye position in the goldfish horizontal oculomotor neural integrator', *Journal of Neurophysiology*, 105(2):896–909, doi:10.1152/JN.00313.2010.

Ding H, Zhu H, Dong J, Zhu W, Yang W, Yang H and Zhou Z (2005) 'Inducible nitric oxide synthase contributes to intermittent hypoxia against ischemia/reperfusion injury1', *Acta Pharmacologica Sinica*, 26(3):315–322, doi:10.1111/j.1745-7254.2005.00046.x.

Fernald RD (1982) 'Retinal projections in the African cichlid fish, Haplochromis burtoni', *Journal of Comparative Neurology*, 206(4):379–389, doi:10.1002/CNE.902060406.

Fernandez C and Goldberg JM (1976) 'Physiology of peripheral neurons innervating otolith organs of the squirrel monkey. I. Response to static tilts and to long-duration centrifugal force', 39(5):970–984, doi:10.1152/JN.1976.39.5.970.

Fetoni AR, Sergi B, Scarano E, Paludetti G, Ferraresi A and Troiani D (2003a) 'Protective effects of alpha-tocopherol against gentamicin-induced Oto-vestibulo

toxicity: an experimental study', *Acta Oto-Laryngologica*, 123(2):192–198, doi:10.1080/00016480310001484.

Flight Standards Division (2005) 航空機乗組員の使用する医薬品の取り扱いに関する指針 (国空乗第 491 号), Ministry of Land, Infrastructure, Transport and Tourism, Civil Aviation Bureau, Aviation Safety and Security Department, Japan, https://www.mlit.go.jp/notice/noticedata/pdf/20180801/10-004.pdf, accessed 5 December 2024.

Gestrin P and Sterling P (1977) 'Anatomy and physiology of goldfish oculomotor system. II. Firing patterns of neurons in abducens nucleus and surrounding medulla and their relation to eye movements', *Journal of Neurophysiology*, 40(3):573–588, doi:10.1152/jn.1977.40.3.573.

Gibb R, Ercoline B and Scharff L (2011) 'Spatial disorientation: Decades of pilot fatalities', *Aviation Space and Environmental Medicine*, 82(7):717–724, doi:10.3357/ASEM.3048.2011.

Gillingham K and Wolfe J (1985) 'Spatial orientation in flight', in R DeHart (ed) *Fundamentals of Aerospace Medicine*, Lea & Febiger, Philadelphia, doi:10.1016/0735-6757(87)90303-2.

Gillingham KK (1992) 'The spatial disorientation problem in the United States Air Force', *Journal of Vestibular Research*, 2:297–306. PMID: 1342404.

Goldstein H (1980) *Classical mechanics*, 2nd ed, Addison-Wesley, https://ci.nii.ac.jp/ncid/BA00434784, accessed 14 September 2023.

Goto F, Ide R, Yabe H, Kunihiro T and Ogawa K (2009) 'Oxidative stress and Ménière's disease and benign paroxysmal positional vertigo', *Equilibrium Research*, 68(1):9–13, doi:10.3757/JSER.68.9.

Grabherr L, Nicoucar K, Mast FW and Merfeld DM (2008) 'Vestibular thresholds for yaw rotation about an earth-vertical axis as a function of frequency', *Experimental Brain Research*, 186(4):677–681, doi:10.1007/S00221-008-1350-8.

Guo J-S (2003) ‘Expression and activities of three inducible enzymes in the healing of gastric ulcers in rats’, *World Journal of Gastroenterology*, 9(8):1767, doi:10.3748/wjg.v9.i8.1767.

Hess BJM and Angelaki DE (1997) ‘Inertial vestibular coding of motion: concepts and evidence’, *Current Opinion in Neurobiology*, 7(6):860–866, doi:10.1016/S0959-4388(97)80147-X.

Hester FJ (1968) ‘Visual contrast thresholds of the goldfish (*Carassius auratus*)’, *Vision Research*, 8(10):1315–1336, doi:10.1016/0042-6989(68)90053-9.

Highstein SM, Rabbitt RD, Holstein GR and Boyle RD (2005) ‘Determinants of spatial and temporal coding by semicircular canal afferents’, *Journal of Neurophysiology*, 93(5):2359–2370, doi:10.1152/JN.00533.2004.

Holmes SR, Bunting A, Brown DL, Hiatt KL, Braithwaite MG and Harrigan MJ (2003) ‘Survey of spatial disorientation in military pilots and navigators’, *Aviation, Space, and Environmental Medicine*, 74(9):957–65, PMID: 14503674.

Inoue M and Kuroiwa H (1975) ‘The effect of symmetrical stimuli on the optomotor reaction of fish’, *Bulletin of the Japanese Society of Scientific Fisheries*, 41(12):1219–1227, doi:10.2331/suisan.41.1219.

Jiang H, Sha S-H, Forge A and Schacht J (2006) ‘Caspase-independent pathways of hair cell death induced by kanamycin in vivo’, *Cell Death & Differentiation*, 13(1):20–30, doi:10.1038/sj.cdd.4401706.

Kaneko CRS (1997) ‘Eye movement deficits after ibotenic acid lesions of the nucleus prepositus hypoglossi in monkeys. I. Saccades and fixation’, *Journal of Neurophysiology*, 78(4):1753–1768, doi:10.1152/JN.1997.78.4.1753.

Kang TH, Hong BN, Park C, Kim SY and Park R (2010) ‘Effect of baicalein from Scutellaria baicalensis on prevention of noise-induced hearing loss’, *Neuroscience Letters*, 469(3):298–302, doi:10.1016/j.neulet.2009.12.009.

Kawamura G (1979) ‘Fundamental study on application of the vision of spotted mackerel, Pneumatophorutsa peinocephalus (Bleeker) , to angling techniques: I Importance of vision estimated from brain pattern, visual acuity of retina, and accommodation’, *Bulletin of the Japanese Society of Scientific Fisheries*, 45(3):281–286, doi:10.2331/suisan.45.281.

Kawamura G and Ohashi S (1988) ‘The habit of cutlassfish as inferred from the retina’, *Bulletin of the Japanese Society of Scientific Fisheries*, 54(5):889–889, doi:10.2331/suisan.54.889.

Kawamura G and Tamura T (1973) ‘Morphological studies on the retina of two teleosts Scomber tapeinocephalus and Halichoeres poecilopterus’, *Bulletin of the Japanese Society of Scientific Fisheries*, 39(7):715–726, doi:10.2331/suisan.39.715.

Kelley MW (2007) ‘Cellular commitment and differentiation in the organ of Corti’, *The International Journal of Developmental Biology*, 51(6–7):571–583, doi:10.1387/ijdb.072388mk.

Kheradmand A and Otero-Millan J (2019) ‘Spatial orientation: Model-based approach to multi-sensory mechanisms’, *Progress in Brain Research*, 248:209–223, doi:10.1016/BS.PBR.2019.04.029.

Kikkawa YS, Nakagawa T, Horie RT and Ito J (2009) ‘Hydrogen protects auditory hair cells from free radicals’, *NeuroReport*, 20(7):689–694, doi:10.1097/WNR.0B013E32832A5C68.

Kimura K and Tamura T (1966) ‘On the direction of the lens movement in the visual accommodation of teleostean eyes’, *Bulletin of the Japanese Society of Scientific Fisheries*, 32(2):112–116, doi:10.2331/suisan.32.112.

Kishimoto-Urata M, Urata S, Fujimoto C and Yamasoba T (2022) ‘Role of oxidative stress and antioxidants in acquired Inner ear disorders’, *Antioxidants*, 11(8):1469, doi:10.3390/antiox11081469.

Kleinschmidt A (2002) ‘Neural correlates of visual-motion perception as object- or self-motion’, *NeuroImage*, 16(4):873–882, doi:10.1006/nimg.2002.1181.

Kono T (2010) ‘Topical application of Hangeshashinto (TJ-14) in the treatmentof chemotherapy-induced oral mucositis’, *World Journal of Oncology*, 1(6), doi:10.4021/wjon263w.

Kuki Y, Hirata Y, Blazquez PM, Heiney SA and Highstein SM (2004) ‘Memory retention of vestibuloocular reflex motor learning in squirrel monkeys’, *NeuroReport*, 15(6):1007–1011, doi:10.1097/00001756-200404290-00015.

L. Poirrier A, Pincemail J, Van Den Ackerveken P, P. Lefebvre P and Malgrange B (2010) ‘Oxidative stress in the cochlea: an update’, *Current Medicinal Chemistry*, 17(30):3591–3604, doi:10.2174/092986710792927895.

Laurens J and Angelaki DE (2011) ‘The functional significance of velocity storage and its dependence on gravity’, *Experimental Brain Research*, 210(3–4):407–422, doi:10.1007/s00221-011-2568-4.

Laurens J and Angelaki DE (2017) ‘A unified internal model theory to resolve the paradox of active versus passive self-motion sensation’, *eLife*, 6, doi:10.7554/ELIFE.28074.

Laurens J and Droulez J (2007) ‘Bayesian processing of vestibular information’, *Biological Cybernetics*, 96:389–404, doi:10.1007/s00422-006-0133-1.

Lichtenberg BK, Young LR and Arrott AP (1982) ‘Human ocular counterrolling induced by varying linear accelerations’, *Experimental Brain Research*, 48(1):127–136, doi:10.1007/BF00239580.

Liou H-L and Brennan NA (1997) ‘Anatomically accurate, finite model eye for optical modeling’, *Journal of the Optical Society of America A*, 14(8):1684–1695, doi:10.1364/JOSAA.14.001684.

Liu H, Chi F and Gao W (2008) ‘Taurine attenuates aminoglycoside ototoxicity by inhibiting inducible nitric oxide synthase expression in the cochlea’, *NeuroReport*, 19(1):117–120, doi:10.1097/WNR.0b013e3282f3b0ec.

MacNeilage PR, Ganesan N and Angelaki DE (2008) ‘Computational approaches to spatial orientation: From transfer functions to dynamic bayesian inference’, *Journal of Neurophysiology*, 100(6):2981–2996, doi:10.1152/jn.90677.2008.

Madhani A, Lewis RF and Karmali F (2022) ‘How peripheral vestibular damage affects velocity storage: a causative explanation’, *Journal of the Association for Research in Otolaryngology : JARO*, 23(4):551–566, doi:10.1007/S10162-022-00853-3.

Major G, Baker R, Aksay E, Seung HS and Tank DW (2004) ‘Plasticity and tuning of the time course of analog persistent firing in a neural integrator’, *Proceedings of the National Academy of Sciences*, 101(20):7745–7750, doi:10.1073/pnas.0401992101.

Marsh E and Baker R (1997) ‘Normal and adapted visuooculomotor reflexes in goldfish’, *Journal of Neurophysiology*, 77(3):1099–1118, doi:10.1152/JN.1997.77.3.1099.

Mehlman ML and Taube JS (2018) ‘In vivo electrophysiological approaches for studying head direction cells’, *Handbook of Behavioral Neuroscience*, 28:169–187, doi:10.1016/B978-0-12-812028-6.00009-4.

Merfeld DM (1995) ‘Modeling the vestibulo-ocular reflex of the squirrel monkey during eccentric rotation and roll tilt’, *Experimental Brain Research*, 106(1):123–134, doi:10.1007/BF00241362.

Merfeld DM, Park S, Gianna-Poulin C, Black FO and Wood S (2005a) ‘Vestibular perception and action employ qualitatively different mechanisms. I. Frequency response of VOR and perceptual responses during translation and tilt’, *Journal of Neurophysiology*, 94(1):186–198, doi:10.1152/jn.00904.2004.

Merfeld DM, Park S, Gianna-Poulin C, Black FO, Wood S (2005b) ‘Vestibular perception and action employ qualitatively different mechanisms. II. VOR and

perceptual responses during combined tilt and translation', *Journal of Neurophysiology*, 94(1):199–205, doi:10.1152/JN.00905.2004.

Merfeld DM, Young LR, Oman CM and Shelhamer MJ (1993) 'A multidimensional model of the effect of gravity on the spatial orientation of the monkey', *Journal of Vestibular Research*, 3(2):141–161, doi:10.3233/VES-1993-3204.

Merfeld DM, Zupan L and Peterka RJ (1999) 'Humans use internal models to estimate gravity and linear acceleration', *Nature*, 398(6728):615–618, doi:10.1038/19303.

Mergner T and Glasauer S (1999) 'A simple model of vestibular canal-otolith signal fusion', *Annals of the New York Academy of Sciences*, 871:430–434, doi:10.1111/J.1749-6632.1999.TB09211.X.

Mergner T, Schweigart G, Botti F and Lehmann A (1998) 'Eye movements evoked by proprioceptive stimulation along the body axis in humans', *Experimental Brain Research*, 120(4):450–460, doi:10.1007/S002210050418.

Mergner T, Siebold C, Schweigart G and Becker W (1991) 'Human perception of horizontal trunk and head rotation in space during vestibular and neck stimulation', *Experimental Brain Research*, 85(2):389–404, doi:10.1007/BF00229416.

Migliaccio AA, Minor LB and Santina CC Della (2010) 'Adaptation of the vestibulo-ocular reflex for forward-eyed foveate vision', *Journal of Physiology*, 588(20):3855–3867, doi:10.1113/jphysiol.2010.196287.

Miki S, Baker R and Hirata Y (2018) 'Cerebellar role in predictive control of eye velocity initiation and termination', *Journal of Neuroscience*, 38(48):10371–10383, doi:10.1523/JNEUROSCI.1375-18.2018.

Miki S, Urase K, Baker R and Hirata Y (2020) 'Velocity storage mechanism drives a cerebellar clock for predictive eye velocity control', *Scientific Reports*, 10(1):6944, doi:10.1038/s41598-020-63641-0.

Miles FA, Busettini C, Masson GS and Yang DS (2004) 'Short-latency eye movements: evidence for rapid, parallel processing of optic flow', In: Vaina LM, Beardsley SA, Rushton SK. (eds) Optic Flow and Beyond. Synthese Library, vol. 324, Springer, Dordrecht, pp. 79–107, doi: 10.1007/978-1-4020-2092-6_5.

Møller P, Wallin H and Knudsen LE (1996) 'Oxidative stress associated with exercise, psychological stress and life-style factors', *Chemico-Biological Interactions*, 102(1):17–36, doi:10.1016/0009-2797(96)03729-5.

Momose O, Takei S, Maekawa Y, Uchida M and Somiya H (2003) 'Visual accommodation system and retinal ganglion cell distribution in the retina of a dolphin fish, Coryphaena hippurus', *Bulletin of the Japanese Society of Scientific Fisheries*, 69(6):933–939, doi:10.2331/SUISAN.69.933.

Moore ST, Clément G, Raphan T and Cohen B (2001) 'Ocular counterrolling induced by centrifugation during orbital space flight', *Experimental Brain Research*, 137(3–4):323–335, doi:10.1007/S002210000669.

Niwa K, Matsunobu T, Kurioka T, Kamide D, Tamura A, Tadokoro S, Satoh Y and Shiotani A (2016) 'The beneficial effect of Hangesha-shin-to (TJ-014) in gentamicin-induced hair cell loss in the rat cochlea', *Auris, Nasus, Larynx*, 43(5):507–513, doi:10.1016/J.ANL.2015.12.012.

Nooij SAE, Pretto P and Bülthoff HH (2018) 'More vection means more velocity storage activity: a factor in visually induced motion sickness?', *Experimental Brain Research*, 236(11):3031–3041, doi:10.1007/S00221-018-5340-1.

Nouri S and Karmali F (2018) 'Variability in the vestibulo-ocular reflex and vestibular perception', *Neuroscience*, 393:350–365, doi:10.1016/J.NEUROSCIENCE.2018.08.025.

Okada T, Grunfeld E, Shallo-Hoffmann J and Bronstein AM (1999) 'Vestibular perception of angular velocity in normal subjects and in patients with congenital nystagmus', *Brain : A Journal of Neurology*, 122 (Pt 7)(7):1293–1303, doi:10.1093/BRAIN/122.7.1293.

Paige GD and Seidman SH (1999) ‘Characteristics of the VOR in response to linear acceleration’, *Annals of the New York Academy of Sciences*, 871(1):123–135, doi:10.1111/J.1749-6632.1999.TB09179.X.

Paige GD, Telford L, Seidman SH and Barnes GR (1998) ‘Human vestibuloocular reflex and its interactions with vision and fixation distance during linear and angular head movement’, *Journal of Neurophysiology*, 80(5):2391–2404, doi:10.1152/JN.1998.80.5.2391.

Paige GD and Tomko DL (1991) ‘Eye movement responses to linear head motion in the squirrel monkey. I. Basic characteristics’, *Journal of Neurophysiology*, 65(5):1170–1182, doi:10.1152/jn.1991.65.5.1170.

Pan L, Tang Q, Fu Q, Hu B, Xiang J and Qian J (2005) ‘Roles of nitric oxide in protective effect of berberine in ethanol-induced gastric ulcer mice1’, *Acta Pharmacologica Sinica*, 26(11):1334–1338, doi:10.1111/j.1745-7254.2005.00186.x.

Pastor AM, de la Cruz RR and Baker R (1992) ‘Characterization and adaptive modification of the goldfish vestibuloocular reflex by sinusoidal and velocity step vestibular stimulation’, *Journal of Neurophysiology*, 68(6):2003–2015, doi:10.1152/jn.1992.68.6.2003.

Pettorossi VE, Panichi R, Botti FM, Kyriakareli A, Ferraresi A, Faralli M, Schieppati M and Bronstein AM (2013) ‘Prolonged asymmetric vestibular stimulation induces opposite, long-term effects on self-motion perception and ocular responses’, *Journal of Physiology*, 591(7):1907–1920, doi:10.1113/JPHYSIOL.2012.241182.

Pirvola U, Xing-Qun L, Virkkala J, Saarma M, Murakata C, Camoratto AM, Walton KM and Ylikoski J (2000) ‘Rescue of Hearing, Auditory Hair Cells, and Neurons by CEP-1347/KT7515, an Inhibitor of c-Jun N-Terminal Kinase Activation’, *Journal of Neuroscience*, 20(1):43–50, doi:10.1523/JNEUROSCI.20-01-00043.2000.

Raphan T, Matsuo V and Cohen B (1979) ‘Velocity storage in the vestibulo-ocular reflex arc (VOR)’, *Experimental Brain Research*, 35(2):229–248, doi:10.1007/BF00236613.

Rizzi MD and Hirose K (2007) ‘Aminoglycoside ototoxicity’, *Current Opinion in Otolaryngology & Head & Neck Surgery*, 15(5):352–357, doi:10.1097/MOO.0b013e3282ef772d.

Seidman SH and Paige GD (1996) ‘Perception and eye movement during low-frequency centripetal acceleration’, *Annals of the New York Academy of Sciences*, 781:693–695, doi:10.1111/j.1749-6632.1996.tb15762.x.

Seidman SH, Telford L and Paige GD (1998) ‘Tilt perception during dynamic linear acceleration’, *Experimental Brain Research*, 119(3):307–314, doi:10.1007/S002210050346.

Selimoglu E (2007) ‘Aminoglycoside-induced ototoxicity’, *Current Pharmaceutical Design*, 13(1):119–126, doi:10.2174/138161207779313731.

Sena LA and Chandel NS (2012) ‘Physiological roles of mitochondrial reactive oxygen species’, *Molecular Cell*, 48(2):158–167, doi:10.1016/j.molcel.2012.09.025.

Shaikh AG, Palla A, Marti S, Olasagasti I, Optican LM, Zee DS and Straumann D (2013) ‘Role of cerebellum in motion perception and vestibulo-ocular reflex - Similarities and disparities’, *Cerebellum*, 12(1):97–107, doi:10.1007/S12311-012-0401-7.

Sharma SK (2015) ‘Indian Air Force and US Air Force spatial disorientation countermeasure training : A comparison’, *Indian Journal of Aerospace Medicine*, 59(1):33–41.

Shi X, Dai C and Nuttall AL (2003) ‘Altered expression of inducible nitric oxide synthase (iNOS) in the cochlea’, *Hearing Research*, 177(1–2):43–52, doi:10.1016/S0378-5955(02)00796-7.

Shi X and Nuttall AL (2003) ‘Upregulated iNOS and oxidative damage to the cochlear stria vascularis due to noise stress’, *Brain Research*, 967(1–2):1–10, doi:10.1016/S0006-8993(02)04090-8.

Shieh DE, Liu LT and Lin CC (2000) ‘Antioxidant and free radical scavenging effects of baicalein, baicalin and wogonin.’, *Anticancer Research*, 20(5A):2861–5, PMID: 11062694.

Singh B and Navathe PD (1994) ‘Indian Air Force and world spatial disorientation accidents: a comparison.’, *Aviation, Space, and Environmental Medicine*, 65(3):254–6, PMID: 8185557.

Sobkowicz HM, Loftus JM and Slapnick SM (1993) ‘Tissue culture of the organ of Corti.’, *Acta Oto-Laryngologica. Supplementum*, 502:3–36, PMID: 8475741.

Somiya H and Tamura T (1973) ‘Studies on the visual accommodation in fishes’, *Japanese Journal of Ichthyology*, 20(4):193–206, doi:10.11369/jji1950.20.193.

Sterling P (1977) ‘Anatomy and physiology of goldfish oculomotor system. I. Structure of abducens nucleus’, *Journal of Neurophysiology*, 40(3):557–572, doi:10.1152/jn.1977.40.3.557.

Straube A, Kurzan R and Büttner U (1991) ‘Differential effects of bicuculline and muscimol microinjections into the vestibular nuclei on simian eye movements’, *Experimental Brain Research*, 86(2):347–358, doi:10.1007/BF00228958.

Sugahara K, Rubel EW and Cunningham LL (2006) ‘JNK signaling in neomycin-induced vestibular hair cell death’, *Hearing Research*, 221(1–2):128–135, doi:10.1016/j.heares.2006.08.009.

Tabuchi K, Nishimura B, Nakamagoe M, Hayashi K, Nakayama M and Hara A (2011) ‘Ototoxicity: Mechanisms of cochlear impairment and its prevention’, *Current Medicinal Chemistry*, 18(31):4866–4871, doi:10.2174/092986711797535254.

Tadokoro S, Shinji Y, Yamanaka T and Hirata Y (2024) ‘Learning capabilities to resolve tilt-translation ambiguity in goldfish’, *Frontiers in Neurology*, 15:1304496, doi:10.3389/fneur.2024.1304496.

Takabayashi A, Ohmura-Iwasaki T and Mori S (2003) ‘Changes of vertical eye movements of goldfish for different otolith stimulation by linear acceleration’, *Advances in Space Research*, 32(8):1527–1532, doi:10.1016/S0273-1177(03)90391-7.

Takumida M, Anniko M, Popa R and Zhang DM (2000) ‘Lipopolysaccharide-induced expression of inducible nitric oxide synthase in the guinea pig organ of Corti’, *Hearing Research*, 140(1–2):91–98, doi:10.1016/S0378-5955(99)00188-4.

Takumida M, Popa R and Anniko M (1999a) ‘Free radicals in the guinea pig inner ear following gentamicin exposure’, *ORL; journal for oto-rhino-laryngology and its related specialties*, 61(2):63–70, doi:10.1159/000027643.

Tamura A and Tadokoro S (2019) ‘Spatial disorientation and aeromedicine’, *Equilibrium Research*, 78(4):242–253, doi:10.3757/jser.78.242.

Tamura T (1957) ‘A study of visual perception in fish, especially on resolving power and accommodation’, *Bulletin of the Japanese Society of Scientific Fisheries*, 22(9):536–557, doi:10.2331/suisan.22.536.

Telford L, Seidman SH and Paige GD (1997) ‘Dynamics of squirrel monkey linear vestibuloocular reflex and interactions with fixation distance’, *Journal of Neurophysiology*, 78(4):1775–1790, doi:10.1152/JN.1997.78.4.1775.

Thilo KV., Probst T, Bronstein AM, Ito Y and Gresty MA (1999) ‘Torsional eye movements are facilitated during perception of self-motion’, *Experimental Brain Research*, 126(4):495–500, doi:10.1007/s002210050757.

Tweed D, Sievering D, Misslisch H, Fetter M, Zee D and Koenig E (1994) ‘Rotational kinematics of the human vestibuloocular reflex. I. Gain matrices’, *Journal of Neurophysiology*, 72(5):2467–2479, doi:10.1152/jn.1994.72.5.2467.

Usami E, Mizuno M and Seyama Y (1998) ‘A superoxide anion scavenging activity of traditional chinese medicines (Kampo medicines)’, 病院薬学, 24(2):173–178, doi:10.5649/JJPHCS1975.24.173.

Van De Water T and Ruben RJ (1974) ‘Growth of the inner ear in organ culture’, *Annals of Otology, Rhinology & Laryngology*, 83(14_suppl):1–16, doi:10.1177/0003489474083S1401.

Wei M and Angelaki DE (2001) ‘Cross-axis adaptation of the translational vestibulo-ocular reflex’, *Experimental Brain Research*, 138(3):304–312, doi:10.1007/S002210100695.

Yakusheva TA, Shaikh AG, Green AM, Blazquez PM, Dickman JD and Angelaki DE (2007) ‘Purkinje cells in posterior cerebellar vermis encode motion in an inertial reference frame’, *Neuron*, 54(6):973–985, doi:10.1016/j.neuron.2007.06.003.

Yamanouchi T (1956) ‘The visual acuity of the coral fish Microcanthus strigatus’, *Publications of the Seto Marine Biological Laboratory*, 5(2):133–156, doi:10.5134/174560.

Yamashita T, Araki K, Tomifuji M, Kamide D, Tanaka Y and Shiotani A (2015) ‘A traditional Japanese medicine—Hangeshashinto (TJ-14)—alleviates chemoradiation-induced mucositis and improves rates of treatment completion’, *Supportive Care in Cancer*, 23(1):29–35, doi:10.1007/s00520-014-2315-z.

Ylikoski J, Xing-Qun L, Virkkala J and Pirvola U (2002) ‘Blockade of c-Jun N-terminal kinase pathway attenuates gentamicin-induced cochlear and vestibular hair cell death’, *Hearing Research*, 166(1–2):33–43, doi:10.1016/S0378-5955(01)00388-4.

Zaunreiter M, Junger H and Kotrschal K (1991) ‘Retinal morphology of cyprinid fishes: a quantitative histological study of ontogenetic changes and interspecific variation’, *Vision Research*, 31(3):383–394, doi:10.1016/0042-6989(91)90091-I.

Zupan LH and Merfeld DM (2005) ‘Human ocular torsion and perceived roll responses to linear acceleration’, *Journal of Vestibular Research: Equilibrium and Orientation*, 15(4):173–183, doi:10.3233/VES-2005-15401.

Zupan LH, Merfeld DM and Darlot C (2002) ‘Using sensory weighting to model the influence of canal, otolith and visual cues on spatial orientation and eye movements’, *Biological Cybernetics*, 86(3):209–230, doi:10.1007/S00422-001-0290-1.

Appendix: Glossary of terms and abbreviations

Visual-Vestibular Neural Training to Resolve Tilt-Translation Ambiguity in Goldfish

Spatial Orientation refers to an animal's ability to estimate its relative position, posture, and motion in space, using sensory inputs such as visual, vestibular, and proprioceptive information. This ability is essential for survival and allows animals to interact with their environment effectively (e.g., avoiding obstacles or chasing prey).

Spatial Disorientation occurs when an animal's sensory systems fail to provide consistent or accurate information about its position or motion, leading to a misperception of spatial orientation. This condition is particularly critical in situations where sensory conflicts arise, such as during rapid or complex movements, poor visibility, or altered gravitational environments. For example, in humans, spatial disorientation can result in dangerous errors in activities like flying an aircraft or diving underwater, where misjudging spatial orientation can have life-threatening consequences.

Somatogravic Illusions are a series of spatial disorientation or sensory illusions, characterized by a false perception of changes in an aircraft's attitude when the otolith organs are stimulated by linear acceleration. Among these, pitch illusions—also known as pitch-up or pitch-down illusions—are particularly well-documented. Sometimes referred to as the "dark-night take-off illusion," these phenomena are commonly experienced during high-stakes operations, such as aircraft carrier launches in the Navy, and have also contributed to accidents in commercial and general aviation. For instance, during a forward acceleration in level flight, pilots may experience a false nose-high sensation, which can be dangerous during takeoffs in instrument meteorological conditions (IMC) or at night. If pilots are not fully relying on their instruments, they might push the nose of the aircraft down to correct for this illusory pitch, potentially leading to controlled flight into terrain (CFIT). Conversely, during rapid deceleration, such as when slowing down in

weather conditions, pilots may experience a false nose-down sensation that can also lead to inappropriate control inputs. These illusions highlight the importance of training and strict adherence to instrument flight rules in visually impoverished environments. In contrast, somatogyral illusions are a set of illusions that result from the semicircular canals' inability to accurately register prolonged rotation, i.e., sustained angular velocity.

Vestibulo-Ocular Reflex (VOR) serves as a key indicator of self-motion estimation. It compensates for head motion to stabilize vision, with different VOR types (e.g., torsional VOR around the x-axis and horizontal VOR around the z-axis) helping to estimate roll-tilt and interaural translation, respectively. These reflexes depend on both vestibular and visual information, highlighting the integration of these modalities in motion estimation.

Vestibular System Limitations: The vestibular system, specifically the semicircular canals and otoliths, senses head motion. However, the semicircular canals cannot provide accurate information over prolonged motion, and otoliths struggle to distinguish between tilt and translation (the "tilt-translation ambiguity"), which can lead to spatial disorientation.

Tilt-Translation Ambiguity: This issue arises from otoliths detecting both linear head acceleration and gravitational acceleration, making it difficult to differentiate between head-tilting and translation. It can cause disorientation, particularly in contexts like aviation.

Frequency Segregation Theory suggests that low-frequency accelerations are interpreted as tilts, while high-frequency accelerations are interpreted as translations. This theory is supported by empirical evidence showing that low-frequency accelerations are often associated with tilt, and high-frequency accelerations with translation. Based on this, it is believed that animals have evolved a neural mechanism that is well-suited to distinguish between these two types of motion.

Integration Theory (Internal Model Theory) suggests that the brain combines multiple sensory inputs (e.g., from the semicircular canals, vision, and proprioception) to resolve the tilt-translation ambiguity. This model also implies that animals learn to distinguish between different types of head motion based on their motion experiences.

VOR Adaptation refers to changes in the VOR response due to sensory experience, such as training to reduce the effects of tilt-translation ambiguity. In the context of this thesis, goldfish were used to investigate whether they could adaptively modify their head motion estimation after exposure to specific motion experiences (e.g., training with interaural linear translation and visual stimuli).

Kalman Filter Model is a computational model employed to simulate spatial orientation and motion estimation processes. It was used to understand and predict changes in the VOR following visual-vestibular neural training, where the model was modified to represent the impact of visual and vestibular training on the VOR in goldfish.

Motion Experience plays a key role in resolving the tilt-translation ambiguity. In practical terms, this concept is critical in contexts like aviation, where pilots undergo spatial orientation training to prevent spatial disorientation. The training involves simulating conditions that might induce disorientation, but its effectiveness in improving motion estimation accuracy has yet to be conclusively validated.

TJ-014 effect in inner ear hair cell loss

Hangesha-shin-to (TJ-014) is a traditional Japanese herbal medicine. Main ingredients: Baicalin, Baicalein, Wogonin, Berberine, etc. May have antioxidant effects against oxidative stress. Used for chronic gastritis, stomatitis, psychological disorders, and other conditions.

Hair Cells in the Inner Ear (HCs) are sensory cells in the vestibular organ and cochlear organ, which are vulnerable to oxidative stress.

Oxidative Stress is Tissue damage caused by the excessive production of reactive oxygen species (ROS).

Reactive Oxygen Species (ROS) is important in cellular signaling, redox homeostasis, and metabolic processes; however, excessive production can lead to hair cell death. Factors increasing ROS production are psychological stress, air pollution, smoking, etc.

Gentamicin (GM) is an aminoglycoside antibiotic known to cause irreversible damage to hair cells through ototoxicity. The cell death mechanism involves ROS generation.

Apoptosis is commonly referred to as programmed cell death, a highly regulated biological process crucial for maintaining cellular homeostasis and eliminating damaged or unnecessary cells. This process is characterized by distinct morphological and biochemical features, which include the following terms:
Mitochondrial Pathway (intrinsic pathway of apotosis): Triggered by intracellular stress or ROS, this pathway involves mitochondrial outer membrane permeabilization (MOMP), the release of cytochrome c, and subsequent caspase activation.
Caspase Activation: Central to apoptosis, caspases are proteases that dismantle cellular components. Caspase-3, activated downstream, plays a pivotal role in executing apoptosis.

Main Evaluation Items:

- Fluorescent Labeling (Rhodamine Phalloidin): used to evaluate the number of surviving hair cells and hair cell survival rate.
- Immunostaining for Caspase-3: a marker for apoptosis.
- Anti-8-OHdG Antibody: a marker for oxidative stress, identified through fluorescent signals.
- MitoTracker® Red CMXRos Probe: a marker for mitochondrial membrane potential through color density analysis.

Abbreviations

3D	three-dimensional
GIA	gravito-inertial acceleration
VOR	vestibulo-ocular reflex
OKR	optokinetic response
DAQ	data acquisition
PC	personal computer
OKS	optokinetic stimulus
OKAN	optokinetic after nystagmus
SD	standard deviation
disp.	display
vis.	visual
acc.	acceleration
ang.	angular
vel.	velocity
stim.	stimulation
N.S.	not significant
Trans.	translation
AG	aminoglycosides
GM	Gentamicin
HC	hair cell
ROS	reactive oxygen species
TJ-014	Hangesha-shin-to
8-OHdG	8-hydroxy-2'-deoxyguanosine
DMEM	Dulbecco's Modified Eagle's Medium
FBS	fetal bovine serum
PFA	paraformaldehyde
PBS	phosphate-buffered saline
OHCs	outer hair cells
OHC	outer hair cell
IHC	inner hair cell

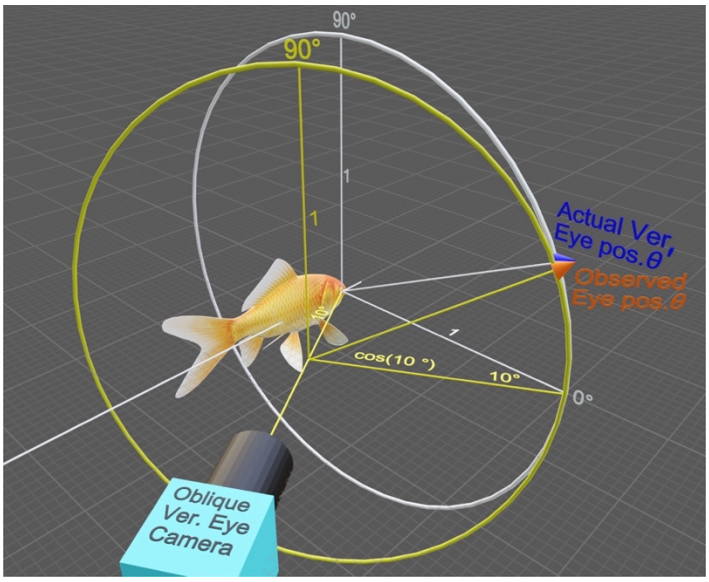
ANOVA	analysis of variance
COX-2	Cyclooxygenase-2
PGE2	Prostaglandin E2
eNOS	endothelial nitric oxide synthase
iNOS	inducible nitric oxide synthase
O^-	superoxide anion
$ONOO^-$	peroxynitrite
LPS	lipopolysaccharide

Supplementary Methods

S2.1 Correction for vertical and horizontal eye positions

S2.2.1 Correction for vertical eye position

Correction for vertical eye position acquired from a 10° horizontally oblique camera (vertical eye camera) was performed using the following analysis method: The vertical eye position (Supplementary Figure S1, orange cone) determined by LABVIEW software (National Instruments, USA) from the camera with a 10° optical axis is a projection of the actual vertical eye position (Supplementary Figure S1, blue cone) that traces a circular path (Supplementary Figure S1, white circle) onto an ellipse (Supplementary Figure S1, yellow ellipse) in a plane orthogonal to the camera's optical axis. The ellipse had a horizontal (short) axis/vertical (long) axis ratio of $\cos 10°$. The distorted vertical eye position θ (Supplementary Figure S1, orange cone) from the camera can be corrected to the actual vertical eye position θ' (Supplementary Figure S1, blue cone) using the function $\theta' = \tan^{-1}(\tan\theta/\cos 10°)$, where θ is the eye position determined by LABVIEW from the camera image relative to where the null position is set to 0°.



Supplementary Figure S1. Relationship between the biasedly observed vertical eye position determined by LabVIEW (θ, angle of the orange corn) and actual vertical eye position (θ', angle of the blue corn). The actual vertical eye position and its circular

orbit (white circle) were projected onto the observed vertical eye position and its elliptical orbit, which flattened horizontally (yellow ellipse orthogonal to the oblique vertical eye camera's optical axis, ellipticity is $\cos 10°$). Note that the angles depicted in the graphic are exaggerated compared with the actual camera placement. Ver.: vertical; pos.: position.

S2.1.2 Correction for horizontal eye position

The slight tilt of the horizontal eye camera (the camera atop the aquarium) away from the z-axis may project a vertical component of eye movement onto the horizontal eye camera, potentially contaminating the eye position data. When the camera's optical axis tilts by the angle α, on the sagittal plane, the actual vertical eye position (Supplementary Figure S2A, blue cone) on the circular trace (Supplementary Figure S2A, white circle) is projected onto the ellipse (Supplementary Figure S2A, yellow ellipse) in the plane orthogonal to the optical axis (Supplementary Figure S2A, yellow ellipse), resulting in contamination of the horizontal eye position data (Supplementary Figure S2A, orange cone). The ellipse has a vertical (short) or horizontal (long) axis ratio of $\sin\alpha$. The contamination effects are usually minimal but significant when the vertical component largely dominates the horizontal component (e.g., during the Roll-Tilt Test). To correct for this, we estimated the pure contamination θ'' due to the vertical component (Supplementary Figure S2I) using the function $\theta'' = \tan^{-1}(\sin\alpha \times \tan\theta')$ and subtracted it from the horizontal eye position data determined by LABVIEW from the eye camera (Supplementary Figure S2C) to obtain the corrected horizontal component (Supplementary Figure S2K), where θ' is the actual vertical eye position estimated by the aforementioned method and α is the tilt angle of the horizontal eye camera estimated by the following method.

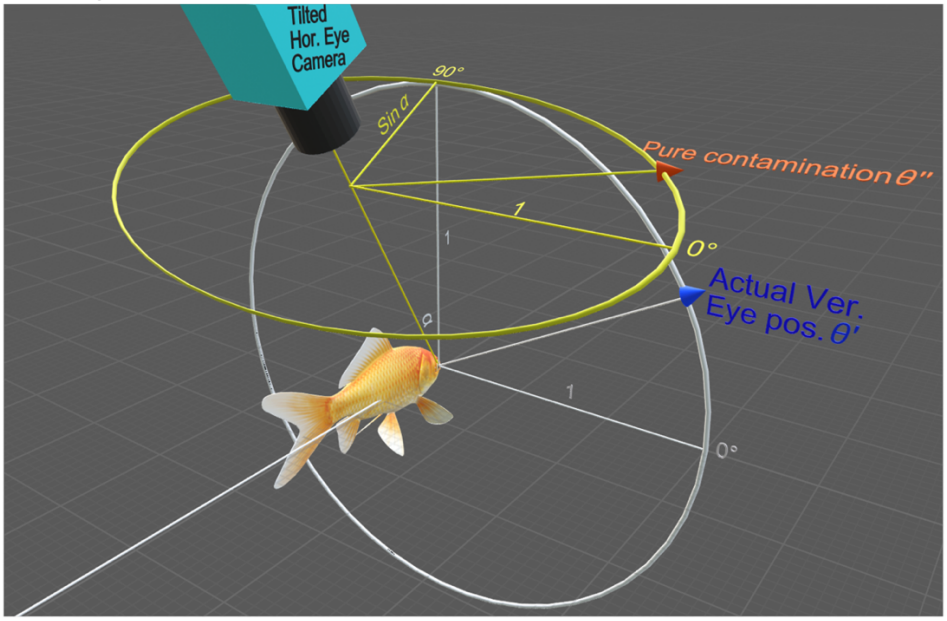
S2.1.3 Estimation of the tilt angle of the horizontal eye camera

The angle α, representing the tilt angle of the optical axis of the horizontal eye camera, was determined as follows (Supplementary Figure S2B–H). We assumed that only saccades and post-saccadic drift caused horizontal eye movements during the roll-tilt test paradigm before training. To identify saccades and high-frequency noise, a custom-made

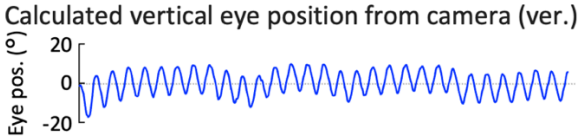
automatic saccade-detection algorithm was applied to approximate the post-saccade drift by connecting a linear line between the end of the saccade and the beginning of the next saccade. The estimated pure horizontal eye position traces (saccades and post-saccadic drifts) and high-frequency noise (Supplementary Figure S2C) were subtracted from the horizontal eye position trace determined by LABVIEW using the horizontal eye camera (Supplementary Figure S2D), leaving a residual trace interpreted as pure contamination.

The angle α in the function $\theta'' = \tan^{-1}(\sin\alpha \times \tan\theta')$ was estimated using curve fitting with MATLAB (MathWorks, USA) 'fit' and 'fittype' functions (Supplementary Figure S2H). Here, θ' represents the actual vertical eye position estimated using the previously mentioned method, averaged over each period of the vestibular stimulus to form a one-period array (Supplementary Figure S2F), and θ'' represents the estimated pure contamination trace similarly averaged to form a one-period array (Supplementary Figure S2G). During the averaging process of the contamination trace, data points with a duration of <0.5 s and those deviating by 2 times the median absolute deviation from the median were excluded.

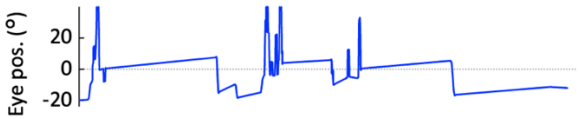
A. Graphical explanation



B. Calculated vertical eye position from camera (ver.)



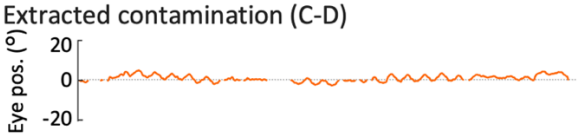
C. Horizontal saccade & eye drift



D. Horizontal eye position from tilted camera (hor.)



E. Extracted contamination (C-D)



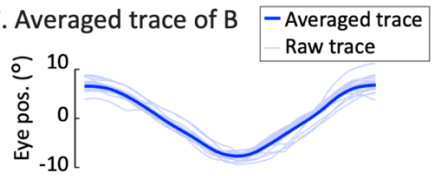
I. Estimated contamination calculated by B & H



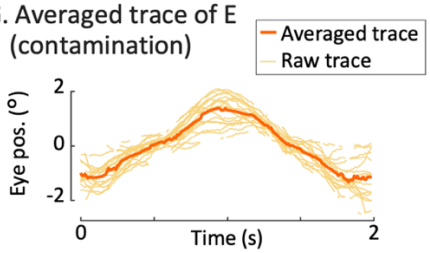
K. Calculated pure horizontal eye pos. (C-I)



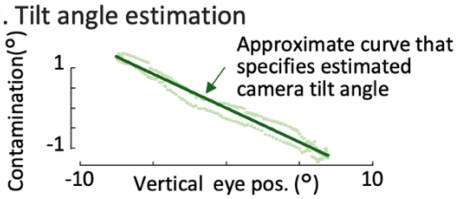
F. Averaged trace of B



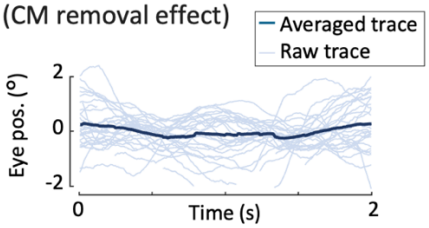
G. Averaged trace of E (contamination)



H. Tilt angle estimation



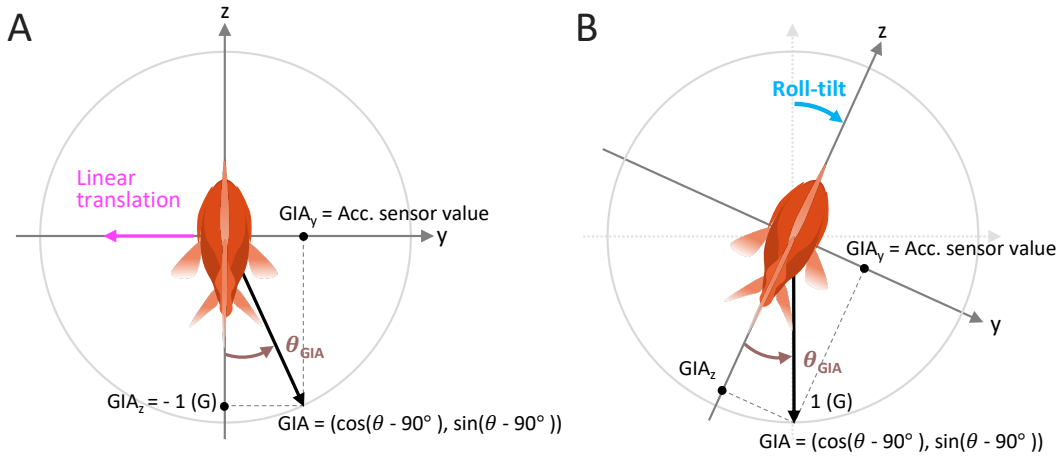
J. Averaged trace of E-I (CM removal effect)



Supplementary Figure S2. Removal of contamination in the horizontal eye position observed from the tilted horizontal eye camera. (A) Graphical explanation of the relationship between the contamination (θ'', angle of the orange corn) and actual vertical eye position (θ', angle of the blue corn). Actual vertical eye position and its circular orbit (white circle) were respectively projected onto the contamination and its elliptical orbit that flattened vertically (yellow ellipse orthogonal to the tilted horizontal eye camera's optical axis; ellipticity is $\sin\alpha$, where α is the camera tilt angle). Note that the angles depicted in the graphic are exaggerated compared with the actual camera placement. (B)–(K) Series of sample analyses aimed at eliminating contamination from the observed horizontal eye position. (B) Actual vertical eye position from the vertical eye camera. (C) Observed horizontal eye position using a tilted horizontal eye camera. The contamination was prominent while horizontally stationary and moving slowly (orange lines). (D) Horizontal saccades and eye drift. It was assumed to be a purely horizontal eye position in the roll-tilt test before training. (E) Contamination extracted using the function $(\mathbf{E}) = (\mathbf{C}) - (\mathbf{D})$. (F) Period-averaged traces of (B). (G) Average traces of (E). This indicates contamination. (H) Approximate curve that curve fitted the (G)–(F) plot based on the function $(\mathbf{G}) = \tan^{-1}(\sin\alpha) \times \tan(\mathbf{F})$ and MATLAB 'fit' function. This curve specifies the estimated camera angle α. (I) Estimated contamination, calculated as $(\mathbf{I}) = \tan^{-1}(\sin\alpha) \times \tan(\mathbf{B})$. (J) Average trace of $(\mathbf{J}) = (\mathbf{E}) - (\mathbf{I})$. This indicates the effectiveness of contamination removal. (K) Calculated pure Horizontal Eye position, given by $(\mathbf{K}) = (\mathbf{C}) - (\mathbf{I})$. (B)–(K) Series of examples in which the horizontal eye camera is extremely tilted to emphasize the effect of contamination removal. The tilt angles of the cameras were generally much smaller. ver.: vertical; hor.: horizontal; pos.: position.

S2.2 Calculation for the rotational angle of the GIA vector.

The gravito-inertial acceleration (GIA) vector is given as a y, z coordinate, (GIA_y, GIA_Z) or $(\cos(\theta_{GIA} - 90°), (\sin(\theta_{GIA} - 90°)$, where θ_{GIA} is the angle of the GIA vector relative to the negative z-axis, rotating around the goldfish's x-axis. GIA_{y} was provided by an acceleration sensor. During translational motion (Translation Test and Training), the GIA vector angle can be obtained by solving equation $GIA_z = -1$ (G) and $GIA_y/GIA_x = \tan(\theta_{GIA} - 90°)$, as $\theta_{GIA} = \tan^{-1}(\text{Acc. Sensor Value})$ following Lichtenberg *et al.,* (1982) (Supplementary Figure S3A). During roll-tilt rotational motion (Roll-Tilt Test), the GIA vector angle can be obtained by solving equation $GIA_{\mathrm{y}} = \cos(\theta_{\mathrm{GIA}} - 90°)$, as $\theta_{GIA} = \sin^{-1}(\text{Acc. Sensor Value})$ (Supplementary Figure S3B).



Supplementary Figure S3. Positioning of the GIA vector. The GIA vector is given as a y, z coordinate, (GIA_y, GIA_Z) or $(\cos(\theta_{GIA} - 90°), (\sin(\theta_{GIA} - 90°)$, where θ_{GIA} is the angle of the GIA vector relative to negative z-axis, rotating around the goldfish's x-axis. GIA_y was provided by an acceleration sensor. (A) GIA_z during linear translational motion (Translation Test and Training) is -1 (G); (B) length of GIA vector during roll-tilt rotational motion (Roll-Tilt Test) is 1 (G). GIA: gravito-inertial acceleration; Acc.: acceleration.

S2.3 Kalman filter model

S2.3.1 Model of head and eye motion with sensors

Model of head motion, eye motion, vestibular sensors and visual sensors

Head rotation velocity	$\Omega_x(t) =$	$\Omega_x^u(t)$	$+\Omega_x^\varepsilon(t)$
	$\Omega_y(t) =$	$\Omega_y^u(t)$	$+\Omega_y^\varepsilon(t)$
	$\Omega_z(t) =$	$\Omega_z^u(t)$	$+\Omega_z^\varepsilon(t)$
Semicircular Canal endolymph velocity	$C_x(t) = k_1 C_x(t-\Delta t) + k_2 \Omega_x(t-\Delta t)$		
	$C_y(t) = k_1 C_y(t-\Delta t) + k_2 \Omega_y(t-\Delta t)$		
	$C_z(t) = k_1 C_z(t-\Delta t) + k_2 \Omega_z(t-\Delta t)$		
Gravity	$G_x(t) = G_x(t-\Delta t) - \Delta t G_z(t-\Delta t)\Omega_y(t-\Delta t) + \Delta t G_y(t-\Delta t)\Omega_z(t-\Delta t)$		
	$G_y(t) = G_y(t-\Delta t) + \Delta t G_z(t-\Delta t)\Omega_x(t-\Delta t) - \Delta t G_x(t-\Delta t)\Omega_z(t-\Delta t)$		
	$G_z(t) = G_z(t-\Delta t) - \Delta t G_y(t-\Delta t)\Omega_x(t-\Delta t) + \Delta t G_x(t-\Delta t)\Omega_y(t-\Delta t)$		
Head liner acceleration	$A_x(t) =$	$A_x^u(t)$	$+A_x^\varepsilon(t)$
	$A_y(t) =$	$A_y^u(t)$	$+A_y^\varepsilon(t)$
	$A_z(t) =$	$A_z^u(t)$	$+A_z^\varepsilon(t)$
Head linear velocity	$B_x(t) = B_x(t-\Delta t) + \Delta t A_x(t-\Delta t)$		
	$B_y(t) = B_y(t-\Delta t) + \Delta t A_y(t-\Delta t)$		
	$B_z(t) = B_z(t-\Delta t) + \Delta t A_z(t-\Delta t)$		
Visual velocity	$\Phi_x(t) =$		$+\Phi_x^\varepsilon(t)$
	$\Phi_y(t) =$		$+\Phi_y^\varepsilon(t)$
	$\Phi_z(t) =$		$+\Phi_z^\varepsilon(t)$
Eye rotation velocity	$P_x(t) = m_1 P_x(t-\Delta t)$	$+ m_2 P_x^u(t-\Delta t)$	$+ m_2 P_x^\varepsilon(t)$
	$P_y(t) = m_1 P_y(t-\Delta t)$	$+ m_2 P_y^u(t-\Delta t)$	$+ m_2 P_y^\varepsilon(t)$
	$P_z(t) = m_1 P_z(t-\Delta t)$	$+ m_2 P_z^u(t-\Delta t)$	$+ m_2 P_z^\varepsilon(t)$

Semicircular canal signal	$V_x(t) = \Omega_x(t) - C_x(t)$	$+ V_x^\eta(t)$
	$V_y(t) = \Omega_y(t) - C_y(t)$	$+ V_y^\eta(t)$
	$V_z(t) = \Omega_z(t) - C_z(t)$	$+ V_z^\eta(t)$
Otolith signal	$F_x(t) = A_x(t) + G_x(t)$	$+ F_x^\eta(t)$
	$F_y(t) = A_y(t) + G_y(t)$	$+ F_y^\eta(t)$
	$F_z(t) = A_z(t) + G_z(t)$	$+ F_z^\eta(t)$
Retina signal	$\Psi_x(t) = L_i(t)\left(\Phi_x(t) - \Omega_x(t) + rB_y(t) - P_x(t)\right)$	$+ \Psi_x^\eta(t)$
	$\Psi_y(t) = L_i(t)\left(\Phi_y(t) - \Omega_y(t) + rB_z(t) - P_y(t)\right)$	$+ \Psi_y^\eta(t)$
	$\Psi_z(t) = L_i(t)\left(\Phi_z(t) - \Omega_z(t) - rB_y(t) - P_z(t)\right)$	$+ \Psi_z^\eta(t)$

Parameters

Time step
$\Delta t = 0.002$ [s]

Canal dynamics time const
$\tau_C = 0.5$ [s]
$k_1 = 1 - \Delta t/\tau_C$
$k_2 = \Delta t/\tau_C$

Muscle dynamics time const
$\tau_m = 0.003$ [s]
$m_1 = 1 - \Delta t/\tau_m$
$m_2 = \Delta t/\tau_m$

Coefficient for linear stimulus
$r = 4$

Variable to describe light or dark

In the real world model, $L_i(t) = \begin{cases} 1 & \text{if the light is ON} \\ 0 & \text{Otherwise} \end{cases}$

In the Kalman filter model, $L_i(t) = 1$

$L_i(t)$ is always set to 1 in $\boldsymbol{M}$ and $\boldsymbol{T}$ used in the Kalman filter to continue the estimation during the dark interval.

S2.3.2 Model in matrix form

State-space equations

$$\boldsymbol{X}(t) = \boldsymbol{D}\,\boldsymbol{X}(t-\Delta t) + \boldsymbol{M}\,\boldsymbol{X}^{u}(t) + \boldsymbol{E}\,\boldsymbol{X}^{\epsilon}(t)$$

Where:

State variables $\boldsymbol{X}(t) = \left[\Omega_x(t)\ \Omega_y(t)\ \Omega_z(t)\ C_x(t)\ C_y(t)\ C_z(t)\ G_x(t)\ G_y(t)\ G_z(t)\ A_x(t)\ A_y(t)\ A_z(t)\ B_x(t)\ B_y(t)\ B_z(t)\ \Phi_x(t)\ \Phi_y(t)\ \Phi_z(t)\ P_x(t)\ P_y(t)\ P_z(t)\right]'$

The dash denotes a transpose of a matrix.

Input variables $\boldsymbol{X}^{u}(t) = \left[\Omega_x^u(t)\ \Omega_y^u(t)\ \Omega_z^u(t)\ A_x^u(t)\ A_y^u(t)\ A_z^u(t)\ \Phi_x^u(t)\ \Phi_y^u(t)\ \Phi_z^u(t)\ P_x^u(t)\ P_y^u(t)\ P_z^u(t)\right]'$

Stimuli variables + Process noises $\boldsymbol{X}^{\epsilon}(t) = \left[\Omega_x^\epsilon(t)\ \Omega_y^\epsilon(t)\ \Omega_z^\epsilon(t)\ A_x^\epsilon(t)\ A_y^\epsilon(t)\ A_z^\epsilon(t)\ \Phi_x^\epsilon(t)\ \Phi_y^\epsilon(t)\ \Phi_z^\epsilon(t)\ P_x^\epsilon(t)\ P_y^\epsilon(t)\ P_z^\epsilon(t)\right]'$

$$\boldsymbol{D} = \begin{bmatrix}
0 & 0 & 0 & 0 & 0 & 0 & 0 & 0 & 0 & 0 & 0 & 0 & 0 & 0 & 0 & 0 & 0 & 0 & 0 & 0 & 0 & 0 \\
0 & 0 & 0 & 0 & 0 & 0 & 0 & 0 & 0 & 0 & 0 & 0 & 0 & 0 & 0 & 0 & 0 & 0 & 0 & 0 & 0 & 0 \\
0 & 0 & 0 & 0 & 0 & 0 & 0 & 0 & 0 & 0 & 0 & 0 & 0 & 0 & 0 & 0 & 0 & 0 & 0 & 0 & 0 & 0 \\
k_2 & 0 & 0 & k_1 & 0 & 0 & 0 & 0 & 0 & 0 & 0 & 0 & 0 & 0 & 0 & 0 & 0 & 0 & 0 & 0 & 0 & 0 \\
0 & k_2 & 0 & 0 & k_1 & 0 & 0 & 0 & 0 & 0 & 0 & 0 & 0 & 0 & 0 & 0 & 0 & 0 & 0 & 0 & 0 & 0 \\
0 & 0 & k_2 & 0 & 0 & k_1 & 0 & 0 & 0 & 0 & 0 & 0 & 0 & 0 & 0 & 0 & 0 & 0 & 0 & 0 & 0 & 0 \\
0 & -\Delta t G_z(t) & \Delta t G_y(t) & 0 & 0 & 0 & 1 & 0 & 0 & 0 & 0 & 0 & 0 & 0 & 0 & 0 & 0 & 0 & 0 & 0 & 0 & 0 \\
\Delta t G_z(t) & 0 & -\Delta t G_x(t) & 0 & 0 & 0 & 0 & 1 & 0 & 0 & 0 & 0 & 0 & 0 & 0 & 0 & 0 & 0 & 0 & 0 & 0 & 0 \\
-\Delta t G_y(t) & \Delta t G_x(t) & 0 & 0 & 0 & 0 & 0 & 0 & 1 & 0 & 0 & 0 & 0 & 0 & 0 & 0 & 0 & 0 & 0 & 0 & 0 & 0 \\
0 & 0 & 0 & 0 & 0 & 0 & 0 & 0 & 0

S2.3.3 Kalman filter algorithm and control feedback

Optimal estimates

$$\widehat{\boldsymbol{X}}^{p}(t) = \boldsymbol{D}\,\widehat{\boldsymbol{X}}(t-\Delta t) + \boldsymbol{M}\,\boldsymbol{X}^{u}(t)$$
$$\widehat{\boldsymbol{S}}^{p}(t) = \boldsymbol{T}\,\widehat{\boldsymbol{X}}^{p}(t)$$
$$\boldsymbol{\Delta S}(t) = \boldsymbol{S}(t) - \widehat{\boldsymbol{S}}^{p}(t)$$
$$\boldsymbol{\Delta}\widehat{\boldsymbol{X}}(t) = \boldsymbol{K}(t)\boldsymbol{\Delta S}(t)$$
$$\widehat{\boldsymbol{X}}(t) = \widehat{\boldsymbol{X}}^{p}(t) + \boldsymbol{\Delta}\widehat{\boldsymbol{X}}(t)$$

Where:

Predicted state variables $\widehat{\boldsymbol{X}}^{p}(t)$

Predicted sensor variables $\widehat{\boldsymbol{S}}^{p}(t) = \left[\hat{V}_x(t)\ \hat{V}_y(t)\ \hat{V}_z(t)\ \hat{F}_x(t)\ \hat{F}_y(t)\ \hat{F}_z(t)\ \hat{\Psi}_x(t)\ \hat{\Psi}_y(t)\ \hat{\Psi}_z(t)\right]'$

Feedback variables $\boldsymbol{\Delta}\widehat{\boldsymbol{X}}(t) = \left[\Delta\hat{\Omega}_x(t)\ \Delta\hat{\Omega}_y(t)\ \Delta\hat{\Omega}_z(t)\ \Delta\hat{C}_x(t)\ \Delta\hat{C}_y(t)\ \Delta\hat{C}_z(t)\ \Delta\hat{G}_x(t)\ \Delta\hat{G}_y(t)\ \Delta\hat{G}_z(t)\ \Delta\hat{A}_x(t)\ \Delta\hat{A}_y(t)\ \Delta\hat{A}_z(t)\ \Delta\hat{B}_x(t)\ \Delta\hat{B}_y(t)\ \Delta\hat{B}_z(t)\ \Delta\hat{\Phi}_x(t)\ \Delta\hat{\Phi}_y(t)\ \Delta\hat{\Phi}_z(t)\ \Delta\hat{P}_x(t)\ \Delta\hat{P}_y(t)\ \Delta\hat{P}_z(t)\right]'$

Predicted sensor errors $\boldsymbol{\Delta S}(t) = \left[\Delta\hat{V}_x(t)\ \Delta\hat{V}_y(t)\ \Delta\hat{V}_z(t)\ \Delta\hat{F}_x(t)\ \Delta\hat{F}_y(t)\ \Delta\hat{F}_z(t)\ \Delta\hat{\Psi}_x(t)\ \Delta\hat{\Psi}_y(t)\ \Delta\hat{\Psi}_z(t)\right]'$

Estimated state variables $\widehat{\boldsymbol{X}}(t) = \left[\hat{\Omega}_x(t)\ \hat{\Omega}_y(t)\ \hat{\Omega}_z(t)\ \hat{C}_x(t)\ \hat{C}_y(t)\ \hat{C}_z(t)\ \hat{G}_x(t)\ \hat{G}_y(t)\ \hat{G}_z(t)\ \hat{A}_x(t)\ \hat{A}_y(t)\ \hat{A}_z(t)\ \hat{B}_x(t)\ \hat{B}_y(t)\ \hat{B}_z(t)\ \hat{\Phi}_x(t)\ \hat{\Phi}_y(t)\ \hat{\Phi}_z(t)\ \hat{P}_x(t)\ \hat{P}_y(t)\ \hat{P}_z(t)\right]'$

$\boldsymbol{K}(t)$ is a Kalman gain matrix. $\boldsymbol{D}$, $\boldsymbol{M}$ and $\boldsymbol{T}$ are coefficient matrices. $\boldsymbol{X}^{u}(t)$ is input variables. $\boldsymbol{S}(t)$ is sensory variables.

Update equation of Kalman gain

$$\boldsymbol{K}(t) = \boldsymbol{L}^{p}(t)\boldsymbol{T}'(\boldsymbol{T}\boldsymbol{L}^{p}(t)\boldsymbol{T}' + \boldsymbol{R})^{-1}$$
$$\boldsymbol{L}^{p}(t) = \boldsymbol{D}\boldsymbol{L}(t-\Delta t)\boldsymbol{D}' + \boldsymbol{Q}$$
$$\boldsymbol{L}(t) = (\boldsymbol{I} - \boldsymbol{K}(t)\boldsymbol{T})\boldsymbol{L}^{p}(t)$$

$\boldsymbol{I}$ is an identity matrix. $\boldsymbol{L}^{p}(t)$ and $\boldsymbol{L}(t)$ are covariances of the predicted and updated estimate.
$\boldsymbol{Q}$ and $\boldsymbol{R}$ are the covariance matrices of $\boldsymbol{E}\,\boldsymbol{X}^{\varepsilon}$ and $\boldsymbol{S}^{\eta}$.

$$\boldsymbol{Q} = \boldsymbol{E}\begin{bmatrix} (\sigma^{\Omega})^2 & 0 & 0 & 0 & 0 & 0 & 0 & 0 & 0 & 0 & 0 & 0 \\ 0 & (\sigma^{\Omega})^2 & 0 & 0 & 0 & 0 & 0 & 0 & 0 & 0 & 0 & 0 \\ 0 & 0 & (\sigma^{\Omega})^2 & 0 & 0 & 0 & 0 & 0 & 0 & 0 & 0 & 0 \\ 0 & 0 & 0 & (\sigma_x^{A})^2 & 0 & 0 & 0 & 0 & 0 & 0 & 0 & 0 \\ 0 & 0 & 0 & 0 & (\sigma_y^{A})^2 & 0 & 0 & 0 & 0 & 0 & 0 & 0 \\ 0 & 0 & 0 & 0 & 0 & (\sigma_z^{A})^2 & 0 & 0 & 0 & 0 & 0 & 0 \\ 0 & 0 & 0 & 0 & 0 & 0 & (\sigma^{\Phi})^2 & 0 & 0 & 0 & 0 & 0 \\ 0 & 0 & 0 & 0 & 0 & 0 & 0 & (\sigma^{\Phi})^2 & 0 & 0 & 0 & 0 \\ 0 & 0 & 0 & 0 & 0 & 0 & 0 & 0 & (\sigma^{\Phi})^2 & 0 & 0 & 0 \\ 0 & 0 & 0 & 0 & 0 & 0 & 0 & 0 & 0 & (\sigma^{P})^2 & 0 & 0 \\ 0 & 0 & 0 & 0 & 0 & 0 & 0 & 0 & 0 & 0 & (\sigma^{P})^2 & 0 \\ 0 & 0 & 0 & 0 & 0 & 0 & 0 & 0 & 0 & 0 & 0 & (\sigma^{P})^2 \end{bmatrix}\boldsymbol{E}' \qquad \boldsymbol{R} = \begin{bmatrix} (\sigma^{V})^2 & 0 & 0 & 0 & 0 & 0 & 0 & 0 & 0 \\ 0 & (\sigma^{V})^2 & 0 & 0 & 0 & 0 & 0 & 0 & 0 \\ 0 & 0 & (\sigma^{V})^2 & 0 & 0 & 0 & 0 & 0 & 0 \\ 0 & 0 & 0 & (\sigma^{F})^2 & 0 & 0 & 0 & 0 & 0 \\ 0 & 0 & 0 & 0 & (\sigma^{F})^2 & 0 & 0 & 0 & 0 \\ 0 & 0 & 0 & 0 & 0 & (\sigma^{F})^2 & 0 & 0 & 0 \\ 0 & 0 & 0 & 0 & 0 & 0 & (\sigma^{\Psi})^2 & 0 & 0 \\ 0 & 0 & 0 & 0 & 0 & 0 & 0 & (\sigma^{\Psi})^2 & 0 \\ 0 & 0 & 0 & 0 & 0 & 0 & 0 & 0 & (\sigma^{\Psi})^2 \end{bmatrix}$$

Control feedback

Eye motor command

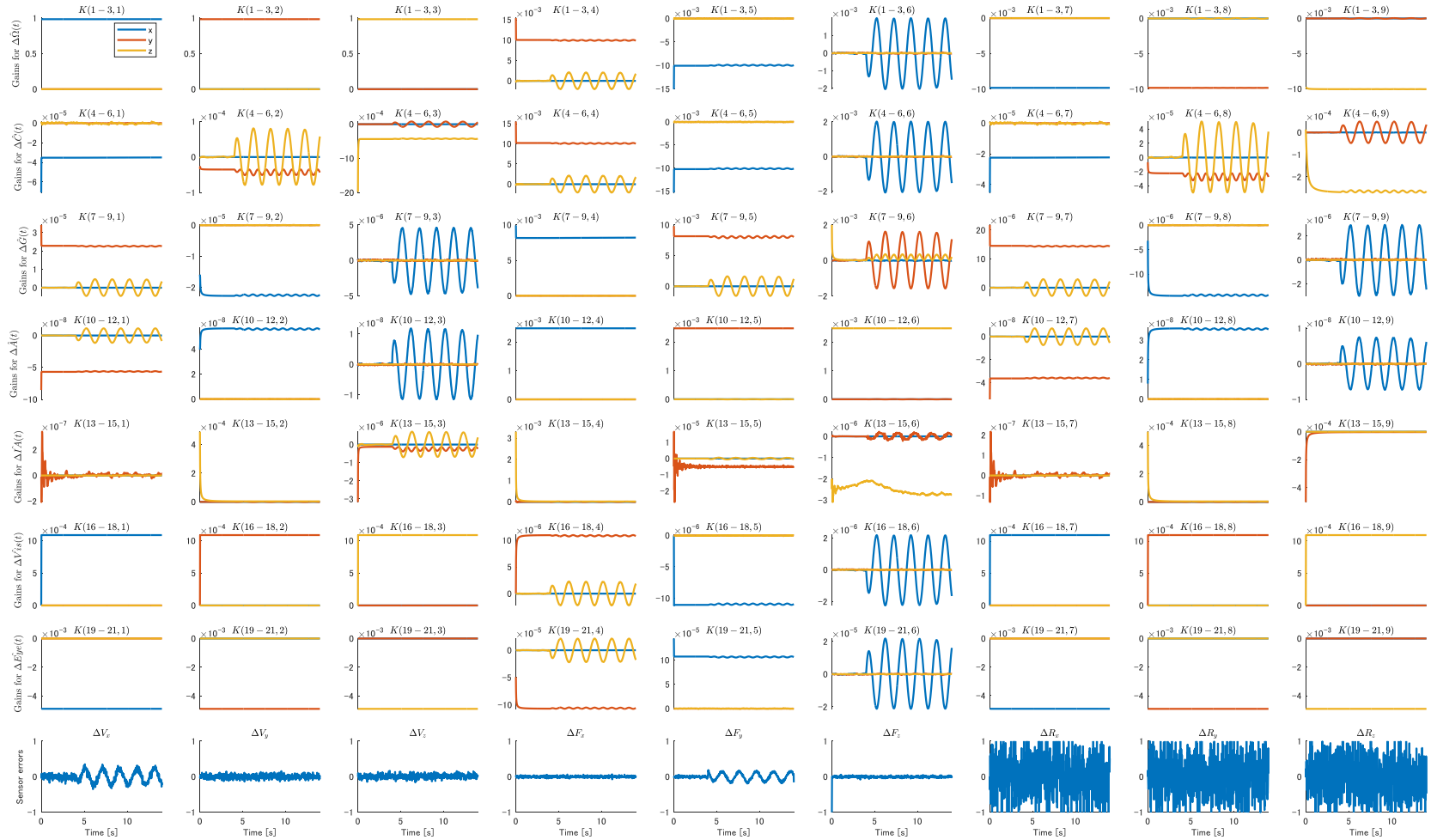
$$P_x^{u}(t) = h\,(\hat{\Phi}_x(t) - \hat{\Omega}_x(t))$$
$$P_y^{u}(t) = h\,(\hat{\Phi}_y(t) - \hat{\Omega}_y(t) + r\hat{B}_z(t))$$
$$P_z^{u}(t) = h\,(\hat{\Phi}_z(t) - \hat{\Omega}_z(t) - r\hat{B}_y(t))$$

Where: control gain $h = 0.8$

Supplementary Results

Kalman gains

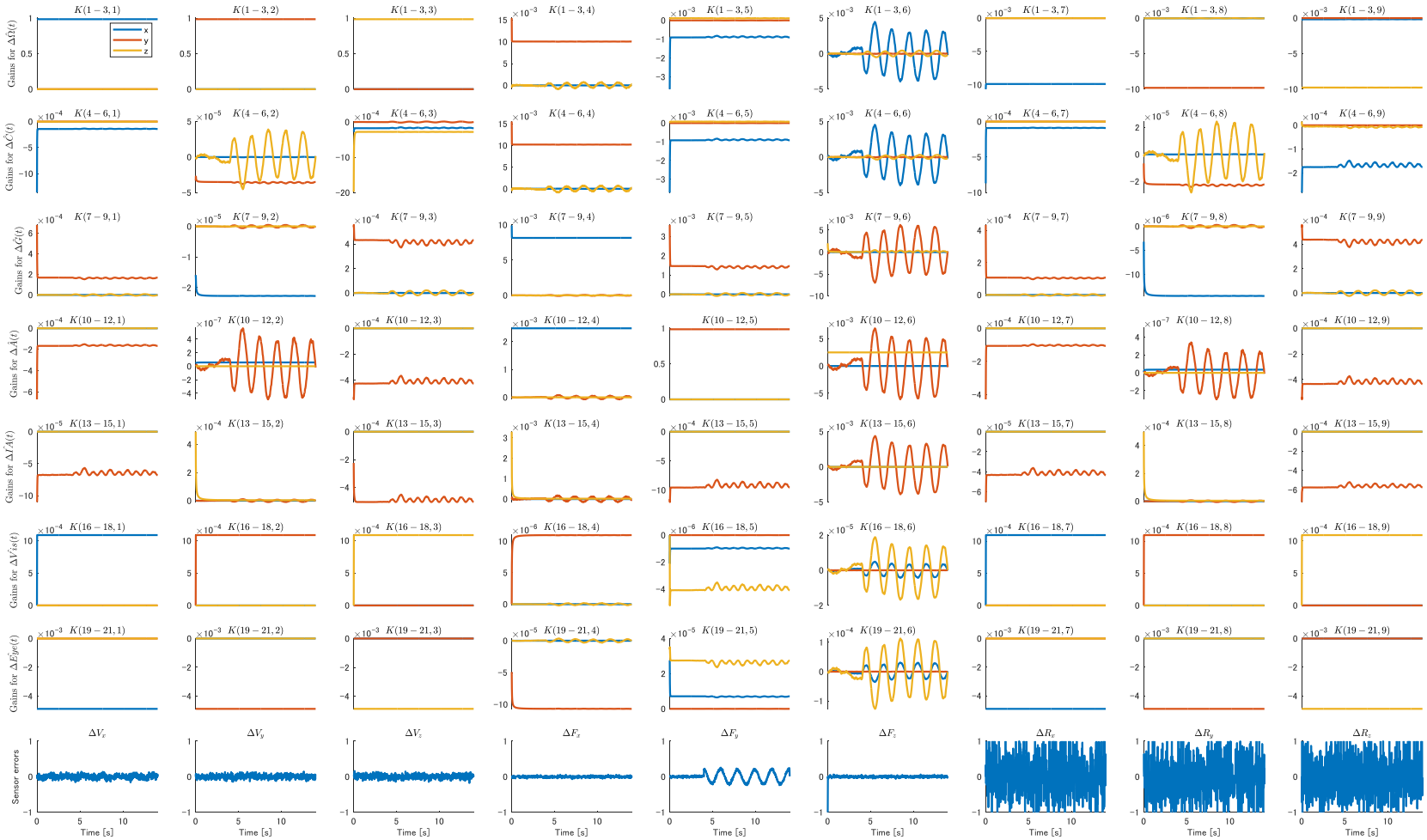
S3.1 Kalman gains in linear VOR dark before training



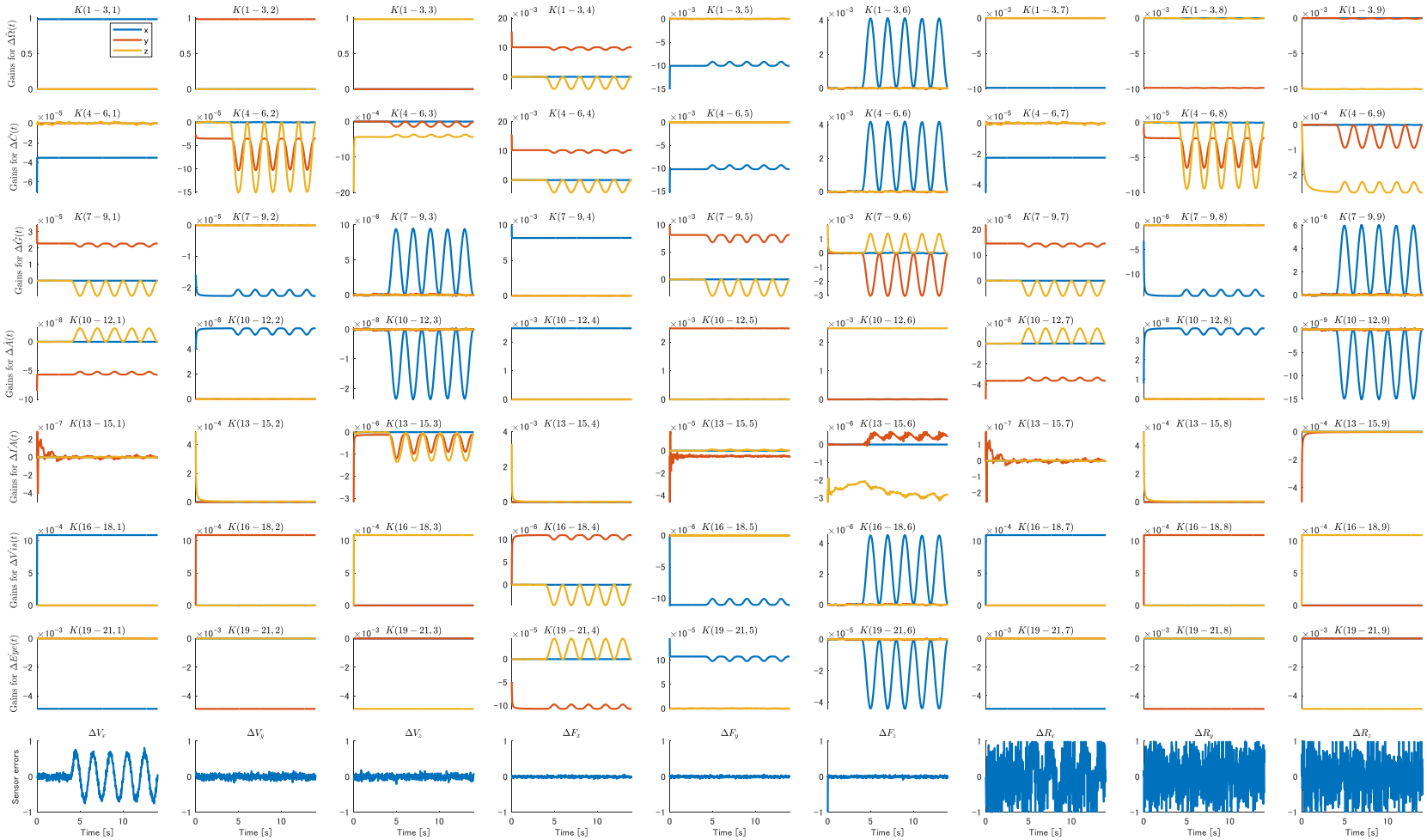
Example:

$$\Delta\hat{\Omega}_x = K(1,1)\Delta V_x + K(1,2)\Delta V_y + K(1,3)\Delta V_z + K(1,4)\Delta F_x + K(1,5)\Delta F_y + K(1,6)\Delta F_z + K(1,7)\Delta R_x + K(1,8)\Delta R_x + K(1,9)\Delta R_z$$
$$\Delta\hat{\Omega}_y = K(2,1)\Delta V_x + K(2,2)\Delta V_y + K(2,3)\Delta V_z + K(2,4)\Delta F_x + K(2,5)\Delta F_y + K(2,6)\Delta F_z + K(2,7)\Delta R_x + K(2,8)\Delta R_x + K(2,9)\Delta R_z$$
$$\Delta\hat{\Omega}_z = K(3,1)\Delta V_x + K(3,2)\Delta V_y + K(3,3)\Delta V_z + K(3,4)\Delta F_x + K(3,5)\Delta F_y + K(3,6)\Delta F_z + K(3,7)\Delta R_x + K(3,8)\Delta R_x + K(3,9)\Delta R_z$$

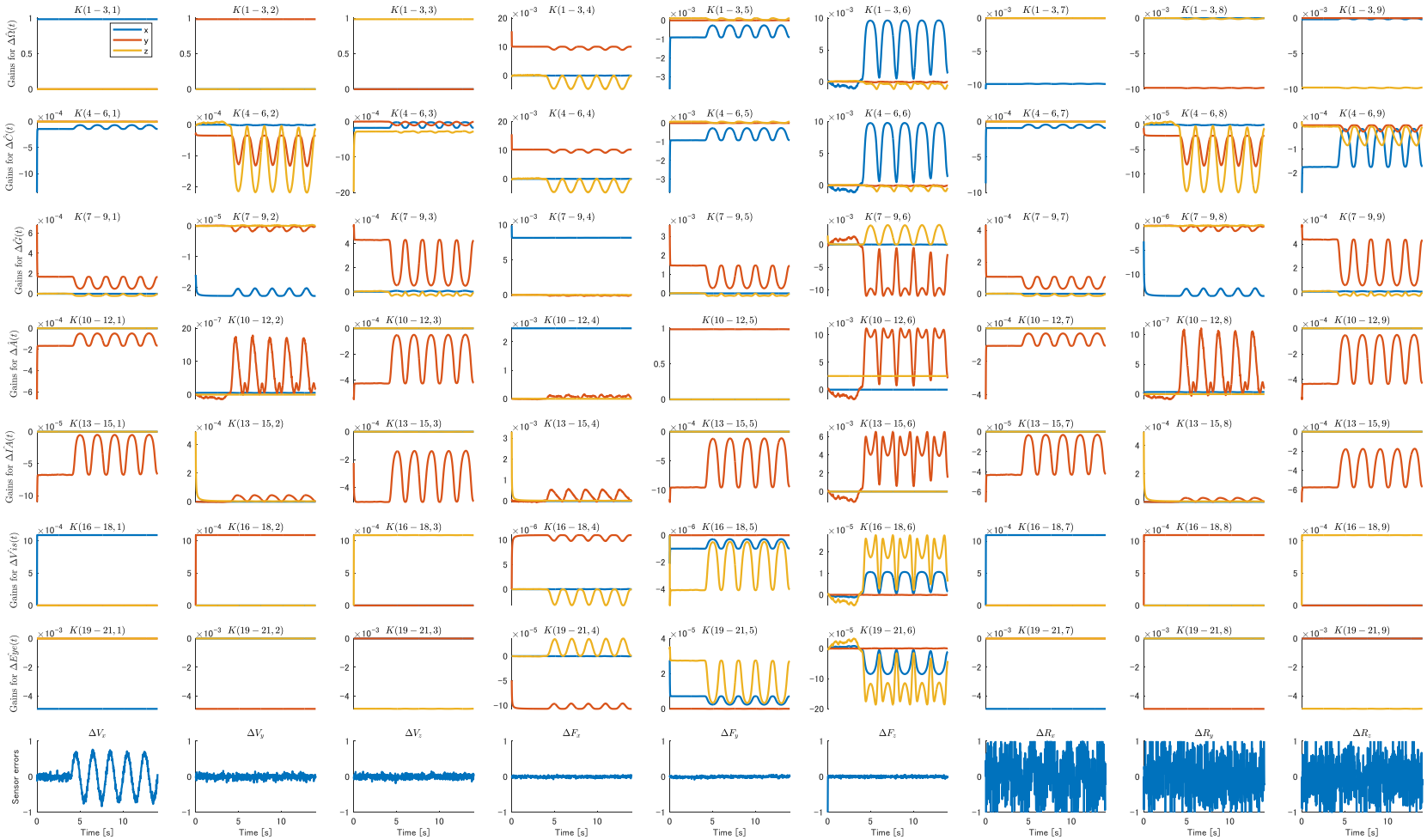
S3.2 Kalman gains in linear VOR dark after training



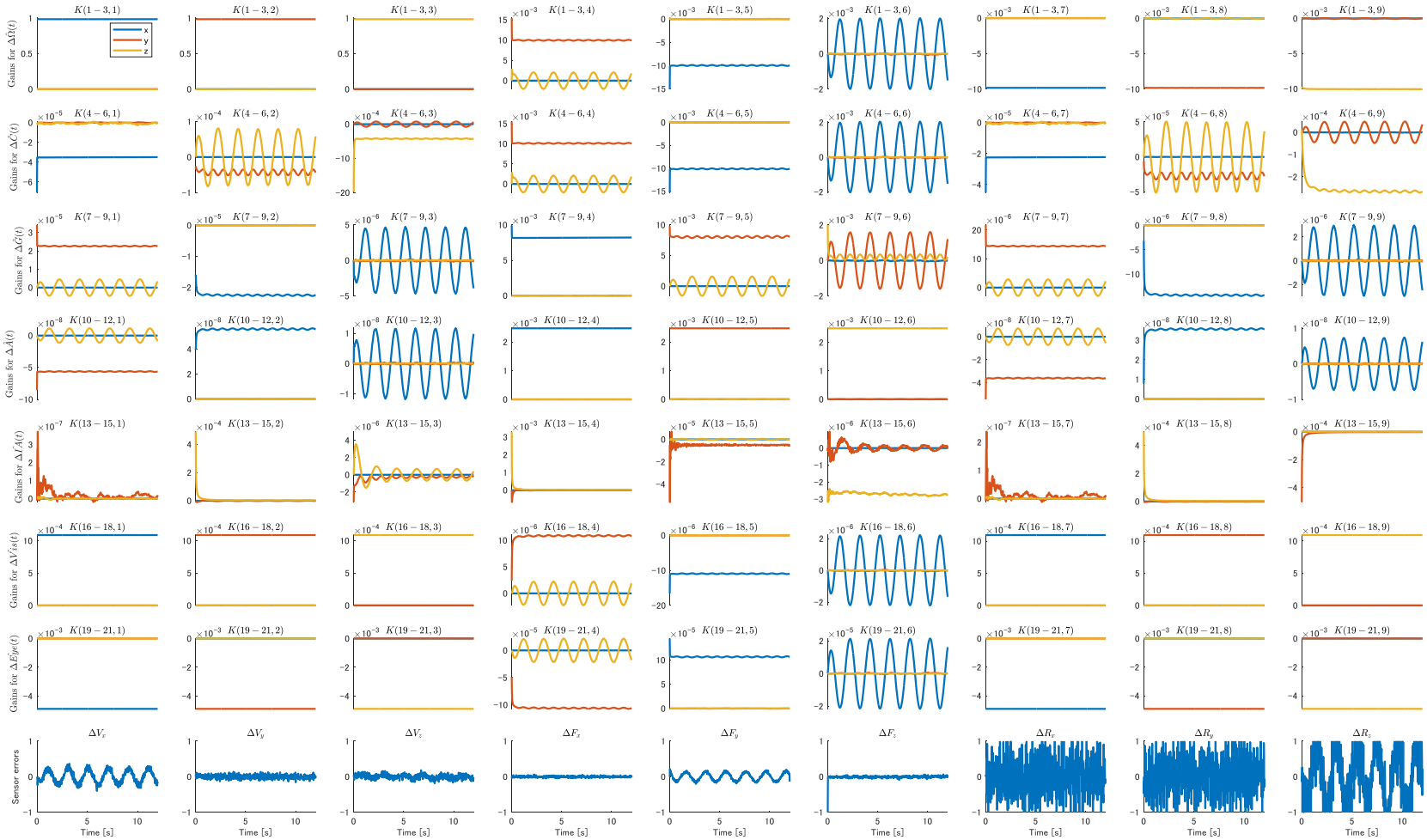
S3.3 Kalman gains in rotate VOR dark before training



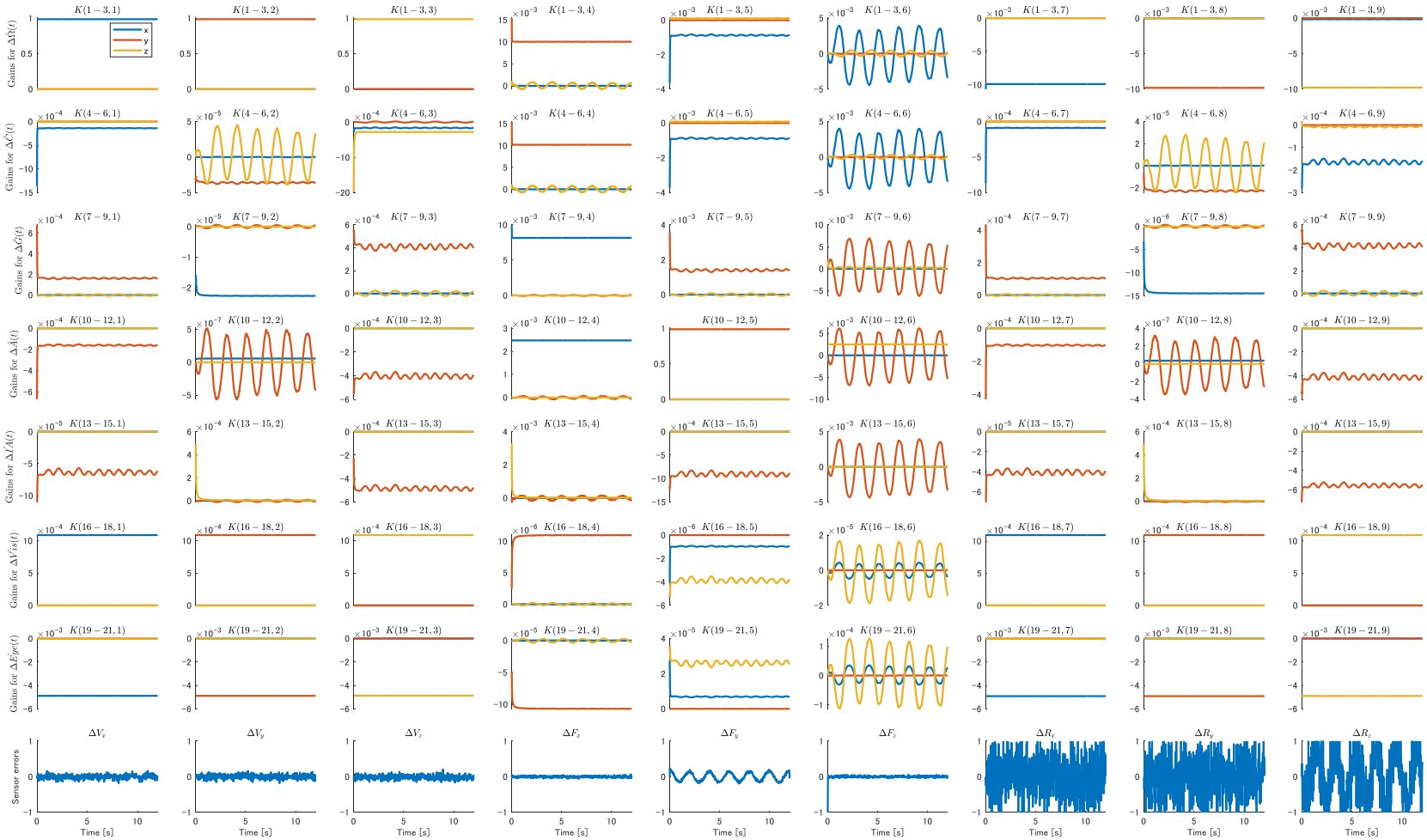
S3.4 Kalman gains in rotate VOR dark after training



S3.5 Kalman gains in linear VOR light beginning of training



S3.6 Kalman gains in linear VOR light end of training



Academic Achievements

Peer-Reviewed Academic Papers (14, including 5 as the first author)

1. Tadokoro, S., Yamanaka, T., Miki, S., Hirata, Y., “Horizontal, vertical, and torsional optokinetic responses and their adaptations in fish”, Journal of Neurophysiology, 2025 (in press).
2. Tadokoro, S., Shinji, Y., Yamanaka, T., Hirata, Y., “Learning capabilities to resolve tilt-translation ambiguity in goldfish”, Frontiers in Neurology, 15:1304496 (23 pages), 2024.
3. Mizokami, D., Takihata, S., Tadokoro, S., Araki, K., Shiotani, A., “Characteristic Findings of Omicron Throat”, Japanese Journal of Hospital General Medicine, vol.4-4, pp194-195, 2022.
4. 関雅彦, 水足 邦雄, 田所 慎, 塩谷 彰浩, “くしゃみを契機に発症した椎骨動脈解離による小脳梗塞”, Equilibrium Research, , vol.79, pp.20-26, 2020.
5. 田村敦, 田所慎, “空間識失調と航空医学”, Equilibrium Research, , vol.78, pp.242-255, 2019.
6. 田村敦, 田所慎, “めまいを伴う突発性難聴に罹患した民間パイロットの航空業務復帰のための航空身体検査証明審査申請状況”, Equilibrium Research, vol.78, pp.192-195, 2019.
7. 田村敦, 田所慎, “メニエール病を抱えた民間パイロットの航空業務復帰のための航空身体検査証明審査申請状況” Equilibrium Research, vol.77, pp.260-263, 2018.
8. Higashino, T., Matsuo, H., Okada, Y., Nakashima, H., Shimizu, S., Sakiyama, M., Tadokoro, S., Nakayama, A., Kawaguchi, M., Komatsu, M., Hishida, A., Nakatochi, M., Ooyama, H., Imaki, J., Shinomiya, N., “A common variant of MAF/c-MAF, transcriptional factor gene in the kidney, is associated with gout susceptibility”, Human Cell, vol.31, pp.10-13, 2018.
9. 田村敦, 田所慎, “航空身体検査証明審査における民間パイロットの内耳疾患事案とその年齢構成”, Equilibrium Research, vol.76, pp.174-177, 2017.
10. Niwa, K., Matsunobu, T., Kurioka, T., Kamide, D., Tamura, A., Tadokoro, S., Satoh, Y., Shiotani, A., “The beneficial effect of Hangesha-shin-to (TJ-014) in gentamicin-induced hair cell loss in the rat cochlea”, Auris Nasus Larynx, vol.43, pp.507-513, 2016.
11. 田所慎, 溝上 大輔, 原田 栄子, 神藤 英二, 荒木 幸仁, 山下 拓, 塩谷 彰浩, “外科的介入を行った直腸癌甲状腺転移の 1 例”, 耳鼻咽喉科・頭頸部外科, vol.87, pp.341-345, 2015.
12. 田所慎, 吉福 孝介, 吉永 里香子, 西元 謙吾, 松崎 勉, 塩谷 彰浩, “永久気管孔内部の気管粘膜炎に対してグリセリン加ネブライザー療法が有効であった 1 症例”, 耳鼻咽喉科・頭頸部外科, vol.87, pp.1035-1039, 2015.
13. 田所慎, 吉福 孝介, 西元 謙吾, 松崎 勉, 昇 卓夫, 塩谷 彰浩, “失神を伴う声門上癌の 1 例”, 防衛医科大学校雑誌, vol.40, pp.265-270, 2015.
14. Matsuo, H., Takada, T., Ichida, K., Nakamura, T., Nakayama, A., Ikebuchi, Y., Ito, K., Kusanagi, Y, Chiba, T., Tadokoro, S., Takada, Y., Oikawa, Y., Inoue, H., Suzuki, K., Okada, R., Nishiyama, J., Domoto, H., Watanabe, S., Fujita, M., Morimoto, Y., Naito, M., Nishio, K., Hishida, A., Wakai,

K., Asai, Y., Niwa, K., Kamakura, K., Nonoyama, S., Sakurai, Y., Hosoya, T., Kanai, Y., Suzuki, H., Hamajima, N., Shinomiya, N., “Common defects of ABCG2, a high-capacity urate exporter, cause gout: a function-based genetic analysis in a Japanese population”, Science Translational Medicine, vol.1, pp.5-11, 2009.

Non-Peer-Reviewed Academic Paper (1 as the first author)

1. 田所慎, 平田豊, “航空パイロットにおける空間識の特徴”, 体育の科学, 72 巻 11 号, pp757-762, 2022

International Conferences (8, including 5 as the first author)

1. Tadokoro, S., Miki, S., Ueno, T., Yamanaka, T., Hirata, T., Hirata, Y., “Goldfish horizontal, torsional, and vertical OKR adaptations reflect their distinctive head movement experience”, Society for Neuroscience, 2024, Chicago.
2. Hirata, T., Tadokoro, S., Yamanaka, T., Shinji, Y., “The relationship between eye position bias and walking deviation under occluded vision: Evidence that spatial orientation estimation is manifested in eye movements”, Society for Neuroscience, 2024, Chicago.
3. Ueno, T., Tadokoro, S., Shinji, Y., Yamanaka, T., Hirata, Y., “A three-dimensional eye movement measurement system using a monocular camera for fish and other animal species”, Society for Neuroscience, 2024, Chicago.
4. Hirata, Y., Shinji, Y., Tadokoro, S., Yamanaka, T., Hirata, T., “Enhanced Kalman filter model of spatial orientation formation”, Society for Neuroscience, 2023, Washington DC.
5. Tadokoro, S., Shinji, Y., Hirata, Y., “Evaluation of horizontal, vertical, and torsional optokinetic responses in goldfish as potential indicators of spatial orientation”, Society for Neuroscience, 2022, San Diego.
6. Tadokoro, S., Shinji, Y., Hirata, Y., “Acquisition of vertical and torsional optokinetic response in goldfish”, Neuro2022, Okinawa
7. Tadokoro, S., Shinji, Y., Hirata, Y., “Tilt-translation discrimination in goldfish vestibulo-ocular reflex”, Society for Neuroscience, 2021, online.
8. Tadokoro, S., Matsuo, H., Chiba, T., Nagamori, S., Nakayama, A., Kitamura, Y., Domoto, H., Phetdee, K., Wiriyasermkul, P., Nishiyama, J., Morimoto, Y., Kanai, Y., Shinomiya, N., “Glucose transporter9(GLUT9) as a serum urate regulator and causative gene for renal hypouricemia”, the 36th congress of the international union of physiological sciences (IUPS2009), Journal of Physiological Sciences, vol.59, p.495, 2009, Kyoto.

Domestic Conferences (25, including 16 as the first author)

1. 田所慎, 三木俊太郎, 上野貴祐, 山中都史美, 平田貴士, 平田 豊, “水平, 垂直, 回旋性視

運動性眼球運動とそれらの学習は自然界の頭部運動特性を反映する”, 第 83 回日本めまい平衡医学会総会学術講演会, Equilibrium Research, vol.83, p.416, 2024.名古屋コンベンションホール. （ポスター賞受賞）

2. 上野貴祐, 田所慎, 進士祐介, 山中都史美, 平田豊： “小型魚類用三次元眼球運動の単眼カメラ計測システム”, 第 18 回 Motor Control 研究会, プログラム p.94, 2024, Aug.大阪大学.
3. 進士祐介, 田所慎, 山中都史美, 平田豊： “Kalman filter による空間識形成過程のモデリングと傾き-並進曖昧性問題への適用”, 第 17 回 Motor Control 研究会, プログラム p.74, 2023. 東京大学.
4. Hirata, Y., Shinji, Y., Tadokoro, S., Yamanaka. T., Hirata, T.: “Simulating eye movements in response to tilt-translation vestibular stimulations using a Kalman filter model for spatial orientation formation”, 第 33 回日本神経回路学会全国大会, 2023. 東京大学.
5. 田所慎, 進士裕介, 山中都史美, 平田 豊, “空間識失調を克服する前庭視覚協調学習：金魚行動実験とモデルシミュレーション”, 第 69 回日本宇宙航空環境医学大会, 2023. 岐阜じゅうろくプラザ.
6. 田所慎, 進士裕介, 山中都史美, 平田 豊, “前庭・視覚協調学習は金魚の慣性力・重力識別を可能にする”, 電気・電子・情報関係学会東海支部連合大会講演論文集, F3-3, 2023 豊橋技術科学大学.（東海支部連合大会奨励賞受賞）
7. 田所慎, 山中都史美, 平田貴士, 進士裕介, 細野貴嗣, 平田豊, “歩行者及び航空パイロットの視線から推定する空間識形成”, 第 19 回空間認知と運動制御研究会学術集会, p.5, 2024. 京都大学.
8. 田所慎, 進士裕介, 山中都史美, 平田 豊, “前庭・視覚協調学習による慣性力・重力識別を担う空間識の変容：金魚における前庭動眼反射を用いた評価”, 第 124 回日本耳鼻咽喉科頭頸部外科学会 総会・学術講演会, 2023. 福岡国際会議場.
9. 田所慎, “眼球運動から推定する空間識”, JST CREST マルチセンシング領域「空間識の幾何による重力覚解明と感覚拡張世界創出」チーム 第 1 回 シンポジウム, 2023. 中部大学
10. 田所慎, 進士裕介, 平田豊, “慣性力・重力識別を担う自己運動知覚の変容：視覚・前庭協調学習前後の金魚前庭動眼反射を用いた評価”, 第 18 回空間認知と運動制御研究会学術集会, 2023. 京都大学.
11. 田所慎, 進士裕介, 平田豊, “多感覚情報統合履歴に依存した空間識変容 : 金魚の視運動性眼球運動による評価”, 第 81 回日本めまい平衡医学会総会学術講演会, 2022. 奈良県コンベンションセンター.

12. 田所慎, 進士裕介, 山中都史美, 平田 豊, “空間識形成過程の計算論に関する一考察”, 第 25 回 視覚科学フォーラム 2022 研究会, p24, 2022. 生理学研究所(愛知).
13. 田所慎, 進士裕介, 平田豊, “感覚情報統合履歴に依存した空間識変容の金魚における評価”, 第 17 回空間認知と運動制御研究会学術集会, p.10, 2022. Online.
14. 田所慎, 進士 裕介, 中野 仁賀, 平田 豊, “空間識失調に関わる並進・傾き識別曖昧性問題と反射性眼球運動の関係評価” 第 80 回日本めまい平衡医学会総会学術講演会, Equilibrium Research, vol.80, p.487, 2021. JP タワー内 KITTE ホール&カンファレンス(東京)
15. 山崎直弥, 冨藤 雅之, 田所 慎, 木村 朱里, 田中 伸吾, 塩谷 彰浩, “頸部食道癌と術前診断した有茎性下咽頭癌の 1 例”, 第 22 回北日本頭頸部癌治療研究会, 耳鼻咽喉科展望, vol.62, p.55, 2019. 北海道がんセンター.
16. 田所慎, 田村敦, “めまいを伴う突発性難聴に罹患した民間航空機操縦者の航空業務復帰までの検討”, 第 77 回日本めまい平衡医学会総会学術講演会, Equilibrium Research, vol.77, p.503, 2018. ホテルニュータナカ(山口)
17. 溝上大輔, 井部 達也, 田所 慎, 児玉 裕章, 濱元 陽一郎, 塩谷 彰浩, “肺癌・下咽頭癌の重複癌(扁平上皮癌)をペンブロリズマブで治療したところ、異なる治療効果を示した 1 例”, 第 119 回日本耳鼻咽喉科学会総会学術講演会, 日本耳鼻咽喉科学会会報, vol.121, p.603, 2018. パシフィコ横浜
18. 山崎直弥, 冨藤 雅之, 田所 慎, 木村 朱里, 田中 伸吾, 塩谷 彰浩, “頸部食道癌と術前診断した有茎性下咽頭癌の 1 例”, 第 42 回日本頭頸部癌学会学術講演会, 頭頸部癌, vol.44, p.237, 2018. 京王プラザホテル(東京)
19. 田所慎, 冨藤 雅之, 松野 直樹, 田中 伸吾, 宇野 光祐, 荒木 幸仁, 塩谷 彰浩, “食道壁内転移を来した下咽頭癌の 1 症例”, 第 69 回日本気管食道科学会総会学術講演会, 日本気管食道科学会会報, vol.69, p.46, 2018. 大阪府立国際会議場
20. 関雅彦, 水足 邦雄, 田所 慎, 塩谷 彰浩, “くしゃみを契機に発症した外リンパ瘻を疑ったが、術前検査で椎骨動脈解離による小脳梗塞と判明した稀な一例”, 第 76 回日本めまい平衡医学会総会学術講演会, Equilibrium Research, vol.76, p.557, 2017. 軽井沢プリンスホテル
21. 田村敦, 田所慎, “内耳疾患を抱えた航空機操縦者の航空業務復帰までの検討”, 第 76 回日本めまい平衡医学会総会学術講演会, Equilibrium Research, vol.76, p.540, 2017. 軽井沢プリンスホテル
22. 田所慎, 他 3 名, “喉頭腫瘍との鑑別を要した喉頭結核の一例”, 日本耳鼻咽喉科学会埼玉

県地方部会第 126 回学術講演会, 2017. 埼玉県県民健康センター

23. 田所慎, 溝上 大輔, 原田 栄子, 神藤 英二, 荒木 幸仁, 山下 拓, 塩谷 彰浩, “直腸癌甲状腺転移の 1 例”, 第 61 回防衛衛生学会, 防衛衛生, vol.64, p.51, 2016. 自衛隊中央病院 (東京)
24. 田村敦, 田所慎, “民間の航空業務における飛行安全と内耳疾患”, 第 75 回日本めまい平衡医学会総会学術講演会, Equilibrium Research, vol.75, p.465, 2016. 大阪国際会議場
25. 田所慎, 松尾 洋孝, 中山 昌喜, 千葉 俊周, 堂本 英治, 北村 陽典, 結城 充正, 西山 純一郎, 櫻井 裕, 四ノ宮 成祥, “海上自衛隊における低尿酸血症の頻度解析及び臨床遺伝学的解析”, 第 54 回防衛衛生学会, 防衛衛生, vol.56, p.83, 2009. 自衛隊中央病院 (東京)

Competitive Research Funding

1. CREST 若手チャレンジ 2023 年度, "歩行者及び航空機操縦者の眼球運動から推定する自己運動・姿勢の知覚と是正", CYC-MS2023004
   https://www.jst.go.jp/kisoken/crest/research/activity/1111117/reports/index.html

Awards

1. 第 83 回めまい平衡医学会学術講演会ポスター賞, 2024
2. 令和 6 年度 中部大学, 学長表彰, 2024
3. 令和 5 年度電気・電子・情報関係学会東海支部連合大会奨励賞, 2023
4. 令和 5 年度 中部大学, 学長表彰, 2023